


2012

Data Driven Prognosis: A Multi-Scale And Multi-Physics Approach

Oliva Kar

Iowa State University

Follow this and additional works at: <https://lib.dr.iastate.edu/etd>

 Part of the [Computer Engineering Commons](#), [Computer Sciences Commons](#), and the [Mechanical Engineering Commons](#)

Recommended Citation

Kar, Oliva, "Data Driven Prognosis: A Multi-Scale And Multi-Physics Approach" (2012). *Graduate Theses and Dissertations*. 12879.
<https://lib.dr.iastate.edu/etd/12879>

This Thesis is brought to you for free and open access by the Iowa State University Capstones, Theses and Dissertations at Iowa State University Digital Repository. It has been accepted for inclusion in Graduate Theses and Dissertations by an authorized administrator of Iowa State University Digital Repository. For more information, please contact digirep@iastate.edu.

Data driven prognosis: a multi-scale and multi-physics approach

by

Oliva Kar

A thesis submitted to the graduate faculty
in partial fulfillment of the requirements for the degree of
MASTER OF SCIENCE

Co-majors: Computer Science; Human Computer Interaction

Program of Study Committee:

Abhijit Chandra, Co-major Professor

David Fernández-Baca, Co-major Professor

Eve Wurtele

Sunanda Roy

Iowa State University

Ames, Iowa

2012

Copyright © Oliva Kar, 2012. All rights reserved.

DEDICATION

*I dedicate this dissertation to family and friends especially to
Ma and Baba for their love and for instilling the importance of hard work and
patience;*

Dadu and Dida for their love, support and encouragement;

Badam and Dadai for their blessings from the world beyond.....

CONTENTS

LIST OF FIGURES	vi
ABSTRACT	x
CHAPTER 1. INTRODUCTION	1
1.1 Overview of Prognostic Systems	1
1.2 Drawbacks	1
1.3 Data Driven Prediction Algorithm	1
1.4 Components of Data Driven Predictive Algorithm	2
CHAPTER 2. CONCEPT OF CURVATURE	3
2.1 Osculating Circle	3
2.2 Tangent Vector to Curve	4
2.3 Mathematical Definition of Curvature	5
2.4 Extrinsic and Intrinsic Curvature	7
2.5 Gaussian Curvature	7
2.6 Occurrence of Curvature in a System	8
2.7 Concept of Path Dependency: Plasticity in crystalline materials	11
2.8 Dislocations and Crystal Plasticity	15
2.9 Curvature Induced Path Dependency	20
CHAPTER 3. LENGTH SCALE DERIVATION	22
CHAPTER 4. ALGORITHMS	25
4.1 LBar and LBarTilda Calculation	25
4.1a Algorithm	25
4.1b Nature of the Roots	26
4.2 Curvature/Kappa Calculation	26
4.2a Range of proportionality variable (alpha)	26
4.2b Algorithm	27
4.3 Post Kappa Processing: Categorizing Points and Assigning PDI	29
4.3a Algorithm	29
4.4 Chain Length Calculation	31
4.4a Algorithm	31

4.5 Critical Localization Index Calculation	33
4.5a Algorithm	34
4.5b Critical localization index for any number of points	35
4.6 Hole Formation Calculation	36
4.6a Algorithm	36
4.7 Trend Reversal Calculation	38
4.7a Algorithm	39
CHAPTER 5. VERIFICATION OF ALGORITHM-BALLOON BURST	40
5.1 System Set Up.....	40
5.2 Verification	41
5.2a Critical Localization Index	41
5.2b Path Dependency Index.....	43
5.2c Residual Curvature.....	47
5.2d Composite Failure Prediction	48
5.3 Results of other datasets for balloon verification	49
5.4 Application of Stability analysis for CMP.....	52
CHAPTER 6. APPLICATION OF ALGORITHM- GULF STREAM.....	54
6.1 Gulf Stream Analysis.....	54
6.2 Feature Model Data Description	54
6.3 Choice of Dimensions	54
6.4 Preprocessing Data Files.....	55
6.5 Analysis Procedure	55
6.5a Critical Localization Index	55
6.5b Path Dependency Index.....	58
6.5c Ring Formation Results	59
6.6 Results of other datasets for Gulf Stream	66
6.6a Data Set 2 - May 21	66
6.6b Data Set 3 - May 21	71
CHAPTER 7. APPLICATION OF ALGORITHM- MACRO ECONOMICS.....	78
7.1 Economic System Analysis.....	78
7.2 Choice of Variables/Dimensions.....	79

7.3 Important Global Economic Events during 1993-2009	79
7.4 External factors that affect economic predictions	80
7.5 Preprocessing Data Files.....	81
7.6 Analysis Procedure	81
7.6a Critical Localization Index	82
7.6b Path Dependency Index.....	86
7.6c Trend Reversal Results.....	86
7.6d Residual Curvature Results.....	108
CHAPTER 8. CONCLUSIONS	111
CHAPTER 9. FUTUREWORK.....	112
BIBLIOGRAPHY.....	114
ACKNOWLEDGEMENTS	116

LIST OF FIGURES

Figure 2.1: An osculating circle. The curvature of curve C at point P is same as the curvature of the osculating circle.	3
Figure 2.2: The T and N vectors at two points on a plane curve, a translated version of the second frame (dotted). $\partial T = \text{change of } T$ And $\partial S = \text{length of line segment between 2 points}$	5
Figure 2.3: Unit tangents at two ends of the arc of length Δs	5
Figure 2.4: Surfaces having Gaussian curvature: Hyperboloid (negative), Cylinder (zero) and Sphere (positive)	8
Figure 2.5: Ants on plane surface, sphere and a hot plate.	9
Figure 2.6: A perfect square and a triangle on a flat surface	9
Figure 2.7: Square, triangle on a circle; Square on a hot plate.	10
Figure 2.8a: Slip Process in a Perfect Crystal	12
Figure 2.8b: Variation of Shear Stress and Lattice/Potential Energy with Atomic Displacement	13
Figure 2.9: Slip between two neighboring rows of atoms	14
Figure 2.10: Point Defects: - (a) Vacancy (b) Interstitial atom (c) Substitution Impurity (d) Interstitial Impurity	16
Figure 2.11: Planar defects: (a) Grain Boundary (b) Twin Boundary (i) and (ii) Stacking faults	17
Figure 2.12: Dislocation in a Crystal (a) Edge Dislocation (b) Screw Dislocation	18
Figure 2.13: Slip by means of edge dislocation	19
Fig 4.1: A shear stress \mathcal{T} is applied to the top of the square while the bottom is held in place. This stress results in a strain, or deformation, changing the square into a parallelogram	27
Figure 5.1: Balloon in the beginning and in the end before bursting	41
Figure 5.2: Zoom Out Plots for Balloon Burst Experiment	42
Figure 5.3: Chain Length Calculations for Balloon Burst	43
Figure 5.4a: Categorization of Points according to Path Dependency Index. (Path Independent and Path Dependent Categories)	44
Figure 5.4b: Path Dependency with Localization Index Category for 100 Points for Color Dimension	45
Figure 5.5: Number of roots having category greater than 5 showing path dependencies in color dimension	46

Figure 5.6: Number of roots having category greater than 5 and having chain length greater than number of points.....	47
Figure 5.7: Number of roots having residual curvature drops more than 80%.....	48
Figure 5.8: Composite Failure Prediction of Sample Data Set 1 (Row 353-362, Col 343-352).....	49
Figure 5.9a: Sample Data Set 2 (Row 363-372, Col 353-362).....	50
Figure 5.9b: Sample Data Set 3 (Row 373-382, Col 363-372).....	51
Figure 5.9c: Sample Data Set 4 (Row 383-392, Col 373-382).....	52
Figure 6.1: Zoom Out Plots for Gulf Stream Analysis.....	57
Figure 6.2: Short Term and Long Term Chain Length Calculations.....	58
Figure 6.3: Categorization of Points according to Path Dependency Index. (Path Independent and Path Dependent Categories).....	59
Figure 6.4a: Grid of April 9 at 6.00 a.m.	60
Figure 6.4b: Grid of April 23 at 6.00 a.m. (Row 16 Col 60).....	61
Figure 6.4c: Point plot of selected region April 9 to April 13.....	62
Figure 6.4d: Point plot of selected region April 13 to April 17.....	63
Figure 6.4e: Point plot of selected region April 17 to April 21.....	64
Figure 6.4f: Point plot of selected region April 21 to April 23.....	65
Figure 6.5a: May 21 Grid with the Selected Area for Analysis (Row 5 Col 105).....	66
Figure 6.5b: Point plot of selected region May 7 to May 11.....	67
Figure 6.5c: Point plot of selected region May 11 to May 15.....	68
Figure 6.5d: Point plot of selected region May 15 to May 19.....	69
Figure 6.5e: Point plot of selected region May 19 to May 21.....	70
Figure 6.6a: May 28 Grid Showing the 2 Areas of May 21 Used For Analysis.....	71
Figure 6.6b: May 21 Grid with the Selected Area for Analysis (Row 16 Col 60).....	72
Figure 6.6c: Point plot of selected region May 7 to May 11.....	73
Figure 6.6d: Point plot of selected region May 11 to May 15.....	74
Figure 6.6e: Point plot of selected region May 15 to May 19.....	75
Figure 6.6f: Point plot of selected region May 19 to May 21.....	76

Figure 7.1: Zoom Out Plots for Macro Economic Analysis.....	84
Figure 7.2: Short Term Chain Length Calculations for Economic Analysis.....	85
Figure 7.3: Categorization of Points according to Path Dependency Index. (Path Independent and Path Dependent Categories)	86
Figure 7.4a: GDP per capita of selected countries against path dependency indices part 1	87
Figure 7.4b: GDP per capita of selected countries against path dependency indices part 2	88
Figure 7.4c: GDP per capita of selected countries against path dependency indices part 3.....	89
Figure 7.4d: GDP per capita of selected countries against path dependency indices part 4	90
Figure 7.4e: GDP per capita of Greece, New Zealand, and Slovenia.....	91
Figure 7.5a: Lending rate of selected countries against path dependency indices part 1	92
Figure 7.5b: Lending rate of selected countries against path dependency indices part 2	93
Figure 7.5c: Lending rate of selected countries against path dependency indices part 3	94
Figure 7.5d: Lending rate of selected countries against path dependency indices part 4	95
Figure 7.5e: Lending rate of Algeria, Australia, Hungary and Israel	96
Figure 7.5f: Lending rate of Nicaragua and South Africa	97
Figure 7.6a: Inflation GDP Deflator of selected countries against path dependency indices part 1	98
Figure 7.6b: Inflation GDP Deflator of selected countries against path dependency indices part 2	99
Figure 7.6c: Inflation GDP Deflator of selected countries against path dependency indices part 3	100
Figure 7.6d: Inflation GDP Deflator of selected countries against path dependency indices part 4	101
Figure 7.6e: Inflation GDP Deflator of some selected countries	102
Figure 7.6f: Inflation GDP Deflator of Dominican Republic	103
Figure 7.7a: Unemployment of selected countries against path dependency indices part 1	104
Figure 7.7b: Unemployment of selected countries against path dependency indices part 2	105
Figure 7.7c: Unemployment of selected countries against path dependency indices part 3	106
Figure 7.7d: Unemployment of selected countries against path dependency indices part 4	107
Figure 7.7e: Unemployment of selected countries against path dependency indices part 4	108
Figure 7.8: Percentage of roots (out of 16) that had a residual curvature drop greater than 80%.	109

Figure 7.9: Percentage of roots (out of 64 summed across all 4 dimensions) that had a residual curvature drop greater than 80% 109

ABSTRACT

All current engineering prognostic practices require prior off-line tests. These are needed to: (1) Determine the exact conservative principle or utility function being satisfied, and (2) Determine associated material, geometric and process parameters. In addition, prediction of onset of instability or failure requires a failure criterion. The data driven prognosis (DDP) approach, developed here, obviates the need for such off-line testing and facilitates true predictive capability using only on-line data being sensed. To achieve this end, the DDP algorithm makes an assumption regarding polynomial order of the potential or utility function in the neighborhood of each observation points. Thus, an assumption regarding the local piecewise behavior replaces any global assumption. The needed system parameters in dimensionless forms are then estimated based on prior data or experience from the same experiment. A multi-physics model based on the concept of excess curvature is then developed to predict short-term and long term stability profiles of any system. The model is first validated against simple "Balloon Burst" experiment and later used for analyzing "Gulf Stream" and "Economics" systems. The proposed DDP algorithm may be used for general conservative systems provided the variables involved in the conservation principle are observable. The developed multi-physics model also provides an objective basis for data driven prediction of system stability and associated decision making in various mechanical, economic and societal systems.

CHAPTER 1. INTRODUCTION

1.1 Overview of Prognostic Systems

Predictive or prognostic ability represents a core competency required in many walks of life. Traditionally, analytical or numerical models based on conservation principles are used for such activities. These models require satisfying primarily three principles: - (1) equilibrium (which embodies satisfaction of a conservative principle), (2) compatibility and (3) constitutive relations. In most cases, the constitutive relations depend on prior knowledge of constitutive or material parameters. Most often, a failure criterion and associated critical or threshold value of a parameter is also required to predict onset of material or geometric instabilities. Such estimation protocols require off-line testing.

1.2 Drawbacks

Numerous applications of practical interest, however, suffer from two major drawbacks: (1) the exact conservation principle or utility function being conserved may be unknown, (2) the system may not be amenable to perform off-line (in particular, destructive) testing. For instance while trying to predict the onset of instability in a material (e.g. necking in a tension test done on a material), the material properties can be found out even before the actual experiment is done. The knowledge of specific material and geometric properties can then ease the process of prediction. But if a non-materialistic or abstract system (e.g. a global economic system, or a genetics system) is considered there is neither any way of knowing the specific material properties, nor there is any method to assess the nature of the conservation function. In such cases there is a need to rely on a predictive algorithm that can function without these parameters known beforehand.

1.3 Data Driven Prediction Algorithm

The present work circumvents these two difficulties by devising a data driven prognosis (DDP) algorithm. The proposed algorithm requires assumption of existence of a conservation principle, but its exact form need not be known a priori. Instead, an assumption is made regarding its piecewise polynomial form around each observation point. Further, the proposed algorithm requires no off-line material or process parameters as input. Instead, it is completely data driven, and only in-situ procured data is utilized to estimate the required dimensionless length scale parameters. The assessment of failure criterion is also done with

this procured data. Thus, the proposed DDP algorithm significantly enhances current prognostic capabilities.

1.4 Components of Data Driven Predictive Algorithm

The current work starts with a discussion of basic methodology adopted for the prognostic approach. In particular, the concept of “Curvature Induced Path Dependency” is introduced. Chapter 2 discusses how curvature of a mathematical manifold may nucleate a “dislocation” when attempting to complete a closed loop. As in material systems, such micro-scale dislocations can induce macro-scale path dependency on a mathematical manifold. Chapter 3 and 4 discusses development of the mechanistic multi-physics formulation along with details of the algorithm. Three types of analysis are considered next. Chapter 5 discusses the verification (a balloon burst experiment) done for this predictive algorithm. In the balloon burst experiment considered here, the prognosis protocol predicts the onset of instability or the point where the balloon will burst from visual data only. Chapter 6 discusses how this predictive algorithm can be utilized in a real world problem (the Gulf Stream Instability Analysis). The development of cold cores in Gulf Stream along the eastern coast of North America is an interesting phenomenon which holds a lot of importance in the fishing community. The knowledge of such cold core rings beforehand would definitely be beneficial for their commercial purposes. Chapter 6 discusses the application of prediction algorithm to anticipate the formation of such cold cores. Another real world application (Economics) of the DDP algorithm is also shown in Chapter 7. A macro-economic example is considered. In each case, the multi-physics prognosis protocol is asked to predict onset of instabilities in an economic system comprising of 81 countries, which are then compared and verified against historical data. Eventually, the conclusion section of this work considers the quality of the prognosis by comparing not only accuracy, but also “false positives” where a false alarm is sounded or a “missed positive” where an instability (that actually happened) is missed. The efficacy and efficiency of the algorithm is then discussed in light of such data “on hindsight”.

CHAPTER 2. CONCEPT OF CURVATURE

Curvature is just a measure of how “curved” a curve is. The measure of “curvature” should depend only on the shape of the curve. Moreover the measure of “curvature” should match with our intuition in the simplest cases. Straight lines are not curved, hence their curvature is zero. Smaller circles which bend more sharply than larger circles should have higher curvature values. Following this, the measure of the curvature of a circle can be thought of as the reciprocal of its radius. Hence the curvature is large if the radius is small and the curvature is small if radius is large. Thus the curvature of a circle is defined as the reciprocal of its radius r .

$$\kappa = \frac{1}{r} \quad (1)$$

2.1 Osculating Circle

Geometrically, given any smooth plane curve C and a point P on it, there is a unique circle called the osculating circle (a circle passing through P and a pair of additional points on the curve infinitesimally close to P) which most closely approximates the curve near P . The curvature of C at P is then defined to be the curvature of that circle [Wikipedia]. [Figure 2.1]

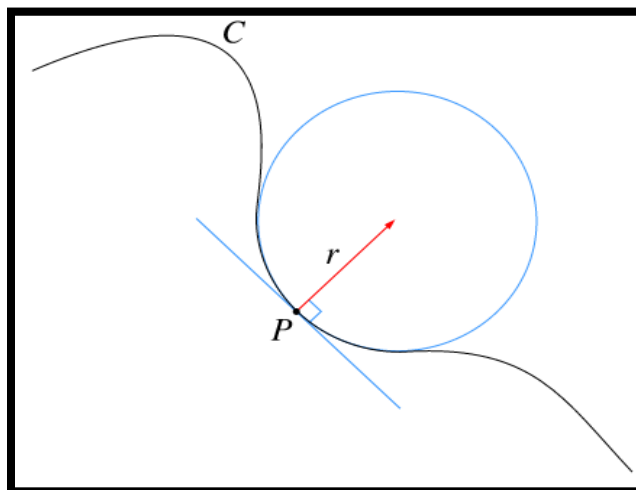


Figure 2.1: An osculating circle. The curvature of curve C at point P is same as the curvature of the osculating circle.

The curvature of the osculating circle is given by equation 1. The radius of curvature is equal to the reciprocal of the radius of the osculating circle.

2.2 Tangent Vector to Curve

Physically, curvature can be understood by imagining a particle moving along that curve (\mathbf{C}) in unit speed. The time t is taken as the parameter for \mathbf{C} (provides a natural parameterization for the curve). The unit tangent vector \mathbf{T} at the point \mathbf{P} also depends on time. The unit tangent vector \mathbf{T} can be also thought as the velocity vector (velocity is always tangential at point \mathbf{P} when a particle is going around a curve or arc or a circle), since the particle is moving with unit speed. The absolute curvature is then the **magnitude of the rate of change of \mathbf{T}** . [Figure 2.2]

$$|\kappa| = \left\| \frac{d\mathbf{T}}{dt} \right\| \quad (2)$$

This signifies magnitude of the acceleration of the particle [Wikipedia 2012]. Geometrically, this measures how fast the unit tangent vector to the curve rotates. If a curve keeps close to the same direction, the unit tangent vector changes minimally and the curvature is small; when the curve undergoes a tight turn, the curvature is large. The absolute value of the curvature is a measure of how sharply the curve bends. Curves which bend slowly, which are almost straight lines, will have small absolute curvature. Curves which swing to the left (counter clockwise) have positive curvature and curves which swing to the right (clock wise) have negative curvature. The two interpretations of curvature (curvature of circle and acceleration of a particle along a curve) are related geometrically. In the first definition the curvature of a circle is actually a ratio between the angles of an arc to its length. For the circle, **arc length** = $2\pi r$ (**circumference**) and **arc angle** = 2π . So $\kappa = \frac{2\pi}{2\pi r} = \frac{1}{r}$. From this understanding, the absolute curvature of a plane curve at a point \mathbf{P} can be given as

$$|\kappa| = \left\| \frac{d\phi}{dt} \right\| = \left\| \frac{d\phi}{ds} \right\| \quad (3)$$

$d\phi =$ *infinitesimal angle in rad between tangents to the curve at the ends of a infinitesimal segment of the curve* And $ds =$ *length of the segment*.

Since the curve is a unit speed one i.e. the particle moving along the curve is having unit speed, the particle would cover the distance ds in ds time. Hence dt in equation (2) of curvature becomes equal to ds and equation (2) can also be written like $|\kappa| = \left\| \frac{d\mathbf{T}}{ds} \right\|$.

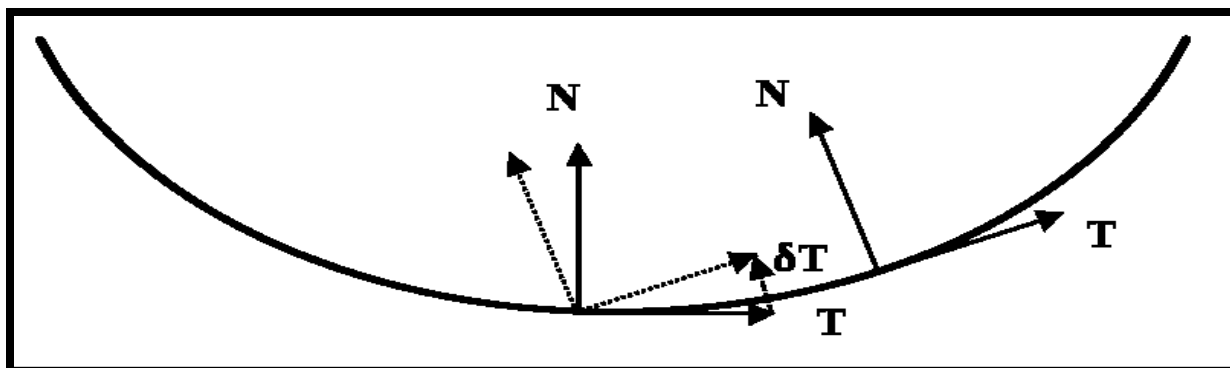


Figure 2.2: The T and N vectors at two points on a plane curve, a translated version of the second frame (dotted).

$\partial T = \text{change of } T$ And $\partial S = \text{length of line segment between 2 points}$.

The change dT happens orthogonal to the direction of T , so it must be along the normal direction N . Equations (2) and (3) can be derived from each other. For instance and replacing $dt = ds$ in equation (2),

$$\kappa = \frac{dT}{ds} \cdot N = \lim_{\Delta s \rightarrow 0} \frac{(T(s + \Delta s) - T(s)) \cdot N}{\Delta s} = \lim_{\Delta s \rightarrow 0} \frac{\Delta \phi \cdot \|T\|}{\Delta s} = \lim_{\Delta s \rightarrow 0} \frac{\Delta \phi}{\Delta s} = \frac{d\phi}{ds}$$

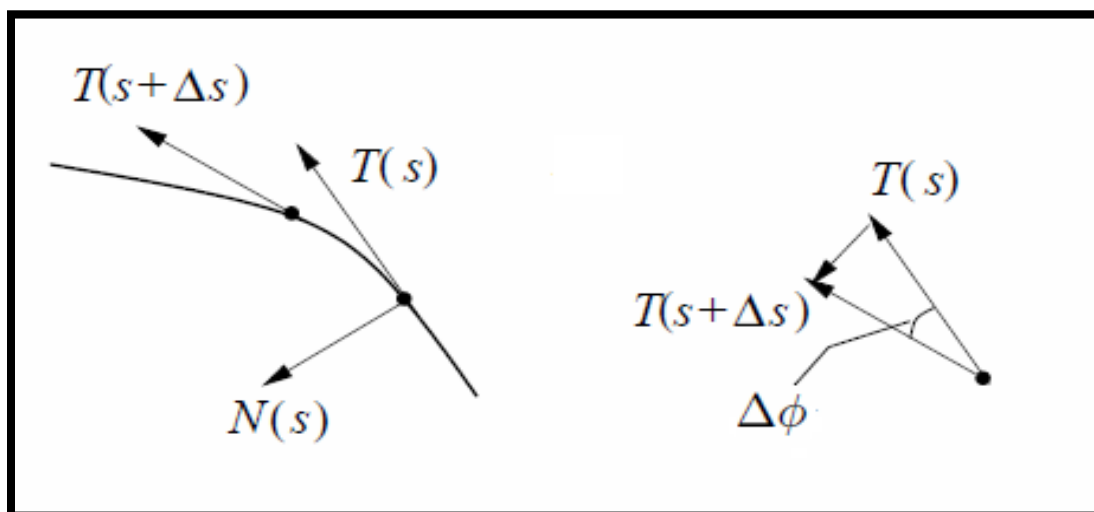


Figure 2.3: Unit tangents at two ends of the arc of length Δs

2.3 Mathematical Definition of Curvature

Let us now consider a plane curve in 2 dimensions which is described by Cartesian parametric equations namely $x = x(t)$ and $y = y(t)$ [Wolfram Math world 2012]. If $\phi =$

tangential angle and $s = \text{arc length}$ then the curvature also called the “first curvature” is given by

$$\kappa = \frac{d\phi}{ds} = \frac{\frac{d\phi}{dt}}{\frac{ds}{dt}} = \frac{\frac{d\phi}{dt}}{\sqrt{\left(\frac{dx}{dt}\right)^2 + \left(\frac{dy}{dt}\right)^2}} = \frac{\frac{d\phi}{dt}}{\sqrt{x'^2 + y'^2}} \quad (4)$$

The numerator of equation (4) can be found using the identity

$$\tan \phi = \frac{dy}{dx} = \frac{\frac{dy}{dt}}{\frac{dx}{dt}} = \frac{y'}{x'} \quad (5)$$

Differentiating equation (5) with respect to time t we get

$$\frac{d(\tan \phi)}{dt} = \sec^2 \phi \frac{d\phi}{dt} = \frac{x'y'' - y'x''}{x'^2} \quad (6)$$

From equation 6 we get

$$\begin{aligned} \frac{d\phi}{dt} &= \frac{1}{\sec^2 \phi} \frac{x'y'' - y'x''}{x'^2} = \frac{1}{1 + \tan^2 \phi} \frac{x'y'' - y'x''}{x'^2} \\ &= \frac{1}{1 + \frac{y'^2}{x'^2}} \frac{x'y'' - y'x''}{x'^2} = \frac{x'y'' - y'x''}{x'^2 + y'^2} \end{aligned} \quad (7)$$

Combining equations (4) and (7) we get

$$\kappa = \frac{x'y'' - y'x''}{(x'^2 + y'^2)^{\frac{3}{2}}} \quad (8)$$

Now let us consider a 2 dimensional curve of the form $y = f(x)$, where x and y are naturally scaled orthogonal coordinates. Natural scaling means $(ds)^2 = (dx)^2 + (dy)^2$. Then the equation of curvature becomes

$$\kappa = \frac{d\phi}{ds} = \frac{dx}{ds} \frac{d\left(\tan^{-1}\left(\frac{dy}{dx}\right)\right)}{dx} = \frac{dx}{ds} \left[\frac{\frac{d^2y}{dx^2}}{\left(1 + \left[\frac{dy}{dx}\right]^2\right)} \right] = \frac{\frac{d^2y}{dx^2}}{\left(1 + \left[\frac{dy}{dx}\right]^2\right)^{\frac{3}{2}}}$$

$$= \frac{y''}{(1+y'^2)^{\frac{3}{2}}} \quad (9)$$

Equation 8 and 9 represents curvature for different curve forms. But the meaning of curvature for each one of them is the same. Curvature represents the change in slope over a length scale.

2.4 Extrinsic and Intrinsic Curvature

Equations (8) and (9) all represent **extrinsic curvature**, which is defined for objects embedded in another space (usually a Euclidean space) in a way that relates to the radius of curvature of circles that touch the object [Weisstein, Eric W. "Curvature." *Wolfram MathWorld*]. Extrinsic curvature depends on the object's particular embedding. It is not detectable to someone who is unaware of the three-dimensional space surrounding the object. There is another curvature called **intrinsic curvature** which is detectable to "inhabitants" residing on the object. Intrinsic curvature is independent of the object's embedding and is a property of the object. It only depends on how the distances are measured on the surface but never on the embedding of the surface in higher dimensions. Example of intrinsic curvature is the **Gaussian curvature**.

2.5 Gaussian Curvature

For explaining the **Gaussian curvature** we need to introduce another term called the **principal curvature**. Consider a one dimensional curve that lies on a two dimensional surface embedded in 3 dimensions. The tangent vector \mathbf{T} to this curve lies on the tangent plane of the surface. The tangent plane of the surface is orthogonal to the surface's unit normal vector \mathbf{U} . The normal curvature (κ_n) is defined as the curvature of the curve projected on the plane containing both \mathbf{T} and \mathbf{U} . All curves with same tangent vector will have same surface normal associated with them. Taking all possible tangent vectors then the maximum and minimum values of the normal curvature at a point are called the principal curvatures and can be denoted by (κ_1) and (κ_2) [Wikipedia 2012]. The Gaussian curvature is defined as the product of the 2 principal curvatures and is given by

$$\kappa_g = \kappa_1 \kappa_2$$

Intrinsically Gaussian curvature can be defined by imagining an ant living on the two dimensional surface on which the smooth curve lies. Now if the ant is tied to a point \mathbf{P} with a thread of length \mathbf{R} and it tries to make a circle around the point P the circumference of the

circle so drawn would not be equal to $2\pi R$. Similarly if the ant tries to draw a triangle the sum of the angles would never be equal to 2π . Then the surface is said to have some Gaussian curvature and it gives a measure of how much convex (positive Gaussian curvature) or concave (negative Gaussian curvature) the surface is. For surfaces not having any Gaussian curvature there will be no deviation from such measurements. Examples include sphere (positive Gaussian curvature), hyperboloid (negative Gaussian curvature). [Figure 2.4]

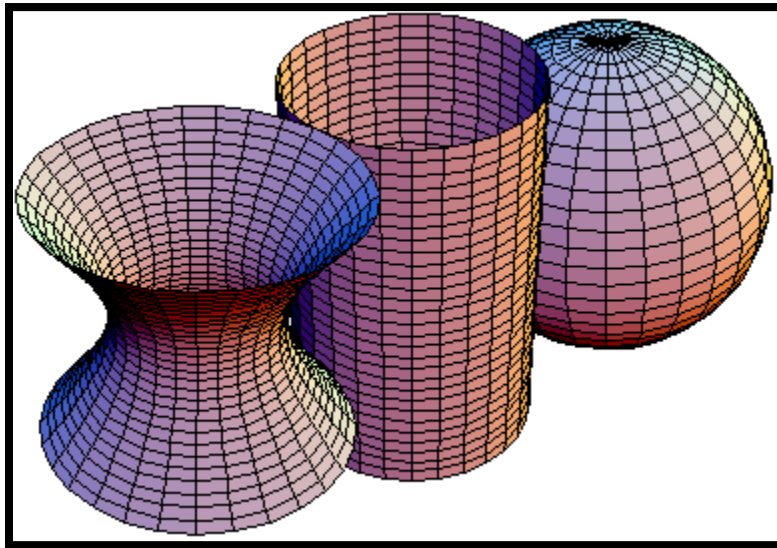


Figure 2.4: Surfaces having Gaussian curvature: Hyperboloid (negative), Cylinder (zero) and Sphere (positive)

2.6 Occurrence of Curvature in a System

There are various ways that a curvature can occur in the system. Let us understand the concept by some imaginative examples. Consider few different situations of 3 different ants living on 3 different surfaces: - 1) A plane surface; 2) A sphere; 3) A plane surface where temperatures are different at different places. All these ants are able to walk on the surface, draw lines, make rulers and measure lengths but they have no idea of the outside three dimensional space. The first situation is to draw a straight line on each of their residing surfaces. The first ant living on the flat surface is able to do that perfectly. The second ant living on the sphere draws the straight line as the shortest distance between 2 points; he has no way of knowing that what he has actually drawn is an arc between 2 points. This happens as the sphere has a curvature and for a proper line to be drawn the ant needs to go through the sphere. When the third ant tries to draw a straight line on his surface with a

ruler, the ruler gets elongated when it comes in contact with the warmer parts of the surface. So the straight line on the third surface curves out towards the warmer regions and ultimately to people outside the ant's world it looks like an arc. [Figure 2.5]

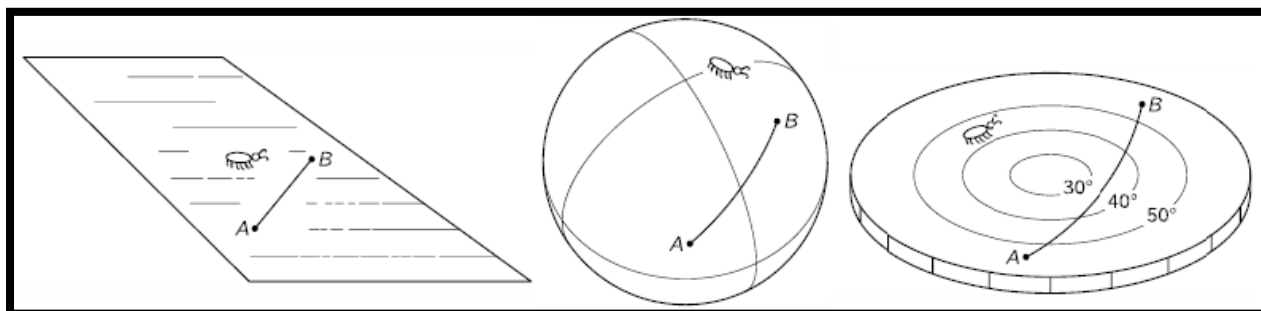


Figure 2.5: Ants on plane surface, sphere and a hot plate.

The second situation happens when each of these ants try to make a square and a triangle on their surfaces. The first ant notices that if he draws a straight line of say 10 cm long starting at point A, then makes a right angle, and repeats this 3 times more he is able to reach at his starting point A. Then he also discovers that if tries to draw a triangle on his surface the sum of the angles is equal to 2π . [Figure 2.6]

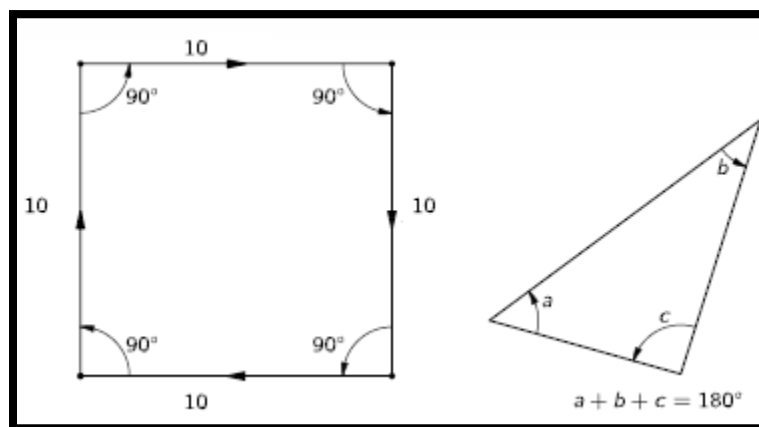


Figure 2.6: A perfect square and a triangle on a flat surface

The second ant on the sphere tries to make a square but his ending point B is different from that of his starting point A. Similarly when he tries to draw a triangle, the sum of the angles of the triangle is not equal to 2π . Rather for him the sum of angles is always greater than 2π . Same situation arises for the ant on the surface of varying temperatures. He too cannot

meet his starting point when he draws a square and he can't ever draw a triangle whose angles' sum is 2π .

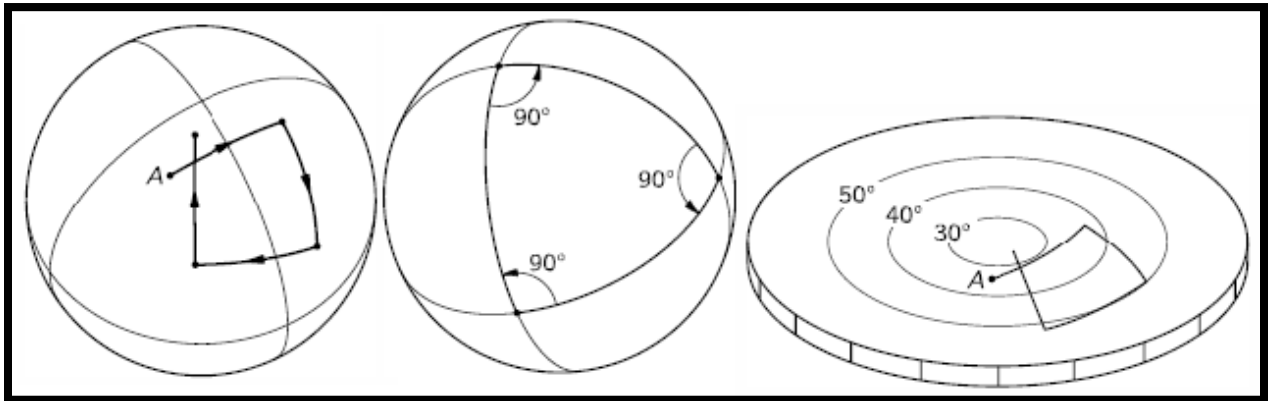


Figure 2.7: Square, triangle on a circle; Square on a hot plate.

So a curved surface can be defined as a surface where the laws of Euclidean geometry (valid for a plane surface) fail. The curvature of the sphere and the hot plate that were described previously are all intrinsic curvatures. That is they are curvatures which only depend upon measurements taken in a local region [*Six Not So Easy Pieces*]. Sphere and the hot plate (where the temperature increases with distance from the center) all have positive intrinsic curvatures. Similarly there are other surfaces which also have negative intrinsic curvature. Examples are the saddle on a horse, or a hot plate where the temperature decreases with distance from center.

Any thermodynamic or mechanical system can be described in terms of a pair of work conjugate variables. For example in thermodynamics the internal energy of the system can be described by temperature and entropy, or pressure and volume. For a mechanical system, a small increment of energy may be expressed in terms of similar work conjugate pairs: a force times a small displacement. Let us consider a system being defined by work conjugate pair of variables \mathbf{U} and \mathbf{V} . A closed loop cycle in such a system is closed in all variables, implying a return to the original state upon completion of the cycle. In other words, if the system is at an initial state of $\mathbf{U} = \mathbf{0}$ and $\mathbf{V} = \mathbf{0}$, and it undergoes a complete cycle, it will return to the final state of $\mathbf{U} = \mathbf{0}$ and $\mathbf{V} = \mathbf{0}$, which is the same as the initial state. When the solution-space (in which the cycle is executed) is curved, then the complete cycle would not be closed in all variables. This means that if after the cycle, $\mathbf{U} = \mathbf{0}$ then \mathbf{V} necessarily would not return to 0 and vice versa.

2.7 Concept of Path Dependency: Plasticity in crystalline materials

Let us establish the physical background for understanding plastic deformations of metals and from there understand the relation between curvature, dislocation and path dependency. Plasticity describes irreversible and path dependent behaviors of ductile materials. Commonly, plasticity is volume conserving (plasticity in soils being an exception) and causes only shape change or distortion in the body. As a body is loaded from its stress free state, it first undergoes elastic or reversible deformation. During this phase, the strain at a point returns to zero if the stress returns to zero, and vice versa. In other words, closed thermodynamic cycles do not dissipate any work.

However, as the stress exceeds a critical threshold, commonly called the yield stress, the behavior of the body becomes path dependent, and closed thermodynamic cycles dissipate work. The work conjugate pair, stress and strain, does not return to zero simultaneously when their excursion amplitude exceeds this critical value. Since, plastic deformation is primarily a distortion; a direct test of plasticity of the material could thus be done by producing a state of simple shearing deformation in a specimen through the application of forces that result in a state of shear stress.

Plasticity theory was primarily developed in order to describe the behavior of ductile metals. Metals in their usual form are polycrystalline aggregates, which are composed of large number of grains, each of which has the structure of a simple crystal. In crystalline materials, plastic flow is related directly to the presence of dislocations and their response to the applied stresses. For instance, relatively lower stresses are required to cause plastic flow in crystals having dislocations, in comparison to the much higher stresses necessary to initiate plastic flow in a perfect crystal, i.e. without dislocations or defects. A crystal is a three dimensional array of atoms forming a regular lattice, it may be regarded as a molecule of indefinite extent. The atoms vibrate about fixed points in the lattice but by and large do not move away from the fixed points being held by the forces exerted by neighboring atoms. The forces may be ionic, covalent or metallic bonding.

Experiments show that plastic deformation is the result of relative motion, or slip on specific crystallographic planes in response to shear stress along these planes. It is found that the slip planes are most often those that are parallel to the planes of closest packing, a simple explanation for this is that the separation between such planes is the greatest and therefore slip between them is the easiest. The cause for this is that the resistance to slip as a result of interatomic forces decreases rapidly with interatomic distance. Within each slip

plane there are preferred slip directions which are those of the atomic rows with greatest density. A slip plane and a slip direction together are said to form a slip system. [Lubliner 1990]

While in slip, atoms in plane slide tangentially from one equilibrium position over to another. The stress needed to displace the atom from equilibrium is the derivative of the bond energy function, the bond energy function being zero at the equilibrium position. The bond energy function is an-anharmonic curve resulting from the balance of attractive and repulsive atomic forces among the atoms. The stress reaches a maximum at approximately quarter of the distance between the two equilibrium positions, dropping to zero at the metastable position midway between them. After that, the stress changes sign, meaning that force is required to hold the atom back (as opposed to application of a force to take the atom away) as it tries to fall toward the new equilibrium position [Roylance 2001] [Figure 2.8b]. Let us understand the stress versus displacement and energy versus displacement curve with the help of Figure 2.8a.

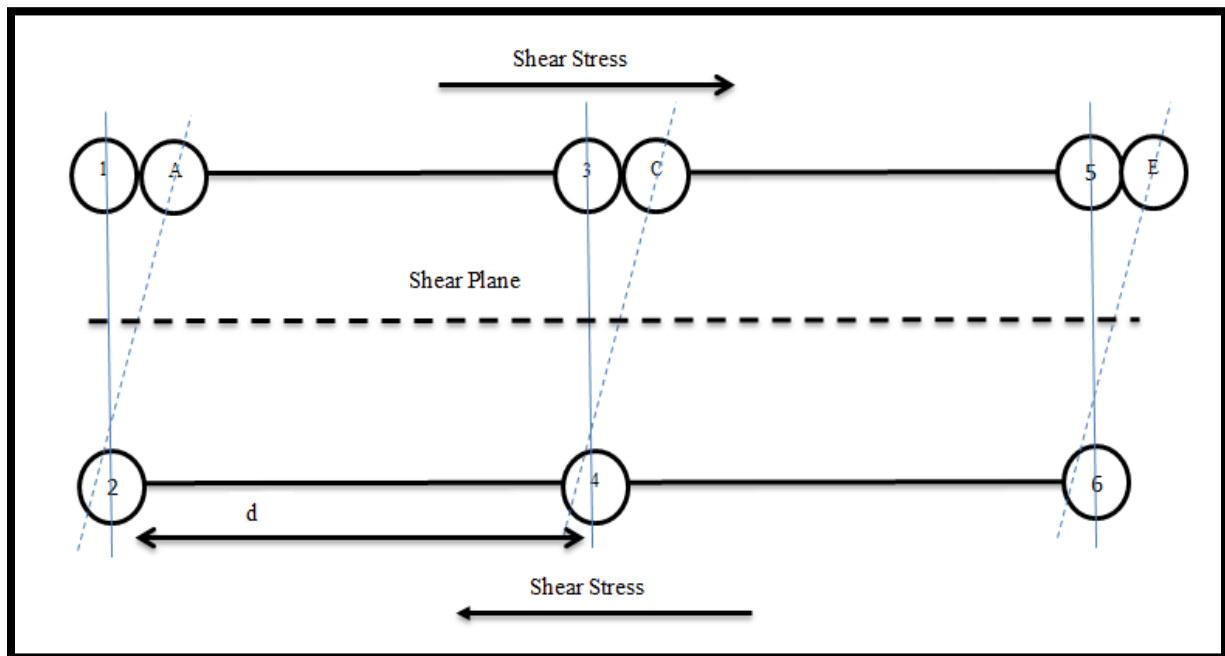


Figure 2.8a: Slip Process in a Perfect Crystal

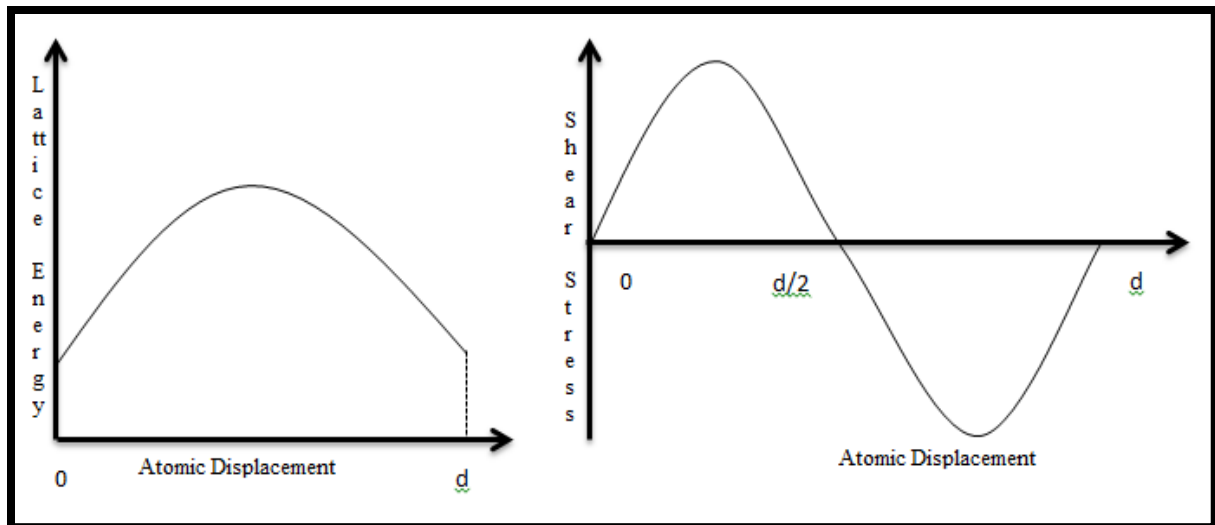


Figure 2.8b: Variation of Shear Stress and Lattice/Potential Energy with Atomic Displacement

Application of a shear stress on a plane within a crystal causes displacement of atoms from their original positions within the crystal lattice. If the atomic displacement is small the strain is elastic, or upon removal of the stress the atom moves back to its original position. If however, the displacement is large enough to take atom 1 to a position midway between atom 2 and 4, atom 1 will become in a state of metastable equilibrium with respect to the two atoms and it has equal chance of taking up a position above atom 4 or above its original neighbor atom 2 [Figure 2.9a]. At the midway point at a distance of $d/2$, the stress required to displace the atom is zero as the atom can go in either direction. This point is unstable and a displacement in either direction will decrease the potential energy. If however under the influence of the stress, atom 1 goes any closer to the position above atom 4, it will move toward the position above atom 4. The symmetry of the lattice will be restored even if atom 1 is above atom 4 but atoms on either side of the shear plane will have nearest neighbors different from their original ones. The crystal is then said to have slipped or undergone plastic deformation. This also means it is no longer in the elastic or reversible regime of deformation.

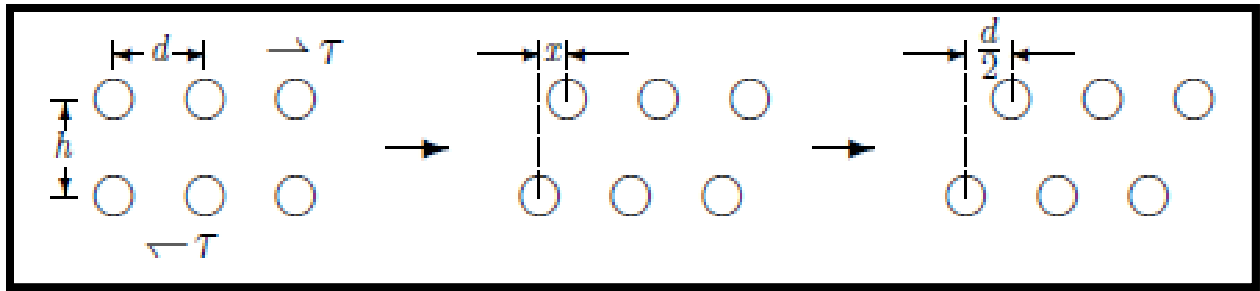


Figure 2.9: Slip between two neighboring rows of atoms

A value of the shear stress necessary to produce slip may be calculated theoretically by assuming that slip takes place by the uniform displacement of adjacent atomic planes. Let us consider two neighboring rows of atoms; the distance between the centers of adjacent atoms in each row being d and the height between the centers lines of the two rows being h . [Figure 2.8]. Let us suppose the two rows are in equilibrium configuration under zero stress. If one row is displaced by a distance d relative to the other, a new configuration is achieved that is not different from the first one. A displacement of $d/2$ on the other hand would lead to an unstable equilibrium configuration at zero stress. When halfway between the two equilibrium positions, the atom has equal probability of going to either of the two positions. Hence the halfway position is a metastable position. When the atom is just quarter of a distance away from one of the positions it has highest chance of going to the position it is closest to. So the critical length scale between 2 equilibrium positions is $d/2$. When the atoms in the upper row slide over those in the lower one, intrinsically strong interatomic forces must be overcome by the applied stress. The crystal energy varies with the relative atomic displacement across the slip plane as shown in Figure 2.8b. When the atoms in the upper plane have been displaced by one-half of their interatomic distance, $d/2$, the crystal energy corresponds to a maximum as going in either direction will only decrease this energy. [Pareja 2008] The force or shear stress required to produce the displacement will be proportional to $\frac{du}{dx}$, where U is the lattice energy. Suppose the lattice energy variation with atomic displacement is given by the equation:

$$U(x) = A - B \cos \frac{2\pi x}{d} \quad (10)$$

The shear stress needed for a relative atomic displacement of x to occur can be given by

$$\frac{du}{dx} = \tau = \tau_{max} \sin \frac{2\pi x}{d} \quad (11)$$

When the displacement x is small, and stress and strain are small then Hooke's law in shear given by $\tau = G\gamma$ is also followed which also means $G = \left(\frac{d\tau}{d\gamma}\right)_0$. Also a small atomic displacement of x between atomic rows which are separated by a distance of h corresponds to a lattice shear of $\gamma = \frac{x}{h}$.

Differentiating equation 11 with respect to x we get

$$\frac{d\tau}{dx} = \tau_{max} \frac{2\pi}{d} \cos \frac{2\pi x}{d} \Rightarrow \left(\frac{d\tau}{dx}\right)_0 = \tau_{max} \frac{2\pi}{d} \quad (12)$$

Using $\frac{d\tau}{dx} = \frac{d\tau}{d\gamma} \frac{d\gamma}{dx}$ and a lattice shear of $\gamma = \frac{x}{h}$ we get

$$\left(\frac{d\tau}{dx}\right)_0 = \frac{1}{h} \left(\frac{d\tau}{d\gamma}\right)_0 \Rightarrow \left(\frac{d\tau}{d\gamma}\right)_0 = h \left(\frac{d\tau}{dx}\right)_0 = h \tau_{max} \frac{2\pi}{d} \quad (13)$$

$$\text{Therefore } G = \left(\frac{d\tau}{d\gamma}\right)_0 = h \tau_{max} \frac{2\pi}{d} \Rightarrow \tau_{max} = \frac{Gd}{2\pi h} \quad (14)$$

$$\text{If } h \text{ is approximately equal to } d \text{ then } \tau_{max} = \frac{G}{2\pi} \cong \frac{G}{10}. \quad (15)$$

So the theoretical shear strength is of the order $\frac{G}{10}$. Actually this has been over estimated as the function $\tau(x)$ is not symmetrical for a real crystal in the range of 0 to $\frac{d}{2}$. A more refined approach lowers the shear stress to $\frac{G}{30}$. These values are much higher than the experimental shear stress values found for single crystals of pure metals. In reality the shear strength of single crystals is less than this by 1 to 3 orders of magnitude that is in the order of $10^{-3}G$ to $10^{-5}G$.

2.8 Dislocations and Crystal Plasticity

There is an observed discrepancy between theoretical and observed shear strength as was seen above. The reason behind low experimental values for the required shear stress was proposed independently by Taylor, Polanyi and Orowan in 1934. It was realized that it is not necessary to slip entire planes of atoms past one another to deform the material plastically. This would require breaking all the bonds connecting the planes simultaneously. The stress needed to do this would be very high, on the order of $\frac{G}{10}$ as described above for the theoretical shear stress. But there is no need to move all the atoms at once; only a few

at a time need to move, requiring a much smaller stress. This discrepancy and the observation of slip bands have led to the theory that slip in ordinary crystals must take place by some mechanism other than movement of whole planes of atoms past one another. This can be attributed to lattice defects and dislocations. A mechanism based on a specific defect called a dislocation was proposed for this reason. A scenario can be imagined of atoms lying in a plane above a single line which are displaced by one atomic distance. This would force this particular plane of atoms previously there into a midway position as shown in Fig. 2.12(a), creating an additional plane of atoms halfway between the normal equilibrium positions. This is an example of a dislocation specifically line defect. [Roylance 2001]

All real crystals contain defects, that is, deviations from the ideal crystal structure. A defect concentrated about a single lattice point and involving only a few atoms is called a point defect; if it extends along a row of many atoms, it is called a line defect; and if it covers a whole plane of atoms, a planar defect.

Point defects can be purely structural, such as (a) a vacancy or (b) an interstitial atom. They can involve foreign atoms also as impurities: (c) a substitution impurity, (d) an interstitial impurity. Point defects distort the crystal lattice locally as seen from the Figure 2.10. The distortion felt for this point defect is significant over a few atomic distances but negligible farther away.

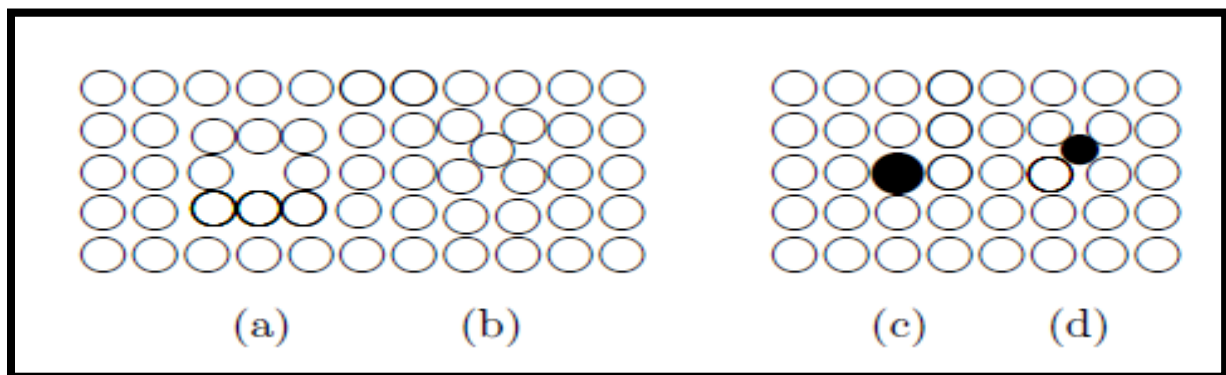


Figure 2.10: Point Defects: - (a) Vacancy (b) Interstitial atom (c) Substitution Impurity (d) Interstitial Impurity

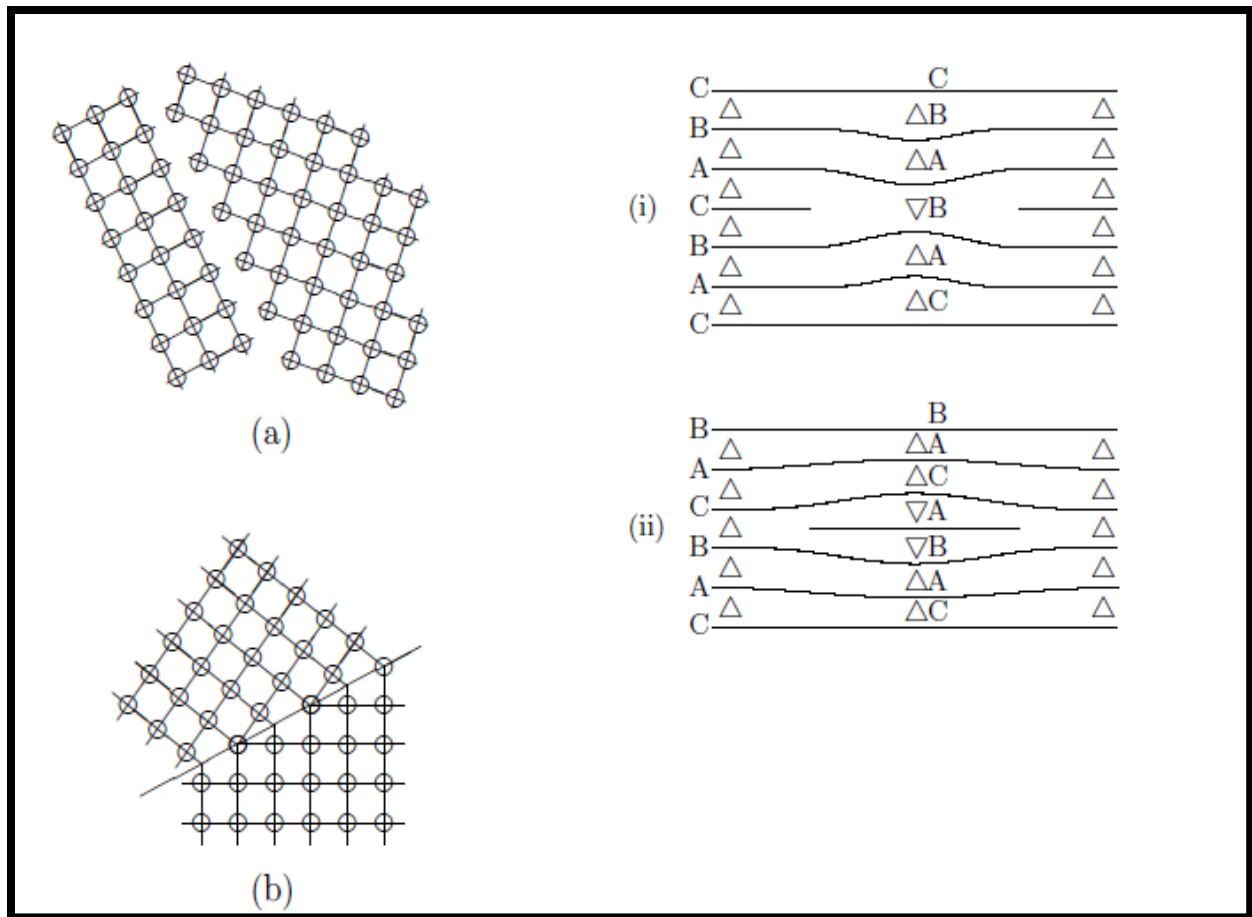


Figure 2.11: Planar defects: (a) Grain Boundary (b) Twin Boundary (i) and (ii) Stacking faults

Planar defects include (a) grain boundaries in poly-crystals and within single crystals they are manifested as (b) twin boundaries and (c) stacking faults. Planar defects are shown in Figure 2.11.

The most important line defects in crystal are dislocations. There are mainly two types of dislocations; edge and screw. An edge dislocation in a crystal can be visualized as a line. It can be imagined as if an extra half-plane of atoms has been introduced on one side of the imaginary line, as illustrated in Figure 2.12(a) for a simple cubic lattice. When the distance from the dislocation line is quite a lot number of atomic distances, the lattice is virtually undisturbed. If now a path through this “good” crystal is considered it would have been closed if the lattice were perfect. But now such a path, consisting of the same number of atom-to-atom steps in each direction and enclosing a dislocation is not closed as shown in the Figure 2.12(a). The vector \mathbf{b} needed to close it is called the Burgers vector of the

dislocation, and the path defining it is called the Burgers circuit. For an edge dislocation, the Burgers vector is necessarily perpendicular to the dislocation line. And this is the defining property of an edge dislocation. Similarly, the defining property for a screw dislocation can be defined as one whose Burgers vector is parallel to the dislocation line as shown in Figure 2.12(b).

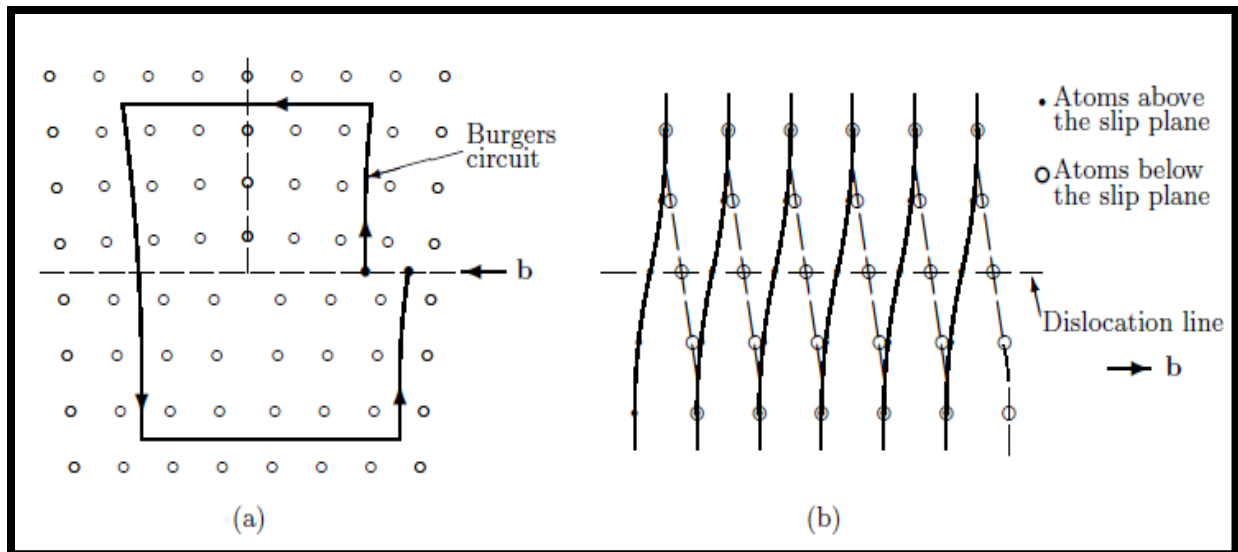


Figure 2.12: Dislocation in a Crystal (a) Edge Dislocation (b) Screw Dislocation

A dislocation in a crystal need not be a straight line. However, the Burgers vector must remain constant. Thus, a dislocation can change from edge to screw, or vice versa. It cannot, however, terminate inside the crystal. It can only terminate at the surface of a crystal or at a grain boundary. It can form a closed loop, or branch into other dislocations (at points called nodes), subject to the conservation of the Burgers vectors: the sum of the Burgers vectors of the dislocations meeting at a node must vanish if each dislocation is considered to go into the node [Frank 1951].

It can be said that plastic deformation in crystals results from the movement of dislocations. In order for an edge dislocation to move one atomic distance in the plane containing it and its Burgers vector (the slip plane), each atom need move only a small fraction of an atomic distance. Consequently, the stress required to move the dislocation is only a small fraction of the theoretical shear strength discussed previously. An approximate value of this stress is given by the Peierls–Nabarro stress given by the following equation.

$$\tau_{PN} = \frac{2G}{1-\nu} \exp \left[\frac{-2\pi h}{d(1-\nu)} \right] \quad (16)$$

h and d denote the distances between adjacent planes of atoms and between atoms in each plane, respectively. The Peierls–Nabarro stress is clearly much smaller than the theoretical shear strength. Its value depends on h/d , and the smallest value is achieved when h/d is largest, that is, for close-packed planes that are as far apart as possible. This explains why farther apart densely packed planes are the most probable to slip.

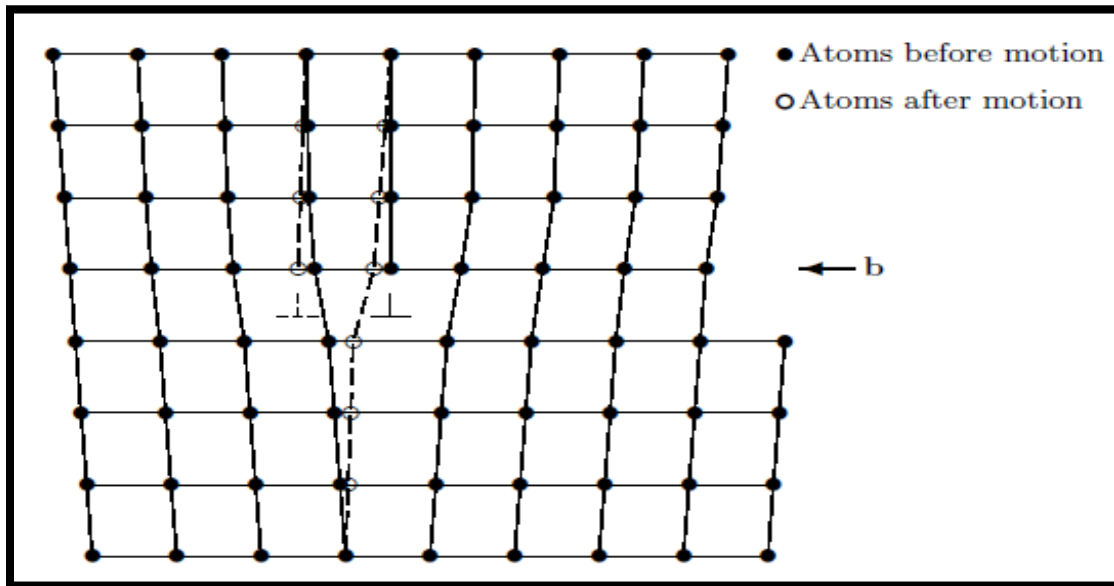


Figure 2.13: Slip by means of edge dislocation

If the stress is maintained, the dislocation will keep on moving to the next position. As the dislocation moves in its slip plane, the portion of the plane that it leaves behind can be regarded as having experienced slip of the amount of one Burgers-vector of magnitude $\mathbf{b} = |\mathbf{b}|$. When the dislocation reaches the crystal boundary, slip will have occurred on the entire slip plane. Suppose that the length of the slip plane is s , and that an edge dislocation moves a distance x in the slip plane; then it contributes a displacement $\frac{bx}{s}$. In case of n dislocations, moving an average distance \bar{x} produce a displacement $\mathbf{u} = \frac{nb\bar{x}}{s}$.

If the average spacing between slip planes is l , then the plastic shear strain is $\mathbf{y}^p = \frac{\mathbf{u}}{l} = \frac{nb\bar{x}}{ls}$. However $\frac{n}{ls}$ is just the average number of dislocation lines per unit perpendicular area or, equivalently, the total length of dislocation lines of the given family per unit crystal volume — a quantity known as the density of dislocations, usually denoted by ρ . Since only

the mobile dislocations contribute to plastic strain, it is their density, denoted by ρ_m that appears in the equation for plastic strain. The final equation is given by $y^p = \rho_m b \bar{x}$. [Lubliner 1990]

2.9 Curvature Induced Path Dependency

Referring to Figure 2.7 it is observed that the ant which started moving from point A on the sphere never returned to point A or to its original state after it underwent a complete cycle. It returned to some other point A' which means it actually returned to another state. Similar kind of phenomenon was shown in Figure 2.12 and 2.13. In crystals this phenomenon can be attributed to lattice defects or more specifically dislocations. In thermodynamics, this phenomenon can be seen as an irreversible change; the difference between A and A' representing the change. A phenomenon or process that is not reversible is called irreversible.

If **(End State) – (Start State) > Critical Value** we conjecture that the solution space will exhibit formation of a dislocation. We hypothesize that formation of such dislocation (or dislocation cluster) is the root cause of path dependency exhibited by a system. Thus, excessive curvature of solution space may nucleate a dislocation, and induce path dependency or irreversibility in a solution space or a mathematical manifold.

The occurrence of curvature and dislocations is related very closely. When a system (be it mathematical or mechanical) is curved it will not behave like a closed loop system, which means there will be a difference in its initial and final state as explained above. If the difference between the initial and final state exceeds a certain critical curvature say K^* then the system will nucleate a formation of dislocation. Once dislocation starts the system will never return to its initial state after undergoing a full process or cycle. Hence a system having dislocation will exhibit path dependency. In a crystalline or metallic system the formation of dislocations can be brought out by the shear stresses that were calculated in previous sections. For example if one atom in a crystalline system is at a distance greater than $d/2$ from its equilibrium position it has a high chance of never returning to its previous equilibrium position thus exhibiting a dislocation in a crystalline system. In a mathematical system, curvature can occur if pair wise relation between two entities A and B is altered by introduction of a third entity C when C enters and demands a share of the resource that is supposed to be conserved. This introduction of C curves the solution space. And on this kind of system a dislocation is nucleated if the curvature exceeds a critical value or the final

state is so much different than the initial state that the difference exceeds a critical curvature dictated by the geometric length scale at that point.

CHAPTER 3. LENGTH SCALE DERIVATION

Let us consider an observable body or a phenomenon. A finite number of observation points are inserted into such a system. At each point, information is collected at multiple dimensions, and at discrete instants of time for the entire duration of the experiment. Let us also consider two points **A** and **B**. At both of these points there are many dimensions where each dimension is denoted by i . The value recorded at these two points in some particular dimension $i = d$ can be denoted as u_d^A and u_d^B . For the present analysis, after all values are recorded at every observation point, a normalized relationship is developed between each pair of points in each dimension. Such a normalized relationship between two points **A** and **B** is given by $\alpha_d^{AB} = \frac{u_d^A - u_d^B}{u_d^A + u_d^B + 2\bar{m}}$, where \bar{m} is an arbitrary small constant that is determined later.

In order to develop a model describing such a phenomenon, it is first assumed that the system under observation is conservative. As a first attempt, it is also assumed that a piecewise second order potential is sufficient to describe the interactions in the system. Thus, the general potential function is assumed to be quadratic in the neighborhood of each observation points. However, the nature of the quadratic potential function (coefficients of the second order polynomial) can vary from one point to the other. The approximations and intrinsic uncertainty introduced in the model predictions due to this approximation will be examined later.

Next, it is attempted to satisfy the three canonical requirements of: (1) compatibility, (2) equilibrium and (3) constitutive relation. It is further acknowledged that objectivity or frame invariance is a requirement for describing the behavior of such a system. Objectivity implies that the state of the observed system remains invariant with respect to variations in the observation procedure. In the present development, compatibility is enforced indirectly by requiring that the system be objective at every observable scale at each location [Chandra and Roy 2012]. Such an indirect approach satisfies compatibility as well as objectivity simultaneously. Using such an approach [Chandra and Roy 2012], the conservation of linear momentum in the neighborhood of point A may be described as,

$$R_i^A - \beta_{ik}^A * \Delta H_k^A = 0 \quad (17)$$

Here R_i^A is the rank at point **A** in dimension i [Chandra and Roy 2012]. Such a rank satisfies both compatibility (and objectivity) as well as equilibrium at **A**. H_k^A represents the

Borda Count [Saari 1999, 2000, and 2001 a, b]. The parameter β_{ik}^A may be described as $\beta_{ik}^A = \frac{1}{(\Delta t)^2} * \frac{\rho}{E_{ijkl}} * \|L_i L_j\|$. The parameter β_{ik}^A is a non-dimensional quantity and essentially represents the square of a length-scale around the point **A**, in which the linearized equation (17) is valid. The length-scale essentially denotes a region around the observation point, in which the piecewise quadratic assumption for the potential function is valid. So replacing β_{ik}^A in the equation above the following equation of length scale (L_l) can be obtained.

$$R_i^A - \frac{1}{(\Delta t)^2} * \frac{\rho}{E_{ijkl}} * L_l L_j * \Delta H_k^A = 0 \quad (18)$$

$$\Rightarrow R_i^A = \frac{1}{(\Delta t)^2} * \frac{\rho}{E_{ijkl}} * L_l L_j * \Delta H_k^A \quad (19)$$

$$\Rightarrow E_{ijkl} \left[\frac{R_i}{L_l L_j} \right] = \frac{\rho}{(\Delta t)^2} * \Delta H_k \quad (20)$$

Out of all the possible transformation laws, the ones that are permissible in the above equation are the ones that conserve angular momentum and the symmetry of potential function. Now the conservation of angular momentum requires that (**i and j**) be interchangeable. Similarly, the interchangeability of (**k and l**) is mandated by the symmetry requirements on the definition of strain. The requirement of work conjugate requires symmetry in potential function and this enforces interchangeability between (**i ; j**) pair and (**k ; l**) pair. After all such transformations, the following equation can be derived:-

$$\frac{E_{ijkl}}{2} * \left[\frac{R_i}{L_l L_j} + \frac{R_j}{L_k L_i} + \frac{R_k}{L_j L_l} + \frac{R_l}{L_i L_k} \right] = \frac{\rho}{(\Delta t)^2} * [\Delta H_i + \Delta H_j + \Delta H_k + \Delta H_l] \quad (21)$$

A constant $m_i^{A,B}$ is evaluated for each observation pair by assuming an order of the interaction potential between the pair under consideration. As a first attempt, only piecewise quadratic potential function is used in the present work. Next, the constant $m_i^{A,B}$ is evaluated by setting the spatial gradient of the observed variable at observation point A ($u_{i,j}^A$) to be exactly the same as the spatial gradient of the normalized variable ($\alpha_{i,j}^A$). Finally, the constant \bar{m} is evaluated from a least square fit of all the $m_i^{A,B}$ values. The constant \bar{m} essentially sets the datum and the coordinate of the origin is set at $-\bar{m}$ in the respective dimension. [Chandra 2012] Since only a least square approximation is used for evaluating \bar{m} , and it is used universally at all points (to set same datum for all observation points), the gradient of the observed variable and that of the normalized variable are not

exactly the same at all points. This introduces an approximation in our formulation. The error introduced due to this approximation is measured in the present work.

CHAPTER 4. ALGORITHMS

The algorithms needed for the prediction, verification and the different applications are explained below.

4.1 LBar and LBarTilda Calculation

This calculation follows a generic approach. This approach is followed so that the algorithm can be applied for any system where the actual Poisson's ratio of the system is not known. For example, an economics system is not a mechanical or a materialistic system and hence the Poisson Ratio of an economics system cannot be known beforehand. It is already known that Poisson's Ratio for pure volumetric deformation or dilatation (ν_v) = -1 and Poisson's Ratio for only shape change (at constant volume) or pure Shear (ν_s) = 0.5. Using these two prior known values we calculate the proportion of volumetric deformation and shear deformation happening.

4.1a Algorithm

1. Two frames consecutive in time are considered. It is assumed that the value of $LBar(\bar{L})$ and $LBarTilda(\tilde{L})$ does not change for points in the 2 frames in such a short time interval. So 1 common value of $LBar(\bar{L})$ and $LBarTilda(\tilde{L})$ is calculated for all points in the 2 frames.
2. The long term (or projected rank upon satisfying both equilibrium and compatibility) $rank(\mathbf{R})$ values for all features/dimensions for the 2nd frame are obtained.
3. The difference between short term (satisfying equilibrium only) $rank(\mathbf{H})$ values of the 2 frames is calculated.
4. Using the above 2 values of \mathbf{R} and \mathbf{H} for a specific dimension and at each data point, 2 sets of simultaneous equations are solved.
 - a) Considering volumetric deformation ($\nu_v = -.99$), values for **1/LBarVolume** ($1/\bar{L}_v$) are obtained.
 - b) Considering deformation due to pure shear ($\nu_s = .5$), values for **1/LBarShear** ($1/\bar{L}_s$) are obtained.
5. The number of equations in each set at each data point for a particular dimension is equal to the number of dimensions. The number of solutions obtained at each data point for a specific dimension is $2^{dimSize}$.

6. Solving the 2 sets of simultaneous equations gives us the reciprocal values. So reciprocal of the values is taken to obtain the actual \bar{L}_V and \bar{L}_S .
7. Since the number of solutions is $2^{dimSize}$ 8 and 16 values of \bar{L} are obtained when number of total dimensions are 3 and 4 respectively. The number of solutions is called to be the number of roots of \bar{L} .

4.1b Nature of the Roots

At each point there are a number of dimensions. So totally for one point there are $2^{dimSize} * dimSize$ number of roots as for 1 specific dimension there are $2^{dimSize}$ number of roots. $2^{dimSize}$ number of roots of 1 dimension corresponds to $2^{dimSize}$ number of roots of any other dimension in 1:1 manner. This means the 1st root of \bar{L} of the 1st dimension is related to the 1st root of \bar{L} of the 2nd dimension and so on. This is a valid assumption as Matlab will always solve simultaneous equations at the same time giving the roots in order of their correspondence. Also it has been noticed that in perfect correlation between the roots the value of any one of the simultaneous equation is $4.68 \times 10^{-71} - 4.16 \times 10^{-72} \times i$ which is almost equal to 0 whereas when the roots are tried to be combined randomly (not 1:1) in the equation the value is $0.006 \times i - 0.004$ which is of the order of 10^{-3} .

4.2 Curvature/Kappa Calculation

This calculation also follows a generic approach. This approach is followed for the same reason as before so that the algorithm can be applied for any system where the actual Poisson's ratio of the system is not known. For example, an economics system is not a mechanical or a materialistic system and hence the Poisson Ratio of an economics system cannot be known beforehand.

4.2a Range of proportionality variable (alpha)

If κ_v is the volumetric curvature and κ_s is the shear curvature then the total or composite curvature (κ) at a given location/point and dimension is given by:

$$\kappa = \alpha \kappa_v + (1 - \alpha) \kappa_s \quad (22)$$

Here α is the proportion by which volumetric curvature takes place. Shear stress is the component of stress coplanar with the material cross section. Shear stress arises from a force vector perpendicular to the surface normal vector of the cross section. Hence shear changes the shape of the object and not the volume. Volume is altered by dilatational deformation (as shown in the figure below).

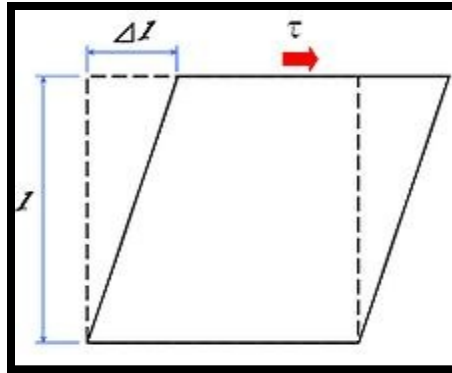


Fig 4.1: A shear stress τ is applied to the top of the square while the bottom is held in place. This stress results in a strain, or deformation, changing the square into a parallelogram

In Solid Mechanics the composite stress is given by:

$$\sigma_{ij} = \lambda \epsilon' \delta_{ij} + 2G(\epsilon_{ij} - \frac{1}{3}\epsilon' \delta_{ij}) \quad (23)$$

Where λ = bulk modulus, G = shear modulus & $\epsilon' = \epsilon_{11} + \epsilon_{22} + \epsilon_{33}$ (volumetric strain for 3 dimensions). Also shear modulus, $G = \frac{E}{2(1+\nu)}$ and bulk modulus $\lambda = \frac{\nu E}{(1+\nu)(1-2\nu)}$.

Comparing the stress equation (23) and curvature equation (22) with each other we find similarity between the two equations. So we can write $\frac{\alpha}{1-\alpha} = \frac{\lambda}{2G} = \frac{\nu}{(1-2\nu)}$. The range of Poisson's Ratio (ν) is $-1 < \nu < 0.5$. When $\nu = -1$ then $\alpha = -\frac{1}{2}$ and when $\nu = 0.5$ then $1 - 2\nu = 0$ which implies $1 - \alpha = 0$, that gives $\alpha = 1$. Hence the range of α should be between $-\frac{1}{2}$ and 1.

4.2b Algorithm

1. **LBarVolume**($\overline{L_V}$) and **LBarShear**($\overline{L_S}$) for all data points and for all features/dimensions are calculated using the algorithm described above for calculating LBar. Let LBarMatrixVolume and LBarMatrixShear be the 2 matrices that contain the results.
2. As explained in the previous algorithm during the calculation of **LBarMatrixVolume** and **LBarMatrixShear**, $2^{\text{featureSize}}$ numbers of roots are calculated for a specific feature and at each point.

3. The reciprocal of **LBarMatrixVolume** is taken and let **LBarMatrixReciprocalVolume** contain these results.
4. The sum of all values of all points of **LBarMatrixReciprocalVolume** for a particular feature and for a specific root is taken. Then the sum is divided by the number of points (sampleSize) to get the average. Let **averageLBarVolumeVectorReciprocal** contain the average results.
5. All the data points in **LBarMatrixReciprocalVolume** are considered and a relation between each pair of point is created. For example if there are 2 points A and B and the value of **LBarReciprocalVolume** ($\frac{1}{L_v}$) at point **A** and point **B** are $\frac{1}{L_v^A}$ and $\frac{1}{L_v^B}$ respectively the relation between **A** and **B** is given by $\frac{\frac{1}{L_v^A} - \frac{1}{L_v^B}}{\frac{1}{L_v^A} + \frac{1}{L_v^B}}$. Like this relations between every pair of points for all features and all roots are created.
6. The matrix of all these relations is homogenized following the algorithm described previously.
7. Each point has relation with every other point. Since there are **sampleSize** number of points there are **sampleSize** number of relations for each point. The relations are all added up for each point for a specific feature and a specific root and then divided by **sampleSize** to get the rank of all the relations for a particular point. Let **rVolFromLBarVol** represent the rank for all points.
8. The 2 averages **averageLBarVolumeVectorReciprocal** and **rVolFromLBarVol** are added for each point and a specific feature and a specific root and **LBarReciprocalTildaVolume** is obtained for that point. Likewise **LBarReciprocalTildaVolume** is calculated for all points.
9. The reciprocal of the values obtained in the previous step is taken and the results are stored inside **LBarTildaVolume**(\widetilde{L}_v).
10. **KappaMatrixVolume**(κ_v) is calculated as $\frac{(R*\widetilde{L}_v - H*\widetilde{L}_v)}{((\widetilde{L}_v^2)*\widetilde{L}_v)*(1+(H/\widetilde{L}_v)^2)^{1.5}}$ for each point, specific feature and a specific root and applied to all points.
11. Steps 3 to 10 are repeated in the same way to calculate **KappaMatrixShear**(κ_s)
12. Equation (22) is solved to find out **alpha**(α) assuming that composite **Kappa**(κ) is minimized to 0.

13. To use a constant ***alpha***(α) absolute values of alpha are taken, the absolute values are squared and then the mean of all the values across all the dimensions are taken. Then the positive square root of the mean is taken to be the least square alpha value that all features of a single point will use.
14. Finally the composite ***Kappa***(κ) is calculated using equation (22) and using the least square ***alpha***(α) value. The Kappa values for all points and all features are stored in the matrix called ***FinalKappaMatrix***.
15. Moreover a composite value for ***LBar*** and ***LBarTilda*** are also calculated in the same manner following equation (22) and using the least square ***alpha***(α) value. These values are stored in ***FinalLBarMatrix*** and ***FinalLBarTildaMatrix***.

4.3 Post Kappa Processing: Categorizing Points and Assigning PDI

There are eight categories that are assigned to the points after their Kappa is calculated. The categories specify the amount of instability that has occurred in each of the points. Assignment of the seven categories will be explained in this section. The 8th last category is assigned after further processing which will be explained in the next section. This section explains only the assignment of the first seven categories. Each of these categories can be defined to be the ***Path Dependent Index (PDI)*** as it measures the amount or severity of the instability.

4.3a Algorithm

1. ***FinalLBarMatrix*** and ***FinalLBarTildaMatrix*** were obtained by the previous algorithm. Two more matrices called ***KappaStarShortAllFeatures*** and ***KappaStarLongAllFeatures*** are created by taking reciprocal ***FinalLBarMatrix*** and ***FinalLBarTildaMatrix*** respectively. For convenience let us call the values of the 2 matrices to be ***KappaShort*** and ***KappaLong*** respectively.
2. For each point, each feature and each root the following steps are done to categorize each point into a specific category that represents the amount of instability that point contains.
3. If the value of $\frac{abs(Kappa)}{abs(KappaLong)} < 1$ and $\frac{abs(Kappa)}{abs(KappaShort)} < 1$ then the point is said to be fully stable and a category of 1 is assigned to that point.

4. Else if the value of $\frac{abs(Kappa)}{abs(KappaLong)} > 1$ and $\frac{abs(Kappa)}{abs(KappaShort)} > 1$ then the point is unstable. It remains to be seen how much instability this point now has.
- (i) If $abs(KappaLong) > abs(KappaShort)$ then $ModKappa = abs(KappaLong)$ or else $ModKappa = abs(KappaShort)$
 - (ii) Another equation of the form $\kappa = \alpha\kappa_v + (1 - \alpha)\kappa_s - ModKappa$ is solved to obtain α value. Here also it is attempted to reduce the curvature of that point even further by calculating a different value for α say α_{prime} . Till now it is only known that this point can be unstable but it might also become stable in the future as the system will always attempt to minimize curvature by adjusting the mode “mixture” between volumetric deformation and shear deformation or shape change.
 - (iii) If the system manages to find a α_{prime} that is in the valid range for **alpha** as determined in section 4.2a i.e. $-\frac{1}{2} < \alpha_{prime} < 1$ then the point is said to be conditionally stable as this point has the capability to reduce its curvature to zero. This point is assigned a category of 4.
 - (iv) Else if however **alpha** is not in valid range then this is noted as occurring in 1 dimension for that point. A vector called **countDOutOfRange** is introduced to keep track of the number of dimensions in which this happens. Another vector called **featureMatrixOutOfRange** stores information about the dimensions in which this happens.
 - (v) If at that particular point the count for the number of dimensions exceed **dimSize** – 1 then that point is assigned a category value of 7 for those particular dimensions. This means that that point is unstable across multiple dimensions and the number of dimensions is definitely greater than 2 which signify that the point is suffering from **volume defect**.
 - (vi) Else if however the count of number of dimensions at that point exceeds 1 then the point is assigned a category value of 6 for those particular dimensions. This means that there are 2 or more dimensions across which the point is unstable and hence the point is suffering from **area defect**.
 - (vii) Else if the count of number of dimensions at that point is equal to 1 then the point is assigned a category value of 5 for that single dimension. This means

that there is 1 dimension across which the point is unstable and hence the point is suffering from **line defect**.

5. Else if however the point was never unstable then after step 4 it is checked whether point is short term or long term unstable.
6. If $\frac{abs(Kappa)}{abs(KappaShort)} > 1$ then the point is said to be short term unstable and is assigned a category value of 2. This signifies that this point might become stable in the long term or in the future but from now it is unstable.
7. If $\frac{abs(Kappa)}{abs(KappaLong)} > 1$ then the point is said to be short term stable and is assigned a category value of 3. This signifies that this point might become unstable in the long term or in the future but from now it is stable.

Thus except the category value of 1 , 2 and 3 all the other categories represent some form of full instability. There is another category value 8 that is done after this to get an idea of the length of the defect that has been produced at each point. Assignment of category value 8 is another full algorithm that is described below.

4.4 Chain Length Calculation

The chain length determination is done at every point for each dimension and each root. This is done to check how long does a defect continue in either directions from one point to another point in order of their ranks. In a materialistic system like the balloon burst the points are oriented geometrically with respect to each other, but in an abstract system like an economical system there is no geometry information. Hence the continuation of defects is checked along the points in order of their ranks so that the algorithm can have a generic approach. Then depending on the threshold chain length value that is obtained from Zoom Out or Critical Localization Index calculations a category of 8 is assigned to such points indicating that these can give rise to highest instability in the future.

4.4a Algorithm

1. The long term or projected rank **Rank(R)** values of all points are sorted in descending order.
2. The curvature **Kappa(κ)** values of all points are sorted in descending order.

3. The highest **Kappa** Value is taken as the reference point say P. The procedure starts with the point which has the highest curvature.
4. The **PDI Category** value of the reference point P is checked that had been assigned in the previous algorithm.
5. If **PDI Category** value is greater than 5 following steps are done :-
 - (i) The position in the descending **Rank Array** where this reference point P occurs is found out.
 - (ii) The Rank Array is traversed in both directions from the above position as long as the upper Index does not reach the full sample size (total number of points in the sample) and the lower index does not hit 0. 2 points above and below the reference point/chain are considered in this manner.
 - (iii) For simplicity (and for initially starting the procedure) these 2 points are considered, one above the reference point P say U and the other below the reference point P say D.
 - (iv) It is checked whether the absolute Kappa Value of the reference point is greater than the absolute Kappa Values of both points U and point D. If it is greater than both, then following steps are done.
 - Find out the minimum of combination of Kappa Values. Combination is done by $\pm Kappa(P) \pm Kappa(U) \pm Kappa(D)$ and this value is called **KappaMix**.
 - Find out the addition of L and LTilda absolute Values and call these **LMix** and **LTildaMix**.
 - If $KappaMix > 1/LTildaMix$ then these 2 points (U and D) along with the reference point will form a chain. So the points U and D are also considered to be a part of the chain.
 - The plotted PDI category values corresponding to these points (U and D) can be changed to 5 and the Chain Length of all these points (P, U, D) is incremented by 2.
 - The Upper Index is incremented by 1 and the Lower index is decremented by 1 for continuing along the chain.
 - (v) Else it is checked whether the absolute Kappa Value of the reference point is greater than the absolute Kappa Values of point U. If is greater than U then the following steps are done :-

- Find out the minimum of combination of Kappa Values. Combination is done by $Kappa(R) \pm Kappa(U)$ and this values is called as KappaMix.
 - Find out the addition of L and LTilda absolute Values and call these LMix and LTildaMix.
 - If $KappaMix > 1/LTildaMix$ then this 1 point (U) along with the reference point will form a chain.
 - The plot value corresponding to these points (U) can be given as 5 and the Chain Length of all these points (P, U) is incremented by 1.
 - Increment the Upper Index by 1 for continuing along Upper part of the Rank Array.
- (vi) Else it is checked whether the absolute Kappa Value of the reference point is greater than the absolute Kappa Values of point D. If is greater than D then the following steps are done :-
- Find out the minimum of combination of Kappa Values. Combination is done by $Kappa(R) \pm Kappa(D)$ and call this value KappaMix.
 - Find out the addition of L and LTilda absolute Values and call these LMix and LTildaMix.
 - If $KappaMix > 1/LTildaMix$ then this 1 point (D) along with the reference point will form a chain.
 - The plot value corresponding to these points (D) can be given as 5 and the Chain Length of all these points (P, D) is incremented by 1.
 - Decrement the Lower Index by 1 for continuing in the Lower part of the Rank Array.
- (vii) Continue in step (ii).
- (viii) Once all the Rank Array points are finished break from the main Loop.
6. Else go to the next highest Kappa Value Point and continue from step (4).

4.5 Critical Localization Index Calculation

This algorithm is done to calculate the critical value of chain length. If the system forms a chain of length equal to this or larger than this value then the system is said to be path

dependent. After the system attains path dependency it can go towards failure depending upon certain other conditions as well.

4.5a Algorithm

1. First the sample data is extracted from the file. The sample data is quite large in this case and preferably a matrix of $3^m * 3^m$ or $4^m * 4^m$ where m is the number of aggregation levels. The algorithm is explained taking the sample data size to be an **81 x 81** matrix. Hence the numbers of levels are 4.
2. In each level, the sample data is divided into squares of size $3 * 3$ or $4 * 4$ matrix based on what initial size of matrix was chosen. For each of the small squares **Kappa, LTilda, L** is calculated for every point.
3. The **Kappa, LTilda, L** values at each point is combined with the **Kappa, LTilda, L** values at every other point. If combined kappa value of a previous point is **Kappa_{prev}** and the **Kappa** value for the next point is **Kappa_{curr}** then the combinations is done by **Kappa_{prev} ± Kappa_{curr}**. This leads to a total number of $2^{no\ of\ points-1}$ combinations for each of the small matrices.
4. Next **average, maximum and minimum** of all the combined values of **Kappa, LTilda, L** from all the small matrices is taken and stored. This unique value so obtained is called to be the **Kappa, LTilda, and L** for that level. If initially an **81 x 81** matrix was chosen then at the first level there were **729 (27 x 27)** small matrices. **Kappa, LTilda, L** s were calculated for all such matrices and combined in the above fashion and the **mean, max or min** of all such values were taken to produce a unique **Kappa, LTilda, L** value for that level. The first level had an aggregation of **3 x 3** points.
5. Next the root mean square value of each of the small matrix is calculated. In the case of **81 x 81** initial data points, there are actually **729(27 x 27)** small matrices of **3 x 3** points. So in the 2nd level the full sample data of **81 x 81** points is reduced into a matrix of **27 x 27** root mean square values. In the 3rd level the **27 x 27** matrix is further reduced into a matrix of **9 x 9** root mean square values. In the 4th level again root mean square is taken for **9(3 x 3)** small matrices and **9 x 9** matrix is reduced into a matrix of **3 x 3** root mean square values. After this this matrix can be further reduced into a single root mean square value but such a point will not have a

- curvature (**Kappa**) or any length scale (**LTilda, L**) value. Hence for a set of **81 x 81** points the number of levels are **4** as $3^4 = 81$.
6. The aggregation levels are the number of points in the smallest matrices which are getting used for **Kappa, LTilda, L** calculations. The first aggregation level is **9** since only a **3 x 3** matrix of points is getting used individually. The second aggregation level is **81** as root mean square is calculated for each **3 x 3** matrixes and then **Kappa, LTilda, L** is calculated for **3 x 3** such root mean square points. In this way the 3rd aggregation level is **729** and the 4th aggregation level is **6561**.
 7. After the root mean square value of the matrix is calculated at any level, the resultant reduced matrix actually becomes the data for the next level. And in a similar fashion as explained above **Kappa, LTilda, L** for each point is calculated, combined and **average/maximum/minimum** is taken across all combined values. This process is repeated until we are left with 1 root mean square point for which **Kappa, LTilda, L** cannot be calculated.
 8. The unique value of **Kappa, 1/LTilda, and 1/L** obtained like this is plotted against the aggregation levels. A log plot is more preferable as it is easier to visualize the nature of the plot.
 9. Next the plot is used to find the critical value of the localization index. The vertical line (parallel to X Axis) at log 9 is taken to be the line of symmetry. Taking this line as the symmetry line another line is drawn which is the mirror image to **Kappa** graph (the part of the graph between log 9 and log 81). After this the $\frac{1}{LTilda}$ line is extended to intersect the mirror of Kappa line. The X value of this intersection point is measured. And the log value of this point is converted to number of points. This number of points represents the chain length that is occurring in a total of **9** points.

4.5b Critical localization index for any number of points

The Zooms-Out plots are drawn on log 10 scales. [Figure 5.2] The different X Axis values representing aggregation levels are log 9, log 81, log 729, and log 6561. The aggregation level represents the number of points that were considered for measuring $\kappa, \frac{1}{LTilda}, \frac{1}{L}$. The vertical line (parallel to X Axis) at log 9 is taken to be the line of symmetry. The information before the aggregation level of Log 9 is not present due to the limitations in resolutions in camera. The first aggregation level should be an absolute flat surface (i.e. when there is no curvature present). So it is attempted to extrapolate the Kappa graph even before the Log 9

aggregation level which for a log graph should start well before zero(at a negative value). Hence the Log 9 is taken as the symmetry line. Another line is drawn which is the mirror image to Kappa graph (the part of the graph between log 9 and log 81). After this the $\frac{1}{LTilda}$ line is extended to intersect the mirror of Kappa line. Every mechanism (the blowing of a balloon or the Gulf Stream) has some process zone. The explanation behind extension of the $\frac{1}{LTilda}$ line to be intersected with the mirror line is that when the process reaches an X value corresponding to point A it jumps to the X value corresponding to point B. This means once localization index (or chain length) of the process reaches point A it very rapidly spreads to the localization index of point B. Hence the X value corresponding to point A is the critical localization index. The X value of this intersection point is measured. And the log value of this point is converted to number of points. This number of points represents the chain length that is occurring in a total of 9 points. If the number of unstable points forms a chain greater than the above length then the system is said to be path dependent. Since this chain length is only valid for 9 points, these needs to be converted to a value that can be applicable to a set of 100 points or even more as required by the experimental analysis.

Chain length calculations for **9** points are given as:-

$$\frac{\log_{10}^x}{\log_{10}^9} = \frac{0.68}{0.95} = 0.715 \Rightarrow x = 9^{0.715} = 4.8 \cong 5$$

Keeping the ratio constant as **0.715** the chain length can be translated to a value in 100 points as given below:-

$$\frac{\log_{10}^x}{\log_{10}^{100}} = \frac{0.68}{2} = 0.715 \Rightarrow x = 10^{2 * 0.715} = 10^{1.43} = 26.9 \cong 27$$

So the critical localization index value is **27** for a set of **100** points. Following the above procedure chain length can be translated to any number of points.

4.6 Hole Formation Calculation

This algorithm is done to locate the ring formations in the Gulf Stream system. For this algorithm geometric length scale and material length scale were both considered in the analysis.

4.6a Algorithm

1. A minimum value of **L** from the previously calculated values of \bar{L} is calculated across all points and across all dimensions considering only the first time index.

2. A matrix **LMateLGeomRatio** containing the material versus geometric ratios **MGRatio** ($\frac{L_M}{L_G}$) is initialized. For the first time instant this ratio is 1 for all points and across all dimensions. For the first time index it is assumed that the material and geometric length scale contribute evenly to the ratio. The algorithm calculates the ratio based on some conditions for the next time indices.
3. Another matrix called **LGeometric** is also initialized. For the first time instant the geometric length scale (L_G) is equal to the square root of the calculated length scale (L) as explained in section 4.1. For the first time instant it is assumed that the material length scale and geometric lengths contribute equally to the actual length scale.
4. The plot categories or path dependency index of the all points across all dimension are calculated following the procedure in section 4.3 and section 4.4. The points are now analyzed from the time indices after time instant 1.
5. If the current plot category of this point is greater than the previous plot category then **loading** is taking place. During loading the ratio $\frac{L_M}{L_G}$ remains same as the ratio during the previous time index. The **LGeometric** (L_G) at this point for the this time index is given by square root of **L/MGRatio**.
6. Else if the current plot category of the point is lesser than previous plot category then **unloading** is taking place. While in unloading there are 2 conditions that need to be checked.
 - (i) If the point was **path dependent** (i.e. if previous plot category value was 5 or above) and **unloading** was occurring then the **LGeometric** does not change while **LMaterial** changes. The value of **LMaterial** (L_M) at this point for this time index is calculated as \bar{L} . The new **MGRatio** is calculated as $\frac{L_M}{L_G}$.
 - To change the **MGRatio** of this point at this current time index, a ratio needs to be checked. This ratio is given as $\left(\frac{MGRatio-1}{MGRatio}\right)$. This ratio is calculated for current and previous time indices. If this ratio has increased from its previous value then the **MGRatio** of the point at the current time is changed to the calculated new value of **MGRatio**.
 - To change the category value of this point at this current time index another ratio needs to be checked. This ratio is given

as $abs\left(\frac{abs(MGRatio-1)}{MGRatio}\right) + abs(1 - MGRatio)$. If this ratio is greater than the minimum value of \bar{L} as calculated in step 1 then the category value of this point is changed to its previous plot category value. This essentially means that the unloading has failed and the point cannot change its category value.

- (ii) If the point was path independent (i.e. if previous plot category value was less than 5) then at this current time index the ratio $\frac{L_M}{L_G}$ remains same as the ratio during the previous time index. The **LGeometric (L_G)** at this point for this time index is given by square root of **L/MGRatio**.
7. The above process is continued for all points across all dimensions starting from time index 2. After all points have undergone categorization again, those points which are having category of 8 and 9 are noted.
 8. Since originally \bar{L} had 2^m roots where $m = \text{number of dimensions}$ such points (category 8 or category 9) can occur across 2^m roots. Out of the above points the points which have category 8 or 9 in more than $\frac{2^m}{2} - 1$ roots are noted again.
 9. For ring formations across the Gulf Streams such points must be occurring in more than 1 dimension. So next, out of the noted above points again those points are noted that have category 8 or category 9 in more than 1 dimension.
 10. Finally these points which have been triggered in more than $\frac{2^m}{2} - 1$ roots and in more than 1 dimension are said to have formed a hole or ring in the Gulf Stream.

4.7 Trend Reversal Calculation

This procedure is done to notice the changes in trend in the Economics System over a time period and across all 4 dimensions (Inflation GDP Deflator, Unemployment, GDP Per Capita, and Lending Rate). For this algorithm the long term rank (**R**) and short term rank (**H**) of all the points are considered to assign them a negative or positive path dependency index.

4.7a Algorithm

1. Firstly the Curvature (*Kappa*) of all the points for all dimensions and across all times are calculated following the algorithm described in section 4.2. This information can be also used from the *Kappa* results if previously stored.
2. Similarly all the points are categorized and assigned a path dependency index following the algorithm described in section 4.3. This information can also be used from previous results if stored.
3. Since there are $2^{dimSize}$ number of roots for *Kappa* calculation, it is required to aggregate the Path Dependency Index information for all roots of a point into a single value so that as single index can be assigned to each point.
4. In order to do so, the $2^{dimSize}$ number of categories is noted. Out of so many values the Path Dependency Index that occurs most frequently (or the maximum number of times) is taken to be the true Path Dependency Index of that point.
5. Lastly the values of Path Dependency Indices are plotted for all countries and for all years.
6. If the absolute Path Dependency Index is greater than category 5 then a trend reversal can be expected from the current trend.

CHAPTER 5. VERIFICATION OF ALGORITHM-BALLOON BURST

The verification experiment consisted of blowing a balloon and ultimately popping it. This experiment allowed us to verify the prediction algorithm developed and described above. The results from the prediction algorithm were matched with the real time when the balloon pops truly. The balloon bursting system is a conservative one. As the balloon is blown it gets bigger and thinner which decreases its color information while the length, breadth and depth information increases. The input files for this experiment were a set of XYZM files that gave the length, breadth, depth and color information of the balloon as a 3-D object. The process of data capture and system set up is explained below.

5.1 System Set Up

The 3-D balloon video is taken as a high-speed real time 3-D shape measurement technique based on a rapid phase-shifting. The system that is developed to take this video takes full advantage of the single-chip DLP (Digital Light Processing) technology for rapid switching of three coded fringe patterns. A color fringe pattern with its red, green, and blue channels coded with three different patterns is created by a personal computer. When this pattern is sent to a single-chip DLP projector, the projector projects the three color channels in sequence repeatedly and rapidly. To eliminate the effect of color, the color filters on the color wheel of the projector are removed. As a result, the projected fringe patterns are all in grayscale. A properly synchronized high-speed black-and-white (B/W) CCD camera is used to capture the images of each color channel from which 3-D information of the object surface is retrieved. A color CCD camera, which is synchronized with the projector and aligned with the B/W camera, is also used to take 2-D color pictures of the object at a frame rate of 26.7 frames/sec for texture mapping. Along with this system, a fast 3-D reconstruction algorithm and parallel processing software is also getting used. This helps us to realize high-resolution, real-time 3-D shape measurement at a frame rate of up to 40 frames/sec and a resolution of 532x500 points per frame. The XYZM files are just the XYZ points that get triangulated (one for every pixel of the 2D image) and then the BMP file is the texture which is simply the three captured images averaged together. [*Song Zhang, Peisen S. Huang , Dec 2006*]

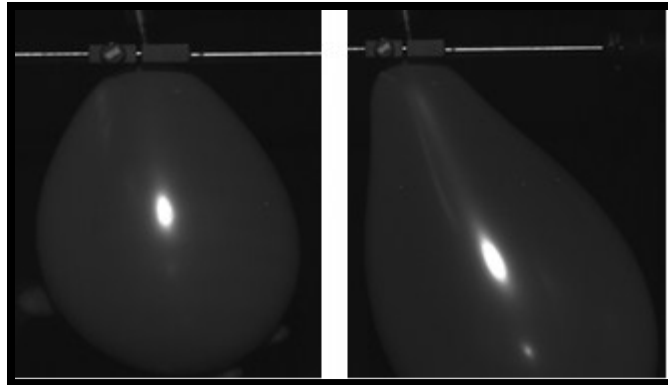


Figure 5.1: Balloon in the beginning and in the end before bursting

5.2 Verification

In the balloon burst verification primarily 3 types of analysis were done. The first one was Zoom Out procedure which was done to get critical localization index. The second and third types of analysis was done for multiple video frames at different instants of time (starting from the beginning and continuing till the end) to verify the predicted results with reality. The results would predict approximately when the balloon was approaching failure. The results would be compared with real time when the balloon had actually burst.

5.2a Critical Localization Index

The zooms out plots for the balloon analysis are given below in Figure 5.2 which shows maximum, minimum and average of absolute values of $\kappa, \frac{1}{L_{Tilda}}, \frac{1}{L}$ against aggregation level. The determination of critical chain length/localization index follows the same procedure as explained in section 4.5b. The intersection point of the symmetrical line of κ and $\frac{1}{L}$ line is taken to be the value of the localization index. The X value of this intersection point is measured. Since the zoom out plots are log scale plots, the log value of this point is converted to an actual number of points. This number of points represents the chain length that is occurring in a total of 9 points. If the number of unstable points forms a chain greater than the above length then the system is said to be path dependent. Since this chain length is only valid for 9 points, these needs to be converted to a value that can be applicable to a set of 100 points.

Chain length calculations for 9 points are given as:-

$$\frac{\log_{10}^x}{\log_{10}^9} = \frac{0.68}{0.95} = 0.715 \Rightarrow x = 9^{0.715} = 4.8 \cong 5$$

Keeping the ratio constant as 0.715 the chain length can be translated to a value in 100 points as given below:-

$$\frac{\log_{10}^x}{\log_{10}^{100}} = \frac{0.68}{2} = 0.715 \Rightarrow x = 10^2 * 0.715 = 10^{1.43} = 26.9 \cong 27$$

So the critical localization index value is 27 for a set of 100 points. Following the above procedure chain length can be translated to any number of points.

The critical localization index value of 27 is used as the threshold value for the chain length of defects for the balloon analysis.

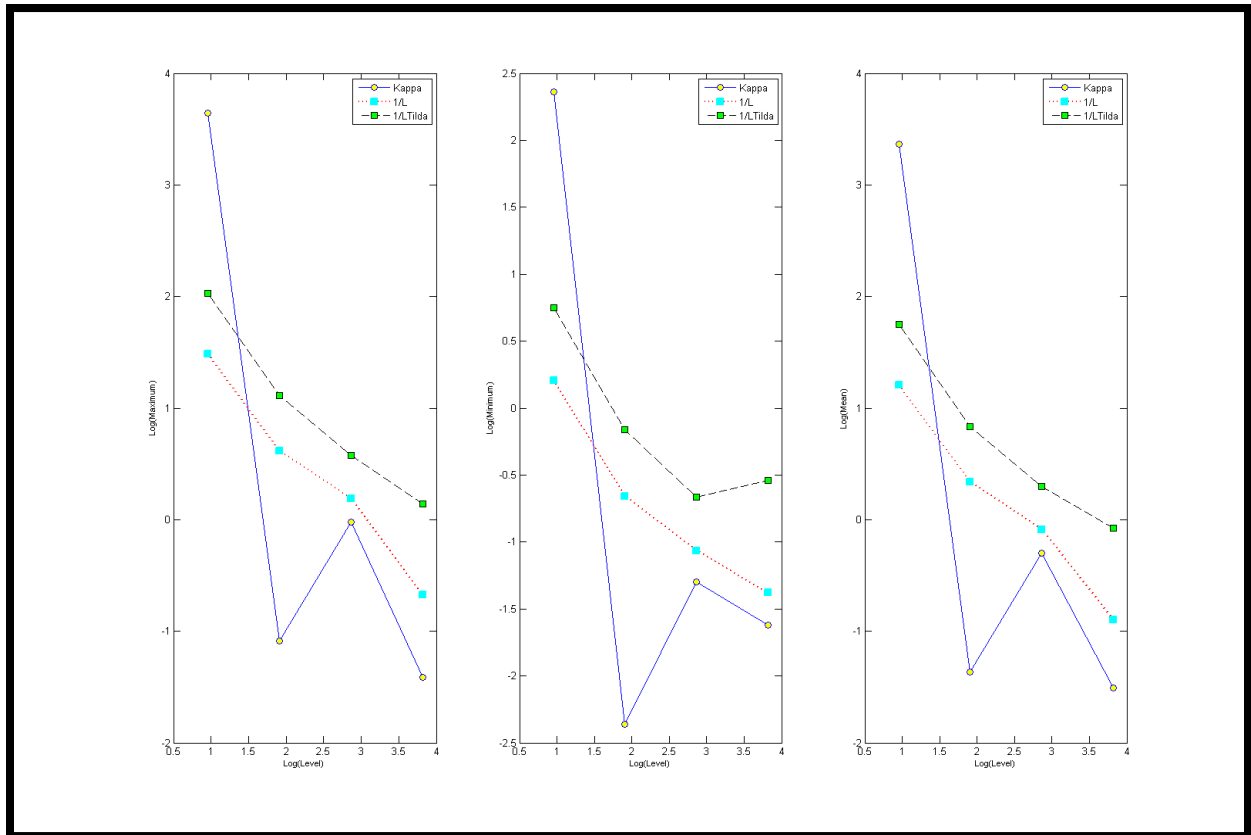


Figure 5.2: Zoom Out Plots for Balloon Burst Experiment

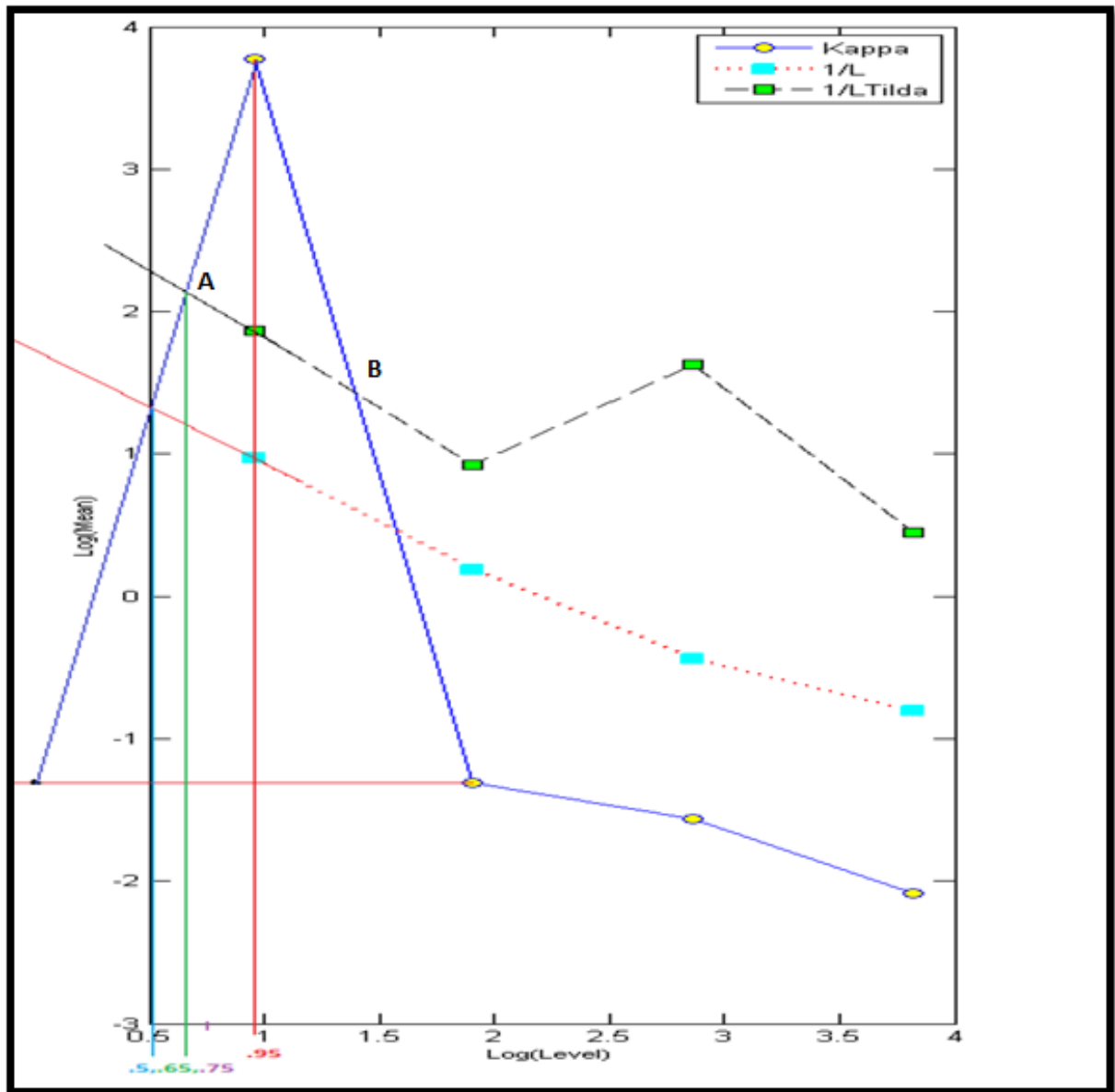


Figure 5.3: Chain Length Calculations for Balloon Burst

5.2b Path Dependency Index

The path dependency index is used individually as well as in conjunction with the above localization index to monitor the process of blowing a balloon and to predict the approximate failure time of the balloon.

Category 1	Full Stability meaning $\frac{abs(Kappa)}{abs(KappaLong)} < 1$ and $\frac{abs(Kappa)}{abs(KappaShort)} < 1$
Category 2	Short term instability or long term stability meaning $\frac{abs(Kappa)}{abs(KappaShort)} > 1$
Category 3	Short term stability or long term instability meaning $\frac{abs(Kappa)}{abs(KappaLong)} > 1$
Category 4	Conditional Stability meaning there is scope to reduce the point's curvature to zero by making $-\frac{1}{2} < \alpha_{prime} < 1$
Category 5	Full Instability in 1 Dimension meaning Line Defect
Category 6	Full Instability in more than 1 Dimensions meaning Area Defect
Category 7 = (Original Category 7 + Category 8 Category 9)	Full Instability in more than 2 Dimensions meaning Volume Defect + Chain Length Greater than Short Term Localization Index + Chain Length Greater than Long Term Localization Index

Figure 5.4a: Categorization of Points according to Path Dependency Index. (Path Independent and Path Dependent Categories)

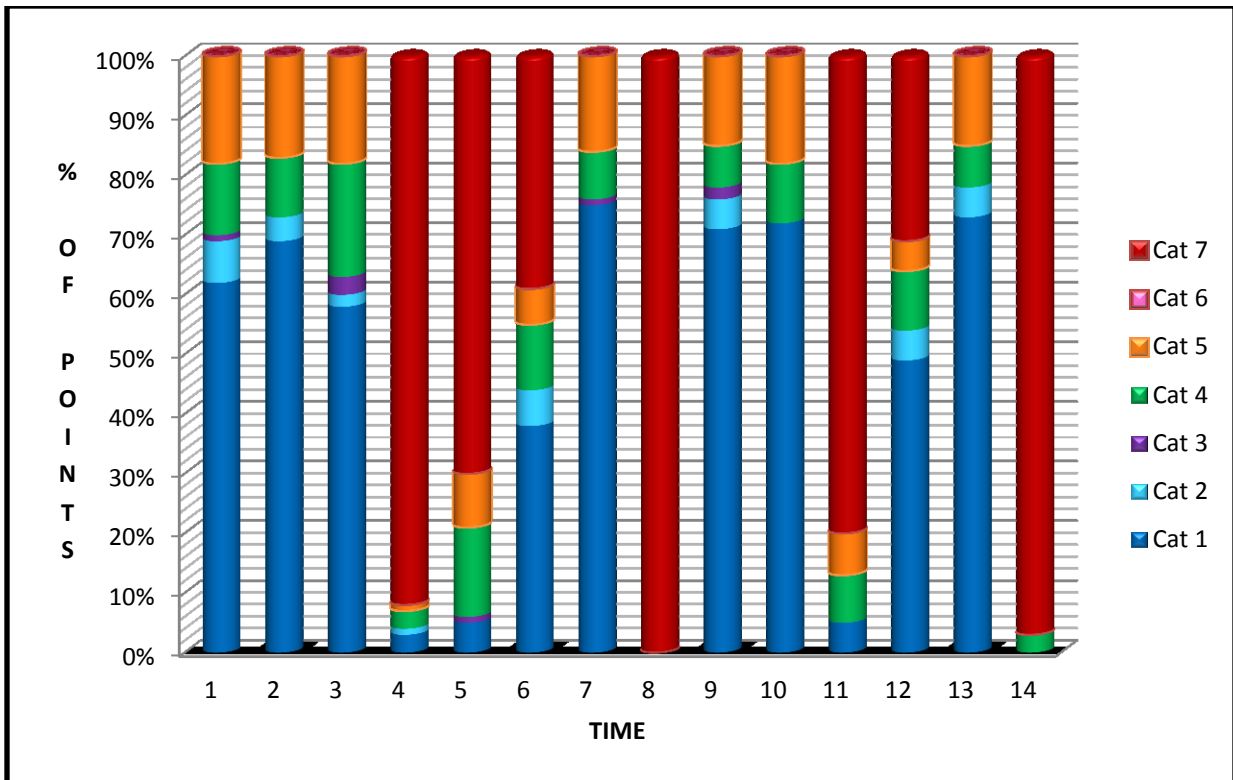


Figure 5.4b: Path Dependency with Localization Index Category for 100 Points for Color Dimension

One of the path dependency with localization index plots for the color dimension across all times are given above (Figure 5.4b) that shows the number of points in 100 points that have reached different levels of instability. The different categories of instability were explained in the algorithm section 4.3a before. Figure 5.5 shows a plot that signifies the moments when the system might have become path dependent only. In other words, it shows the number of roots that have a category value greater than 5 only without the chain length information. The instants of time when the roots are equal to and more than 50% (8 out of 16) in number the balloon is said to path dependent in all those times. So for the balloon path dependency started at time index 4 and the balloon has been path dependent at time indices 13, 16, 22 also.

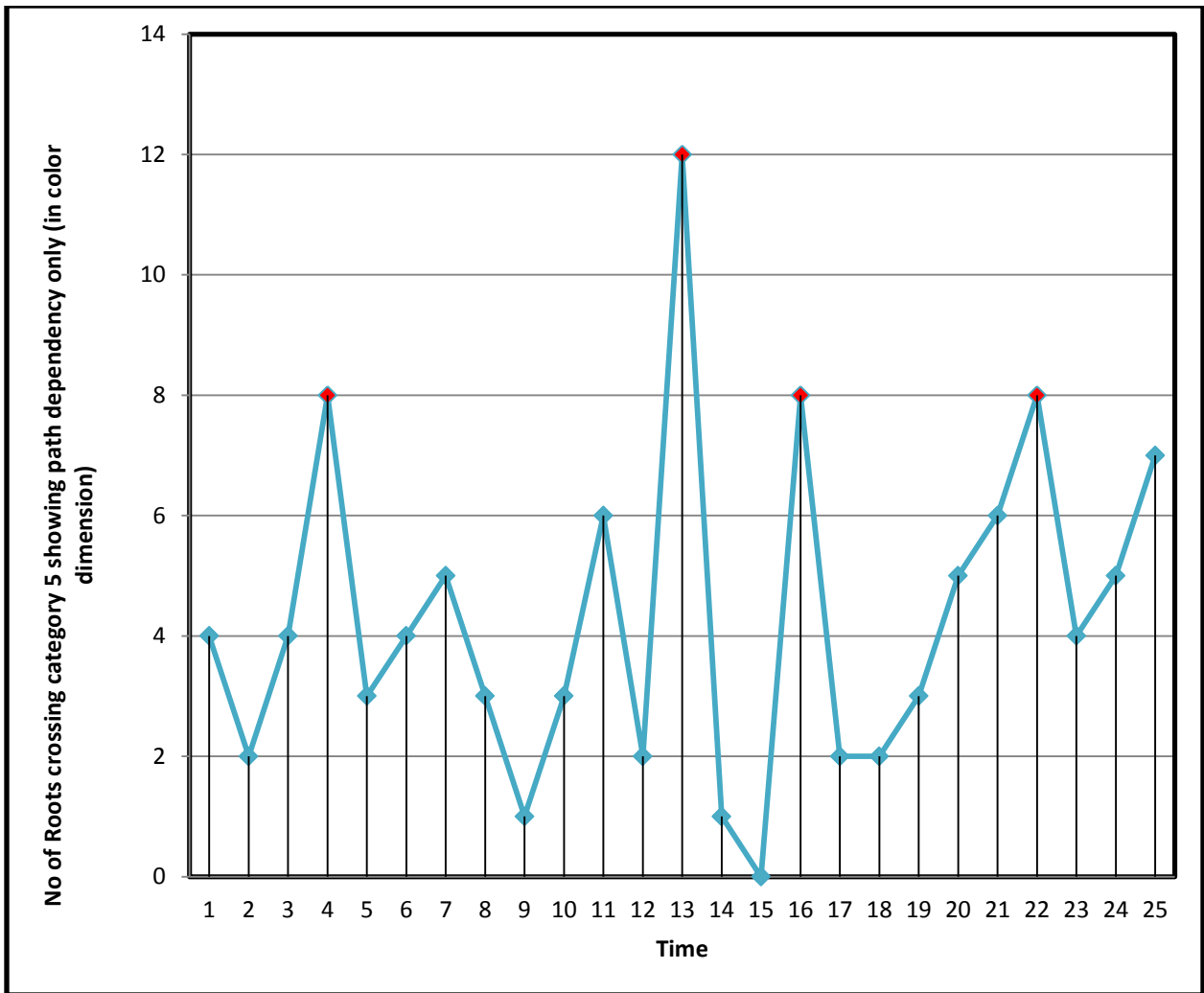


Figure 5.5: Number of roots having category greater than 5 showing path dependencies in color dimension

Figure 5.6 shows the number of roots (out of 16) that had a category value of 5 and above and crossed the localization index threshold (27 in the balloon experiment) as well (in color dimension). The instants of time when the roots are equal and greater than 50% (8 out of 16) in number the balloon is said to near failure in all those times. From figure 5.5 the balloon has crossed the long term localization index at time indices 20, 21, 23, 24 and 25.

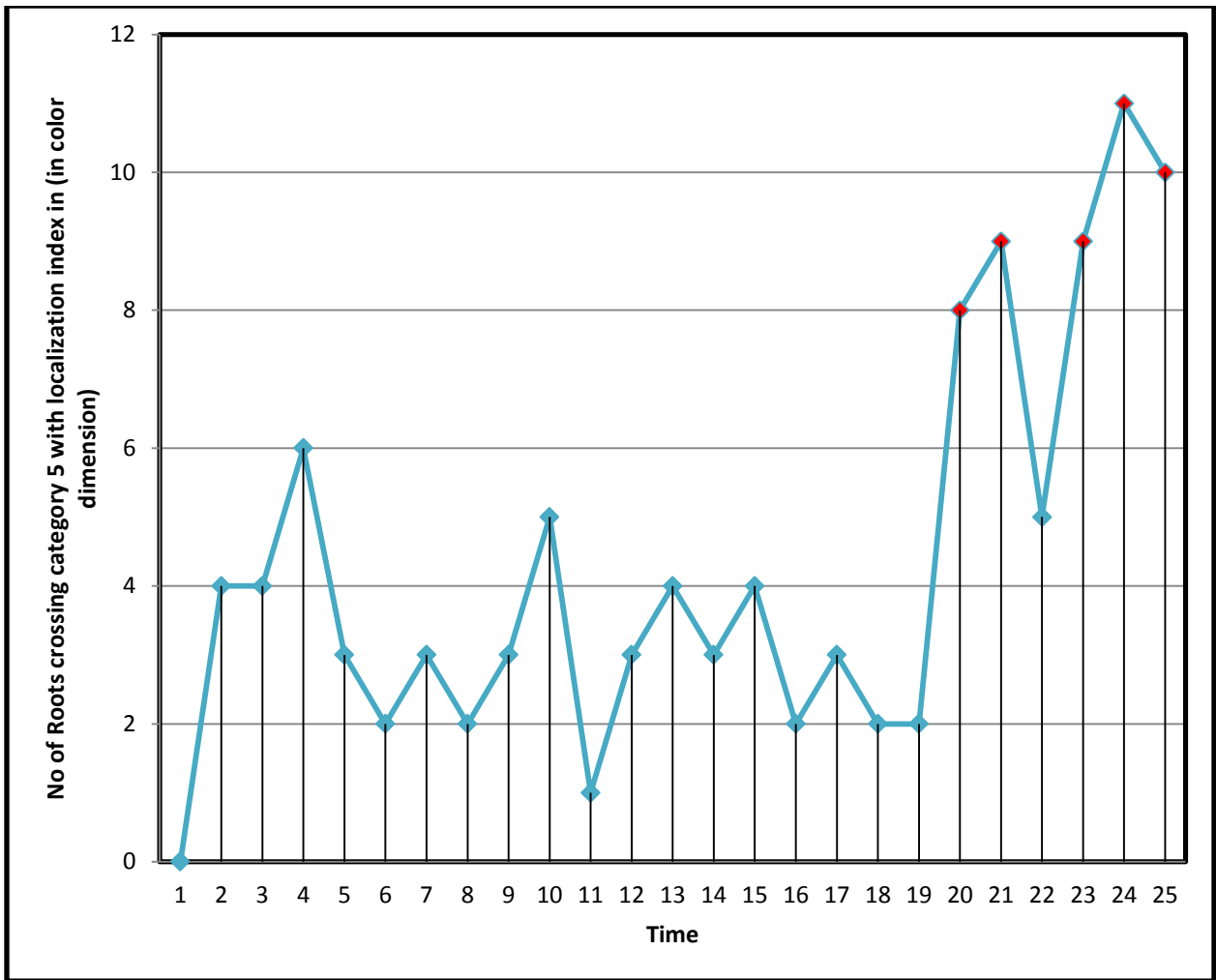


Figure 5.6: Number of roots having category greater than 5 and having chain length greater than number of points.

5.2c Residual Curvature

Figure 5.5 explains when the system is path dependent whereas Figure 5.6 explains when there is a possibility of this system approaching instability in such a manner that the number of points contiguous in rank all become unstable forming a chain greater than the threshold chain length. In addition to Figure 5.5 another analysis based on residual curvature is also used to predict this failure more accurately. It is hypothesized that once all of the path dependency, localization index and residual curvature occurs the balloon would surely approach failure and it is advisable to stop the process. Figure 5.7 shows the percentage of total number of roots in all the 4 dimensions of the balloon (4 dimensions multiplied with 16 roots for each giving total of 64 roots) that had a drop of residual curvature greater than 80%. The instants of time where the number of roots reached a value greater

than 20% (approximately 13 roots out of 64) are said to be the time instants where the balloon is dissipating large amount of energy. The time indices where this happens are 2 , 17 and 22.

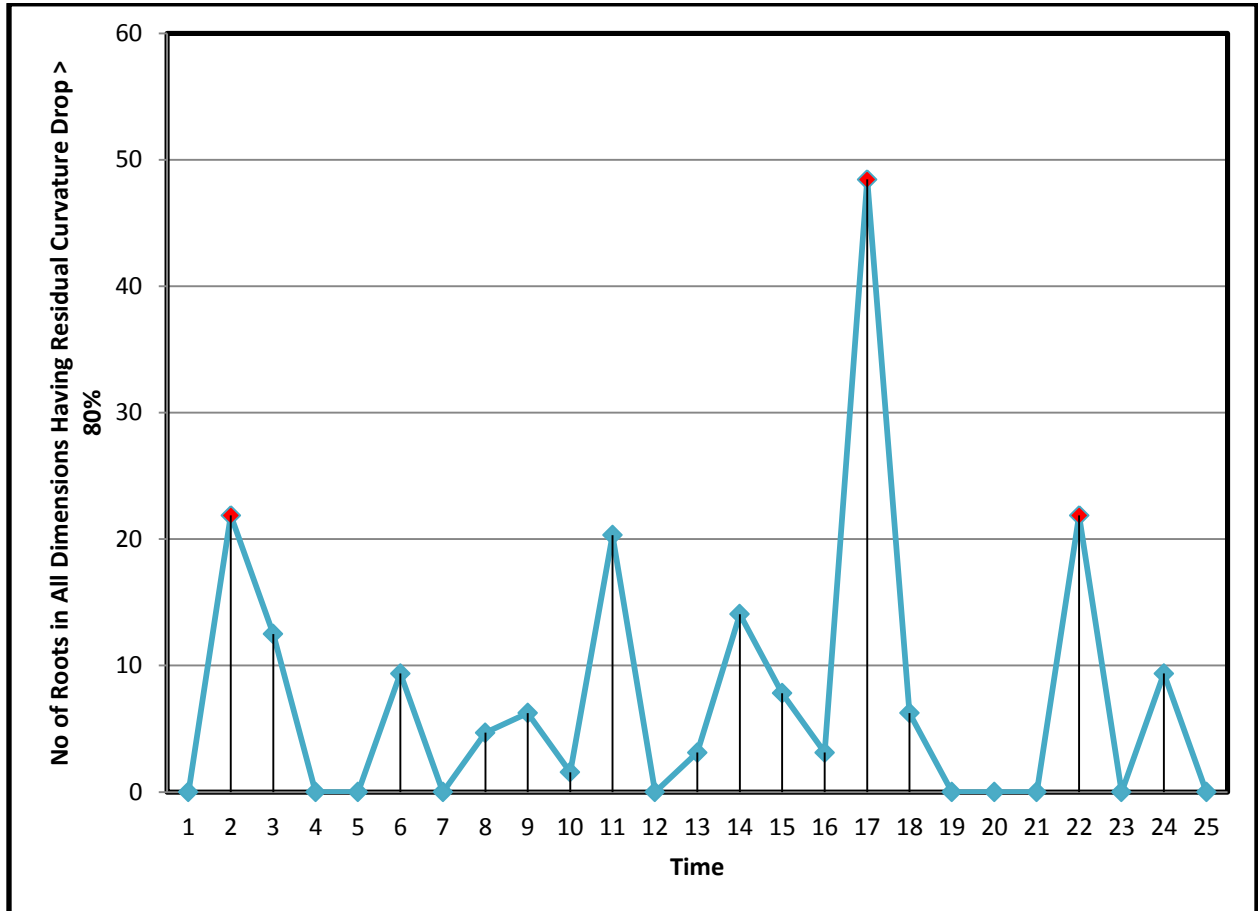


Figure 5.7: Number of roots having residual curvature drops more than 80%.

5.2d Composite Failure Prediction

The full and final failure prediction takes all the above analysis into account. For a failure to occur first the system needs to enter the path dependent stage. A system can be stable even if it is path dependent. While being path dependent the system can nucleate dislocations at multiple points. The points which are only contiguous to each other in rank can actually form a chain. If the chain formed in such a manner exceeds the critical chain length of the system then the dislocations can join and form a huge dislocation which would ultimately give rise to failure. In addition to this the system needs to have huge drop in residual curvature (80%) which would signify that micro crack formation is occurring in the balloon. Once both these (chain formation and micro crack) take place after the system has entered the path dependency mode failure can be predicted for that system. In the case of

balloon the system was under constant monitoring when it entered the path dependency stage at time index 4. After time index 4, it had triggered in long term chain formation at time indices 20, 21, 23, 24 and 25. It had also triggered in residual curvature at time indices 17 and 22 after time index 4. So the time index by which both phenomena had taken place is 20. Hence the balloon was supposed to be approaching failure at that time index and the blowing should be stopped at this instant. Time index 20 corresponds to a frame number of 2099. In reality the balloon had burst at frame 2382. Hence the analysis done predicts failure $\left(1 - \frac{2099}{2382}\right) * 100 = 11.88\%$ ahead of actual time.

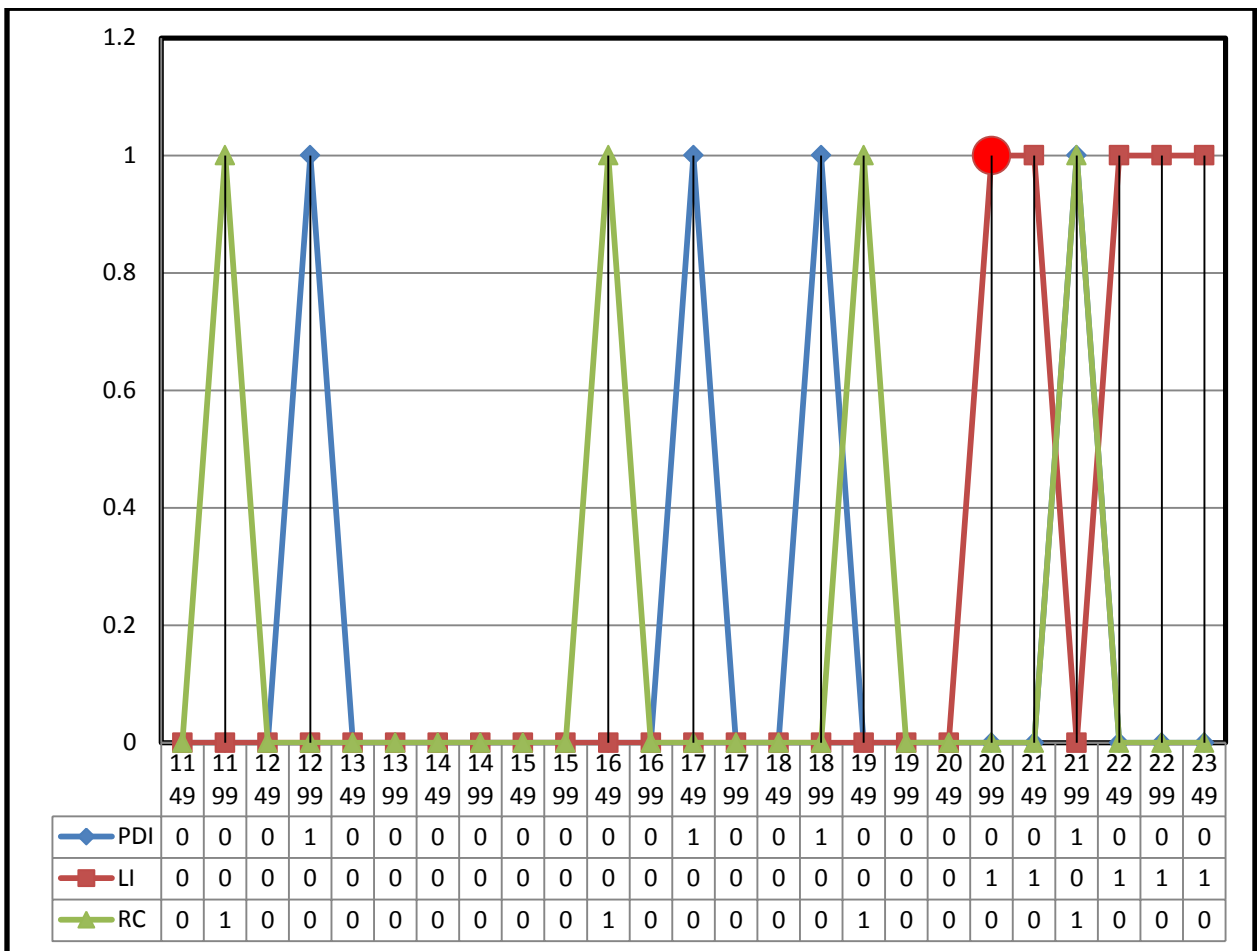


Figure 5.8: Composite Failure Prediction of Sample Data Set 1 (Row 353-362, Col 343-352)

5.3 Results of other datasets for balloon verification

Some results pertaining to other data sets have been given below.

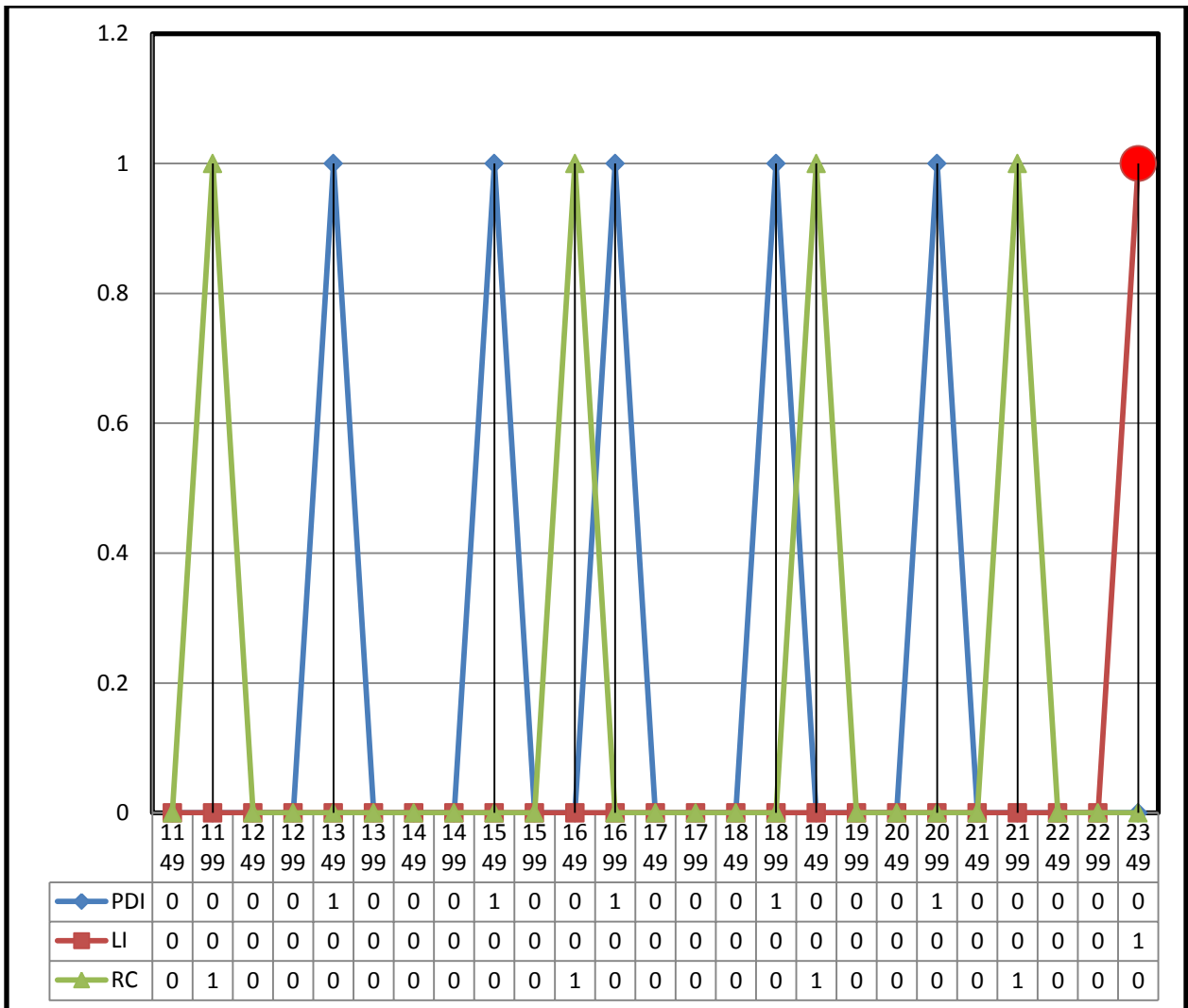


Figure 5.9a: Sample Data Set 2 (Row 363-372, Col 353-362)

Summary Of results

*PATH DEPENDENCY STARTED @1349 AND IN DIMENSION4
 ENERGY DISSIPATION EXCEEDED THRESHOLD @ 1649
 ENERGY DISSIPATION EXCEEDED THRESHOLD @ 1949
 ENERGY DISSIPATION EXCEEDED THRESHOLD @ 2199
 CHAIN FORMATION STARTED @ 2349 AND IN DIMENSION 4
 1.385% PREDICTION AHEAD OF ACTUAL FAILURE.*

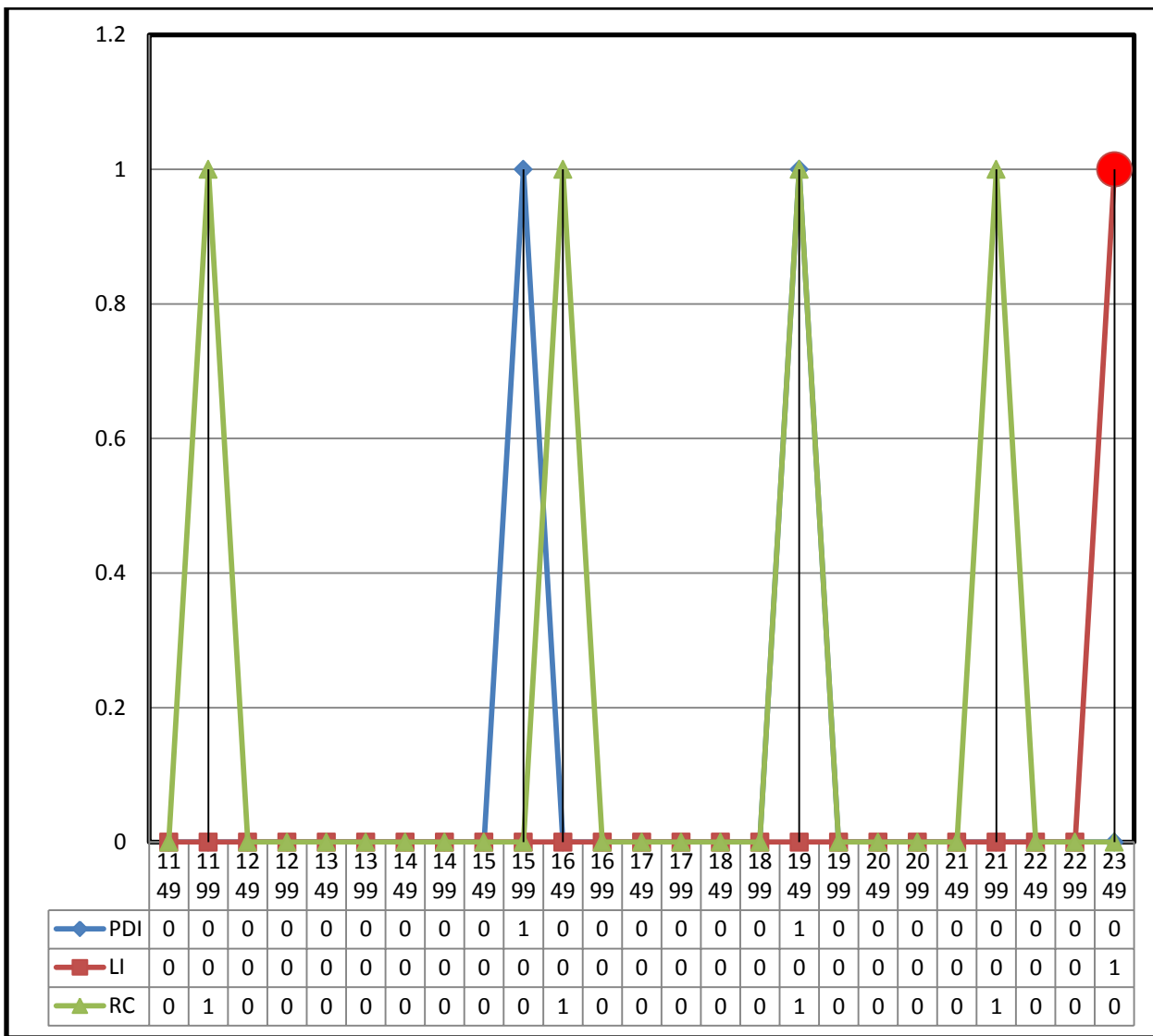


Figure 5.9b: Sample Data Set 3 (Row 373-382, Col 363-372)

Summary Of results

PATH DEPENDENCY STARTED @1599 AND IN DIMENSION 4
ENERGY DISSIPATION EXCEEDED THRESHOLD @ 1649
ENERGY DISSIPATION EXCEEDED THRESHOLD @ 1949
ENERGY DISSIPATION EXCEEDED THRESHOLD @ 2199
CHAIN FORMATION STARTED @ 2349 AND IN DIMENSION 4
1.385% PREDICTION AHEAD OF ACTUAL FAILURE.

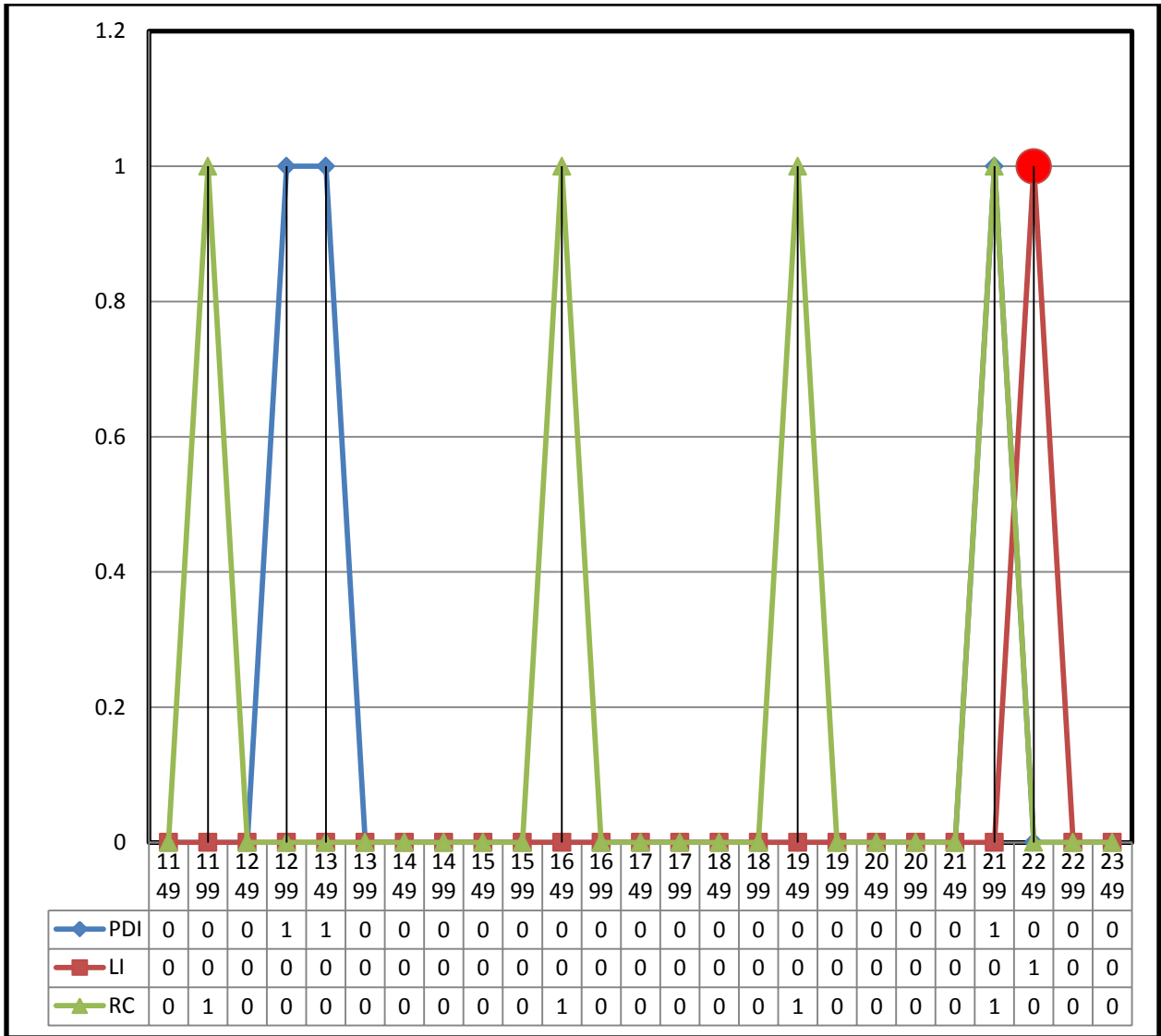


Figure 5.9c: Sample Data Set 4 (Row 383-392, Col 373-382)

SUMMARY OF RESULTS

*PATH DEPENDENCY STARTED @1299 AND IN DIMENSION4
 ENERGY DISSIPATION EXCEEDED THRESHOLD @ 1649
 ENERGY DISSIPATION EXCEEDED THRESHOLD @ 1949
 ENERGY DISSIPATION EXCEEDED THRESHOLD @ 2199
 CHAIN FORMATION STARTED @ 2249 AND IN DIMENSION 4
 5.5835% PREDICTION AHEAD OF ACTUAL FAILURE.*

5.4 Application of Stability analysis for CMP

Over the past 20 years, through significant improvements in design and manufacturing, the CMP process has played an important role in Integrated Circuits manufacturing

advancements. To further understand the interplay between the chemical and mechanical actions in Chemical Mechanical Planarization (CMP), it is useful to build a multi-physics predictive tool that reliably accelerates the development cycle. It is necessary to understand the nature of interactions, at the particle scale, among the porous pad material, the slurry, and the wafer, aided by the CMP machine characteristics. The method adopted for failure prediction in balloon is used in the real life scenario of a CMP machine which improves stability of the process, thereby reducing defectivity and enhancing the associated manufacturing yield. This work is referenced in the paper *Role of Velocity Control for Enhancing Planarization Rate and Stability of Chemical Mechanical Paired Grinding* [Chandra, Bastawros, Wu, Kar and McCleish 2013].

CHAPTER 6. APPLICATION OF ALGORITHM- GULF STREAM

6.1 Gulf Stream Analysis

The first application of the prediction algorithm was Gulf Stream Ring Formation analysis. The regions of interest are the Gulf Stream System, the Gulf of Maine and Mid Atlantic Shelf Region. A feature-oriented regional modeling and simulation (FORMS) of the circulation in the coastal-to-deep region of the above regions are developed. Temperature, Velocity and Salinity profiles are obtained from this feature model. The algorithm developed uses these profiles and tries to predict where ring formations will take place. Ring formations are cold core water rings surrounded on all sides by the warm water of the Gulf Stream. In this cold core rings fishes are trapped which are of interest to the fishing community.

6.2 Feature Model Data Description

The Salinity, Temperature, Velocity data obtained from the feature model needs to be processed before feeding into the prediction algorithm. Each of this data set is a 4 dimensional matrix consisting of data values measured at different times (121 different time instances), different longitudes (130 longitudes) and latitudes (83 different latitudes) and at different depths (16 depths). For the analysis of ring formation, the algorithm however only used the data values on the surface of the ocean i.e. at depth 0. The grid of latitude and longitude points is a rotated as the earth itself is tilted on its axis. So instead of having same longitude value across the 83 different latitudes and same latitude values across the 130 different longitudes the latitude and longitude values both vary from one point to point. Hence all these points (130 x 83) have unique latitude and longitude values. Observations are recorded by the feature model 3 hours apart in a whole day. Generally observations are taken over a period of 15 weeks. Hence in 1 day there are 8 observations and hence across 15 days totally there are 120 observations. 1 extra observation (121st) is provided which is the 12 AM data for the next day.

6.3 Choice of Dimensions

There were many different variables that could have been analyzed in the Gulf Stream System. But out of all the variables, the 4 dimensions of Temperature, Salinity, East Velocity and North Velocity were chosen, since together they can be assumed to form a

conservative system. As the Temperature increases Salinity increases but as Velocity increases, Salinity decreases.

6.4 Preprocessing Data Files

As explained in section 6.2 the output data from the feature model needs to be processed before it can be fed as the input to the prediction algorithm. Each of the Temperature/Salinity/East Velocity/North Velocity feature model output data matrices consists of 121 different time instances. For processing, the input data matrix for Salinity recorded by the feature model from April 9 to April 23 is broken down into 121 different files representing the 121 different times. Hence, at each time instant the data was recorded by the model there is a corresponding time file containing the salinity values at 83 x 130 unique grid points. At each time the 4 dimensions (Temperature, Salinity, North Velocity and East Velocity) recorded at 83 x 130 grid points represents the complete data set at that time instant and a sample snapshot from this complete data set is given to the prediction algorithm as input.

6.5 Analysis Procedure

In the Gulf Stream analysis primarily 2 types of analysis were done almost similar to the balloon burst experiment. The first one was Zoom Out procedure which was done to get critical localization index. The second type of analysis was done for multiple data sets at different instants of time on some selective grid points to observe ring/hole formations. These results were compared with real ring formations on the grid. The results would predict approximately when the ring was getting formed.

6.5a Critical Localization Index

The zooms out plots for the Gulf Stream analysis are given below in Figure 6.1 which shows maximum, minimum and average of absolute values of $\kappa, \frac{1}{LTilda}, \frac{1}{L}$ against aggregation level. For the Gulf Stream analysis 2 types of chain lengths were calculated: - the short term chain length and the long term chain length. The determination of critical chain length/localization index follows the same procedure as explained in section 4.5b. The intersection point of the symmetrical line of κ and $\frac{1}{L}$ line is taken to be the value of the short term localization index. The intersection point of the symmetrical line of κ and $\frac{1}{LTilda}$ line is taken to be the value of the long term localization index. The X values of these intersection points are measured. Since the zoom out plots are log scale plots, the log value of these

point is converted to an actual number of points. This number of points represents the chain length that is occurring in a total of 9 points. If the number of unstable points forms a chain greater than the short term chain length and the long term chain length then those points have potential to form rings. Since this chain length is only valid for 9 points, these needs to be converted to a value that can be applicable to a set of 100 points (or the number of points being considered in the sample data set).

Long term chain length calculations for East Velocity in 9 points are given as:-

$$\frac{\log_{10}^x}{\log_{10}^9} = \frac{0.68}{0.95} = 0.7157 \Rightarrow x = 9^{0.7157} = 4.8 \cong 5$$

Keeping the ratio constant as 0.7157 the chain length can be translated to a value in 100 points as given below:-

$$\frac{\log_{10}^x}{\log_{10}^{100}} = \frac{0.68}{2} = 0.7157 \Rightarrow x = 10^{2 * 0.7157} = 27.013 \cong 28$$

Performing the same procedure as shown above for Short term chain length calculations a chain length of 6 points is obtained among 100 points shown as follows :-

Short term chain length calculations for east velocity in 9 points are given as:-

$$\frac{\log_{10}^x}{\log_{10}^9} = \frac{0.36}{0.95} = 0.3789 \Rightarrow x = 9^{0.3789} = 2.2 \cong 3$$

Keeping the ratio constant as 0.3789 the chain length can be translated to a value in 100 points as given below:-

$$\frac{\log_{10}^x}{\log_{10}^{100}} = \frac{0.36}{2} = 0.3789 \Rightarrow x = 10^{2 * 0.3789} = 5.72 \cong 6$$

So the critical long term and short term localization index value are 28 and 6 respectively for a set of 100 points. These are also used as the corresponding threshold values in the prediction algorithm.

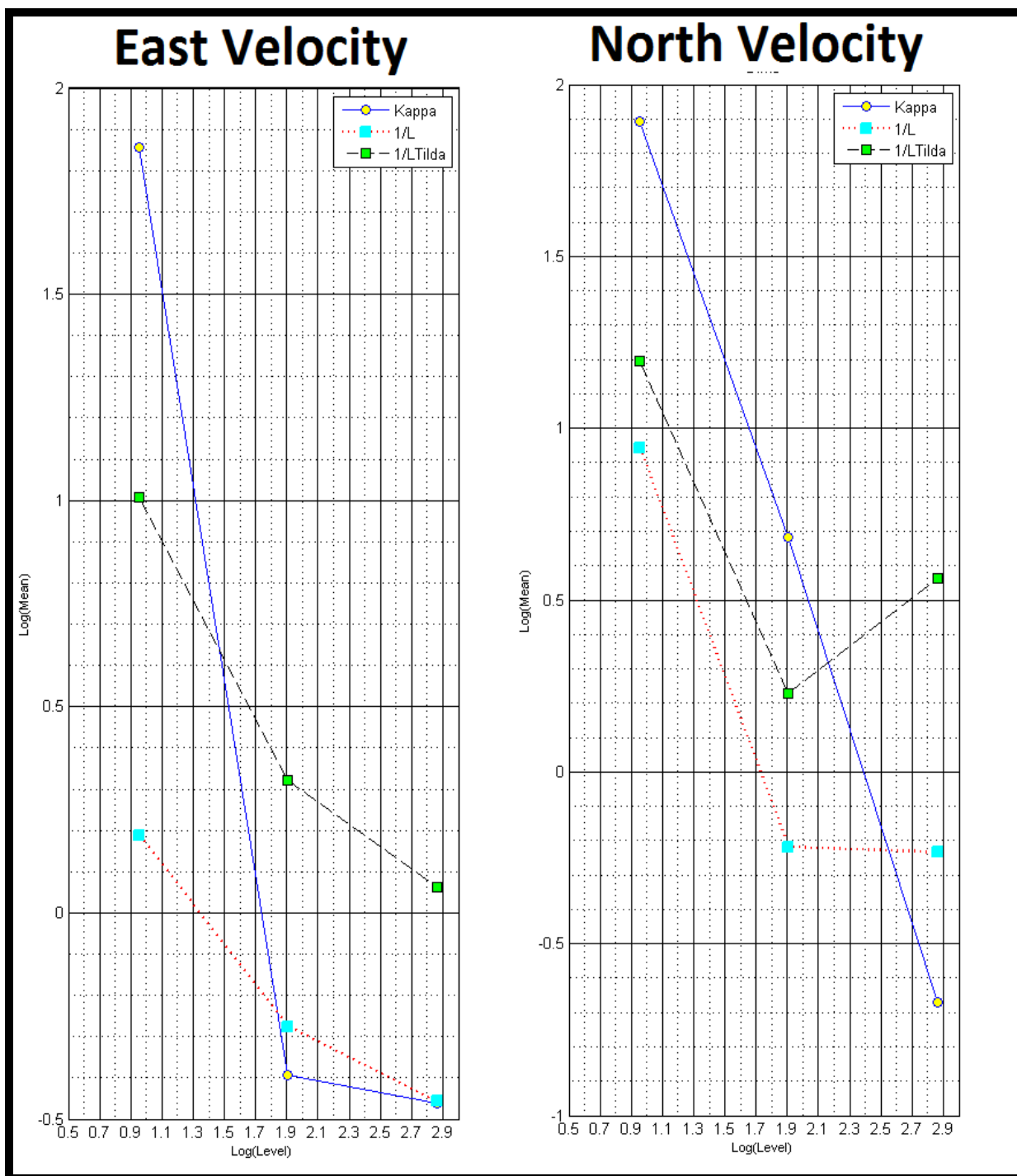


Figure 6.1: Zoom Out Plots for Gulf Stream Analysis

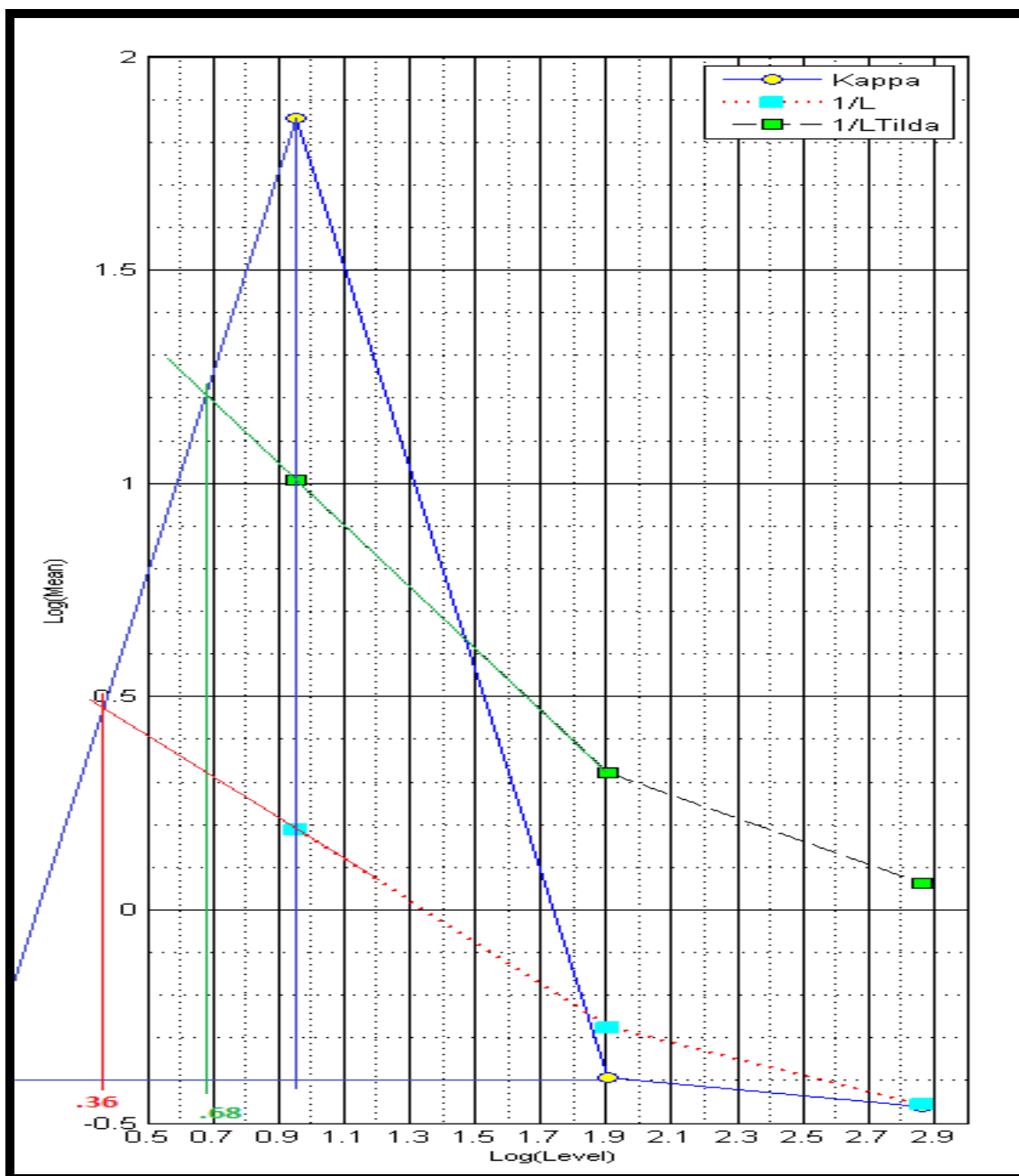


Figure 6.2: Short Term and Long Term Chain Length Calculations

6.5b Path Dependency Index

The path dependency index is used individually as well as in conjunction with the above localization index to look for ring formations in the Gulf Stream. First the points in the sample data set are categorized according to the categories given below.

Category 1	Full Stability meaning $\frac{abs(Kappa)}{abs(KappaLong)} < 1$ and $\frac{abs(Kappa)}{abs(KappaShort)} < 1$
Category 2	Short term instability or long term stability meaning $\frac{abs(Kappa)}{abs(KappaShort)} > 1$
Category 3	Short term stability or long term instability meaning $\frac{abs(Kappa)}{abs(KappaLong)} > 1$
Category 4	Conditional Stability meaning there is scope to reduce the point's curvature to zero by making $-\frac{1}{2} < \alpha_{prime} < 1$
Category 5	Full Instability in 1 Dimension meaning Line Defect
Category 6	Full Instability in more than 1 Dimensions meaning Area Defect
Category 7 = (Original Category 7 + Category 8)	Full Instability in more than 2 Dimensions meaning Volume Defect + Chain Length Greater than Short Term Localization Index

Figure 6.3: Categorization of Points according to Path Dependency Index. (Path Independent and Path Dependent Categories)

Next following the steps outlined in the Hole/Ring formation algorithm the points which were assigned a value equal to or more than category 8 in more than 1 dimension and if this occurs in equal to /greater than 7 roots then those points are triggered for ring formation.

6.5c Ring Formation Results

Next following the steps outlined in the Hole/Ring formation algorithm the points which were assigned a value equal to or more than category 8 in more than 1 dimension and in more than 7 roots then that point is said to be involved in ring formation. Results of some sample data sets selected from particular geographic regions and their ring formation prediction across different days are shown. First the geographic region is shown across multiple days to understand the development of rings across those days. For the same days the predicted point map of that region is shown. The analysis shows that the prediction of ring occurs a day or two before the actual ring forms on the grid.

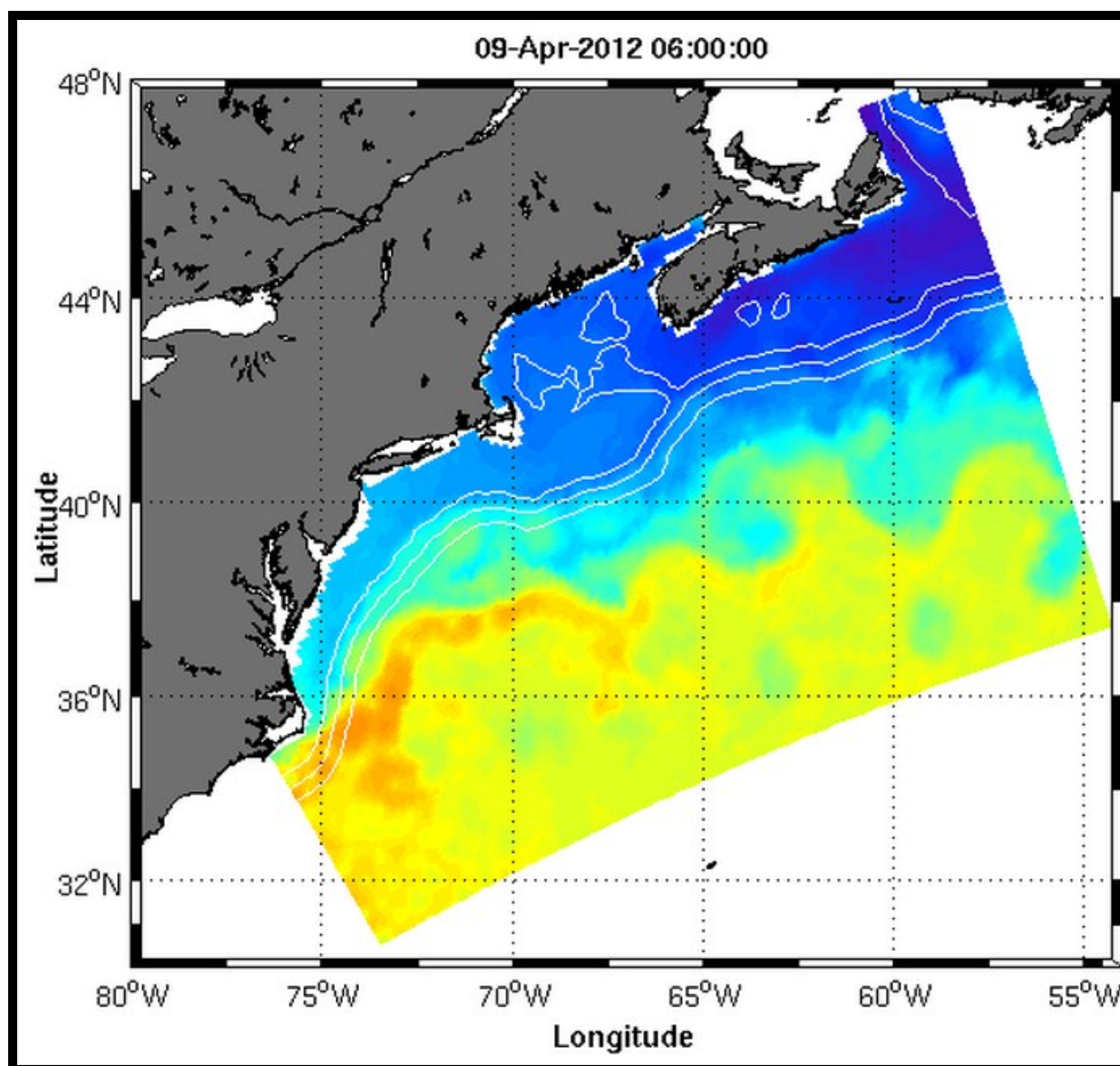


Figure 6.4a: Grid of April 9 at 6.00 a.m.

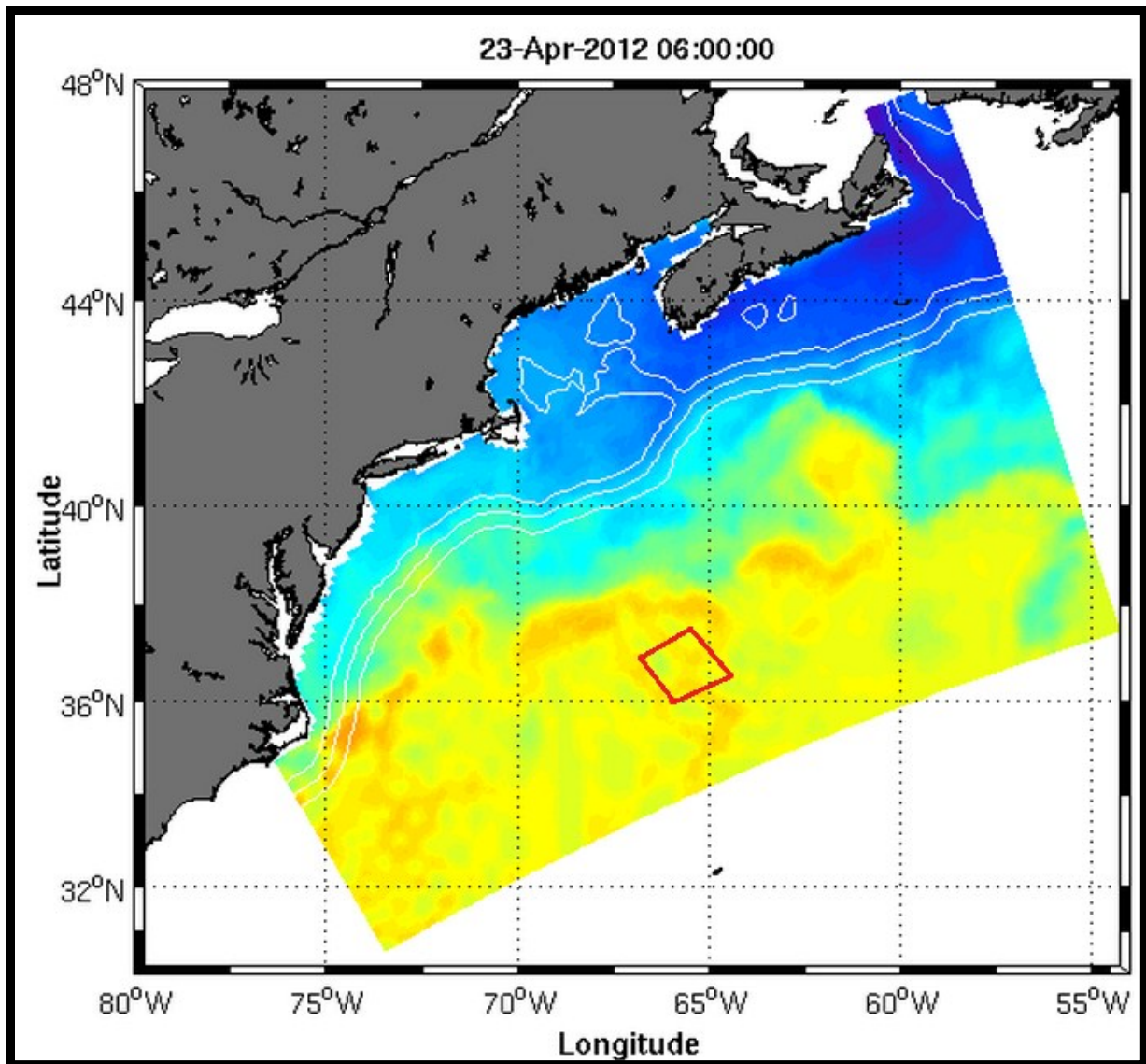


Figure 6.4b: Grid of April 23 at 6.00 a.m. (Row 16 Col 60)

Figure 6.4a shows the condition of the actual geographic grid on April 9, 2012. Starting from this day, the ring formation till April 23, 2012 [Figure 6.4 b] is observed and some results are predicted using the prediction algorithm. The selected red parallelogram region in Figure 6.4b is the first sample dataset that is selected.

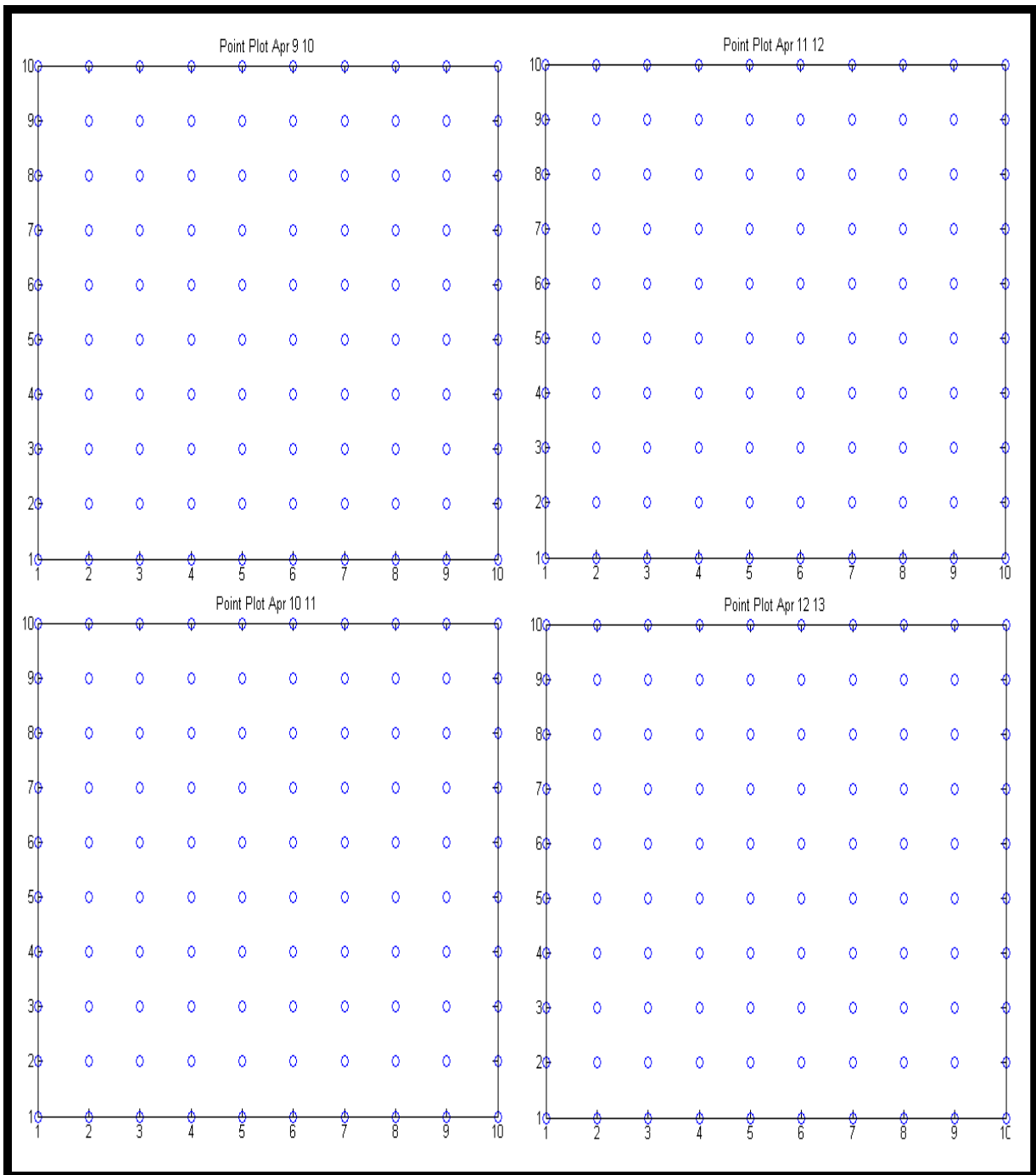


Figure 6.4c: Point plot of selected region April 9 to April 13

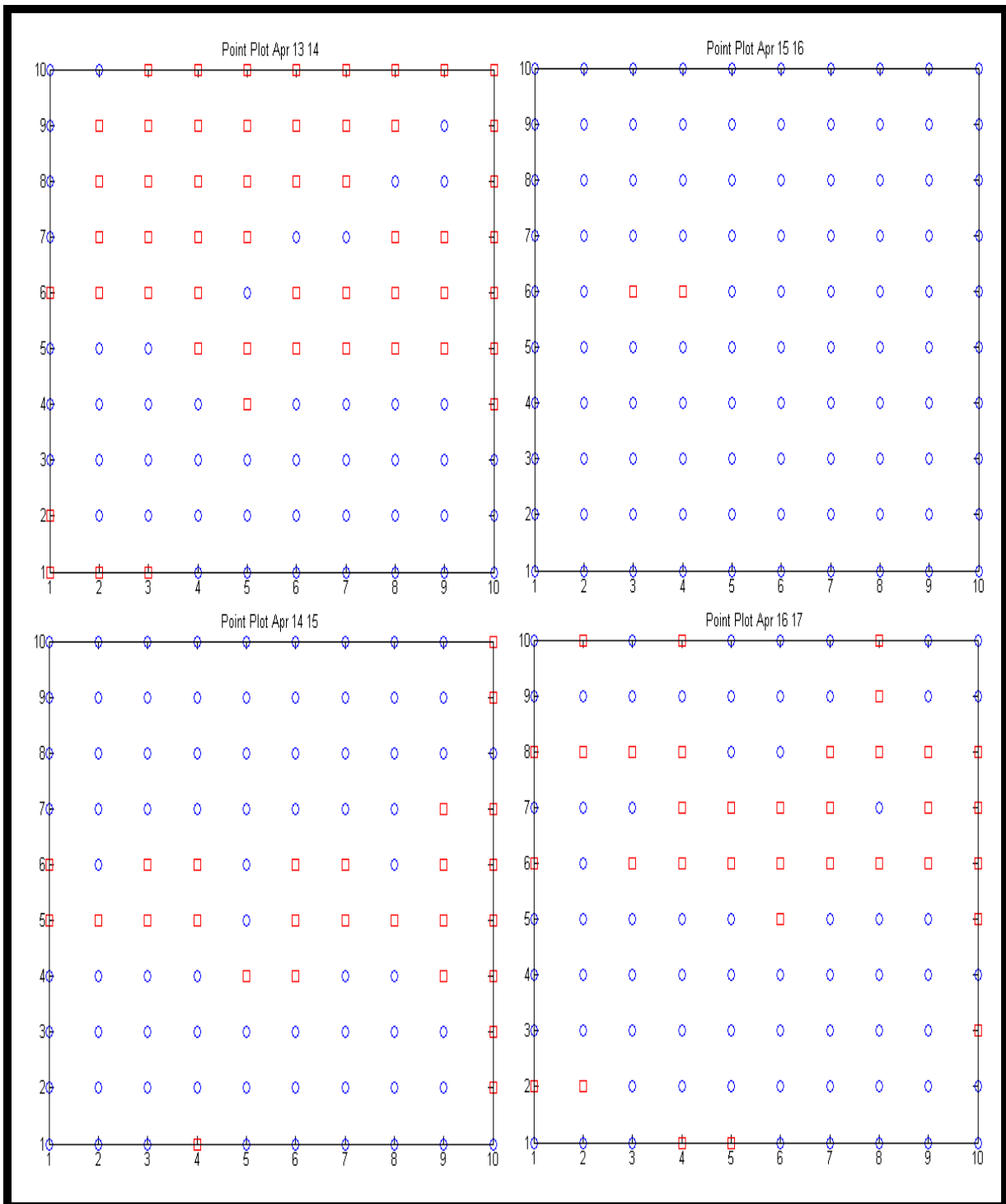


Figure 6.4d: Point plot of selected region April 13 to April 17

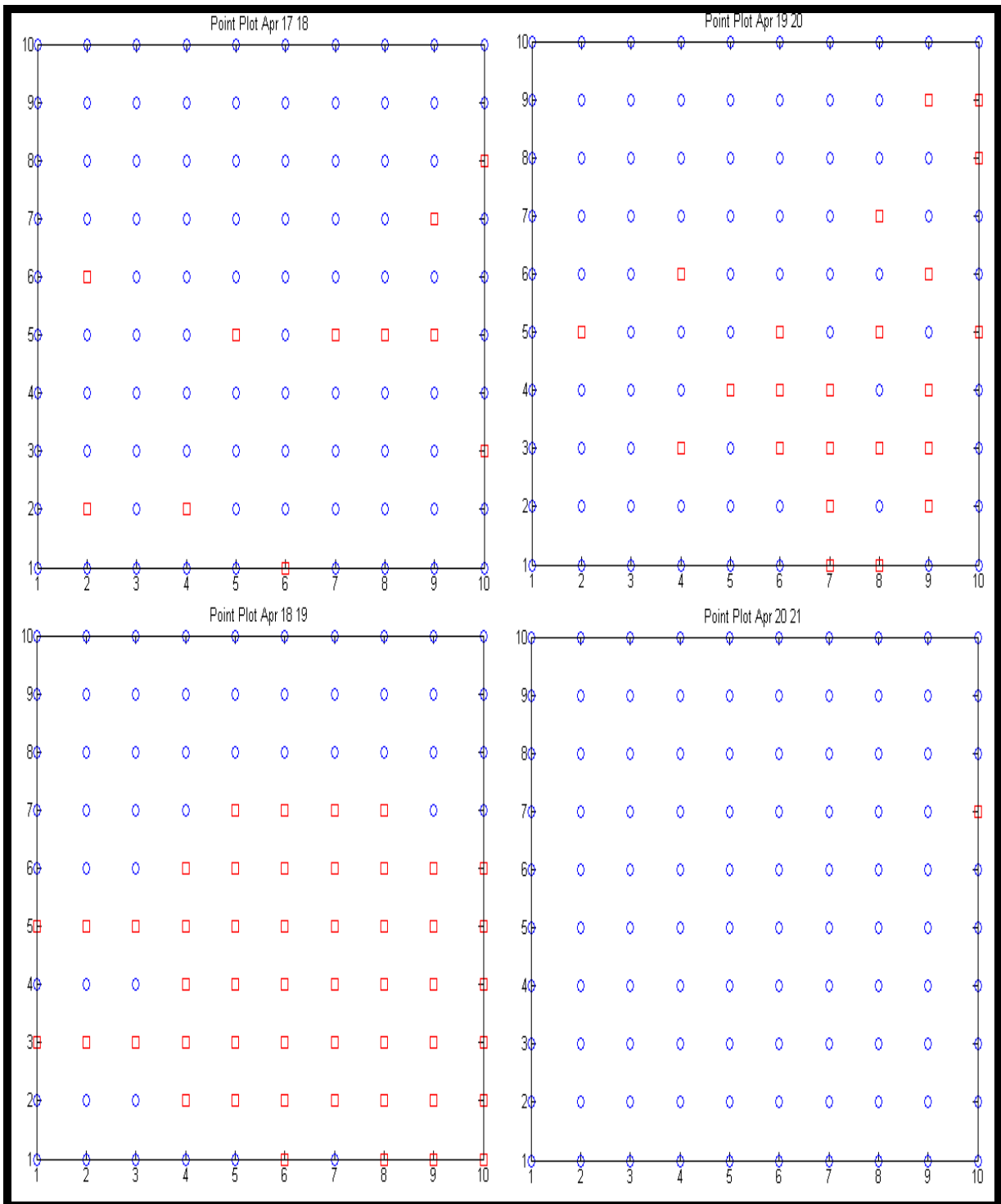


Figure 6.4e: Point plot of selected region April 17 to April 21

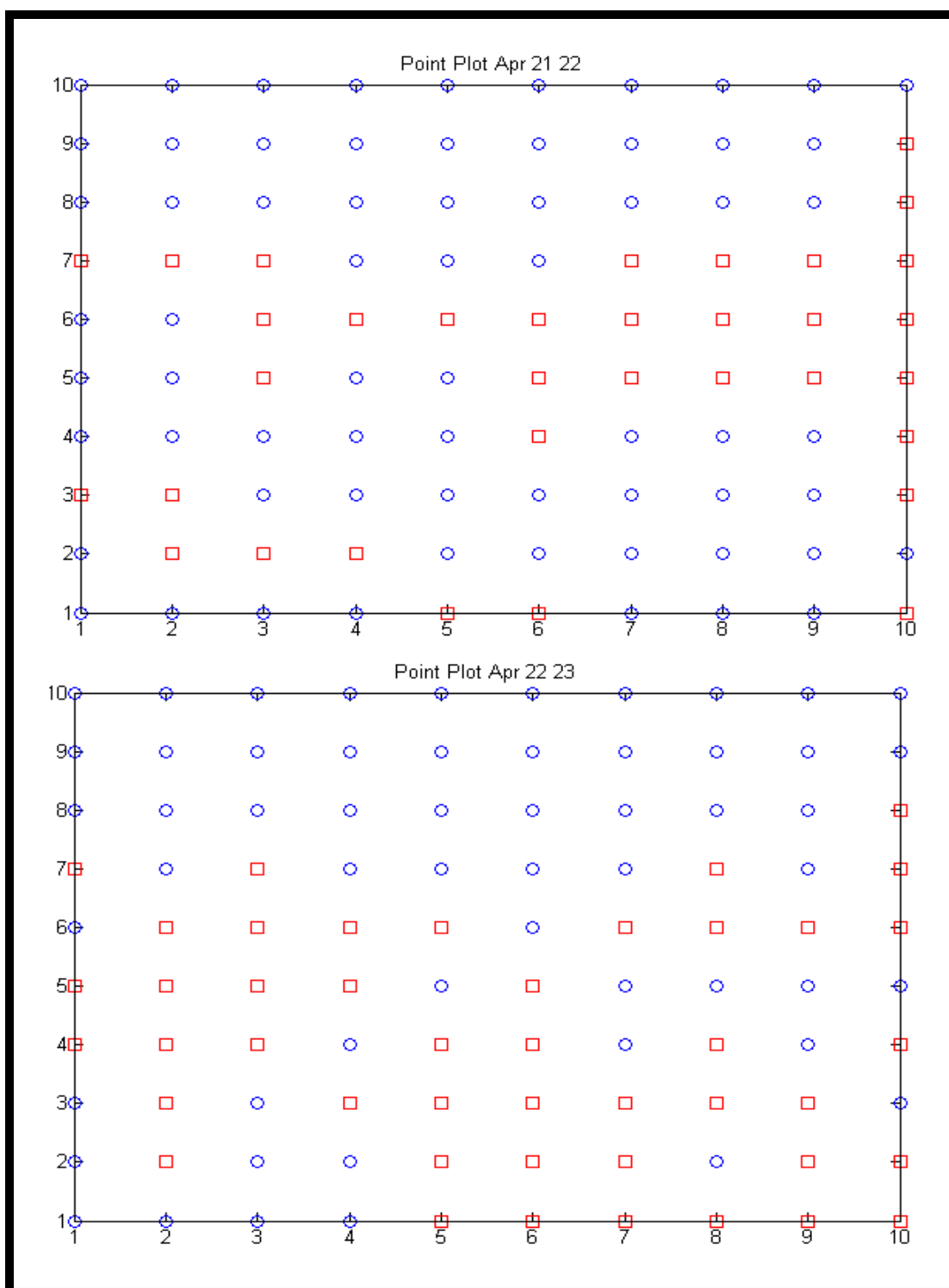


Figure 6.4f: Point plot of selected region April 21 to April 23

As it is observed from the plots there is some similarity in the nature of the ring formations. On April 23, there is a small part of the grid in the northern portion that shows some ring formation. Similarly in the plots, there is a trend to see ring formations in the upper portion of the plots around April 12 and April 13. There are some rings observed in the grid in the south east corner which is shown as red circles in the plots of April 18, 19 and April 22, 23.

6.6 Results of other datasets for Gulf Stream

6.6a Data Set 2 - May 21

Some other datasets are also presented.

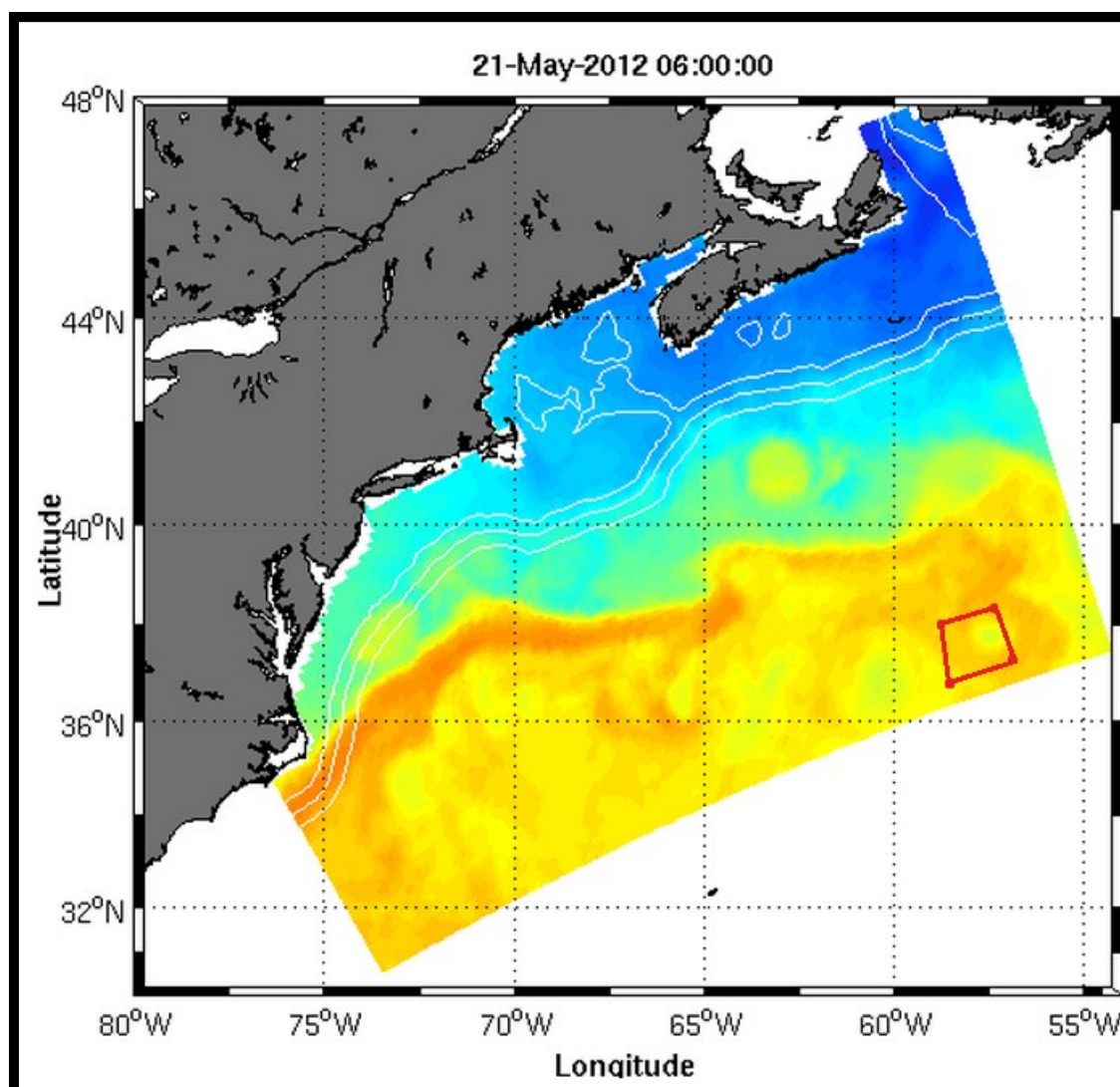


Figure 6.5a: May 21 Grid with the Selected Area for Analysis (Row 5 Col 105)

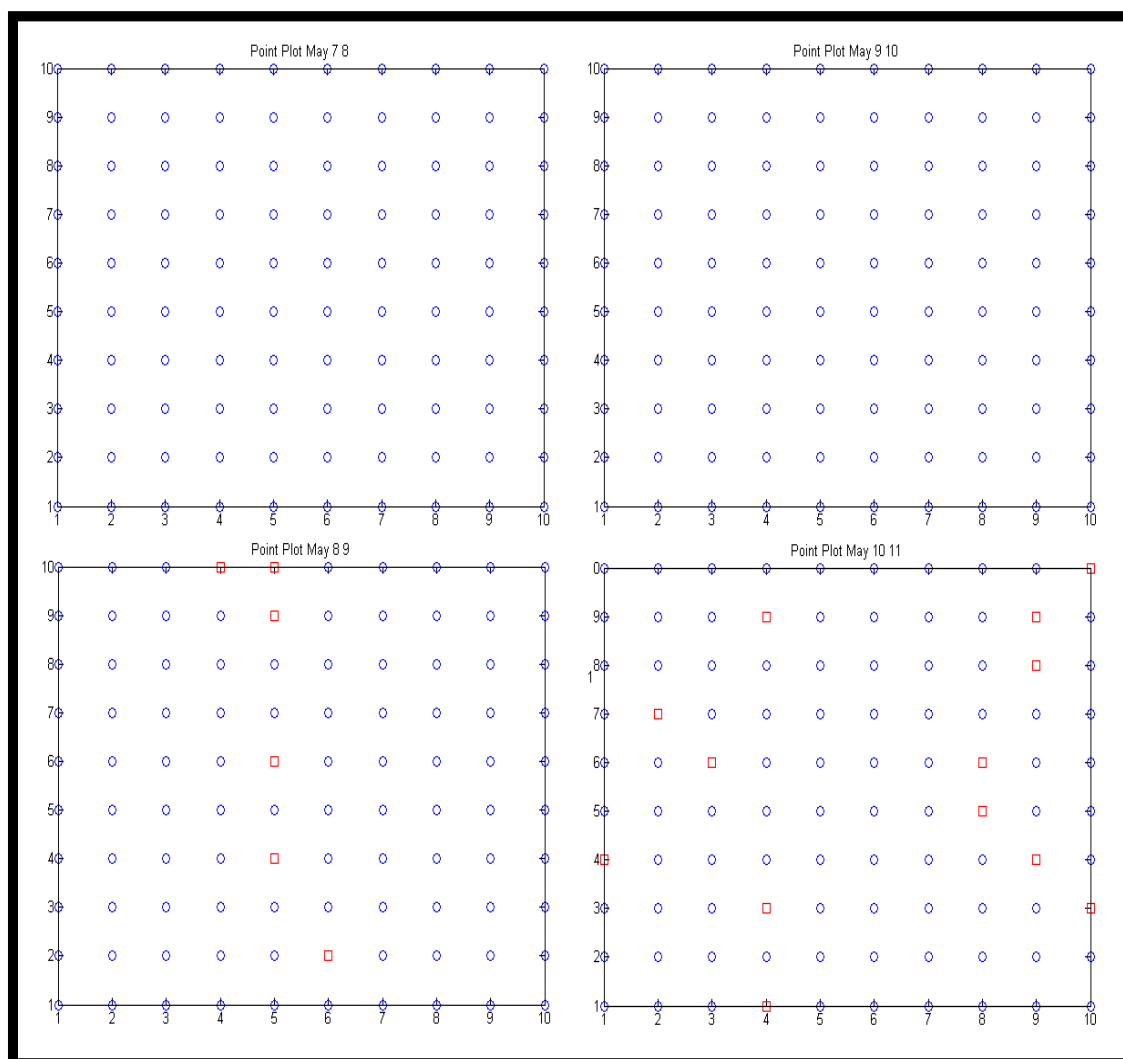


Figure 6.5b: Point plot of selected region May 7 to May 11

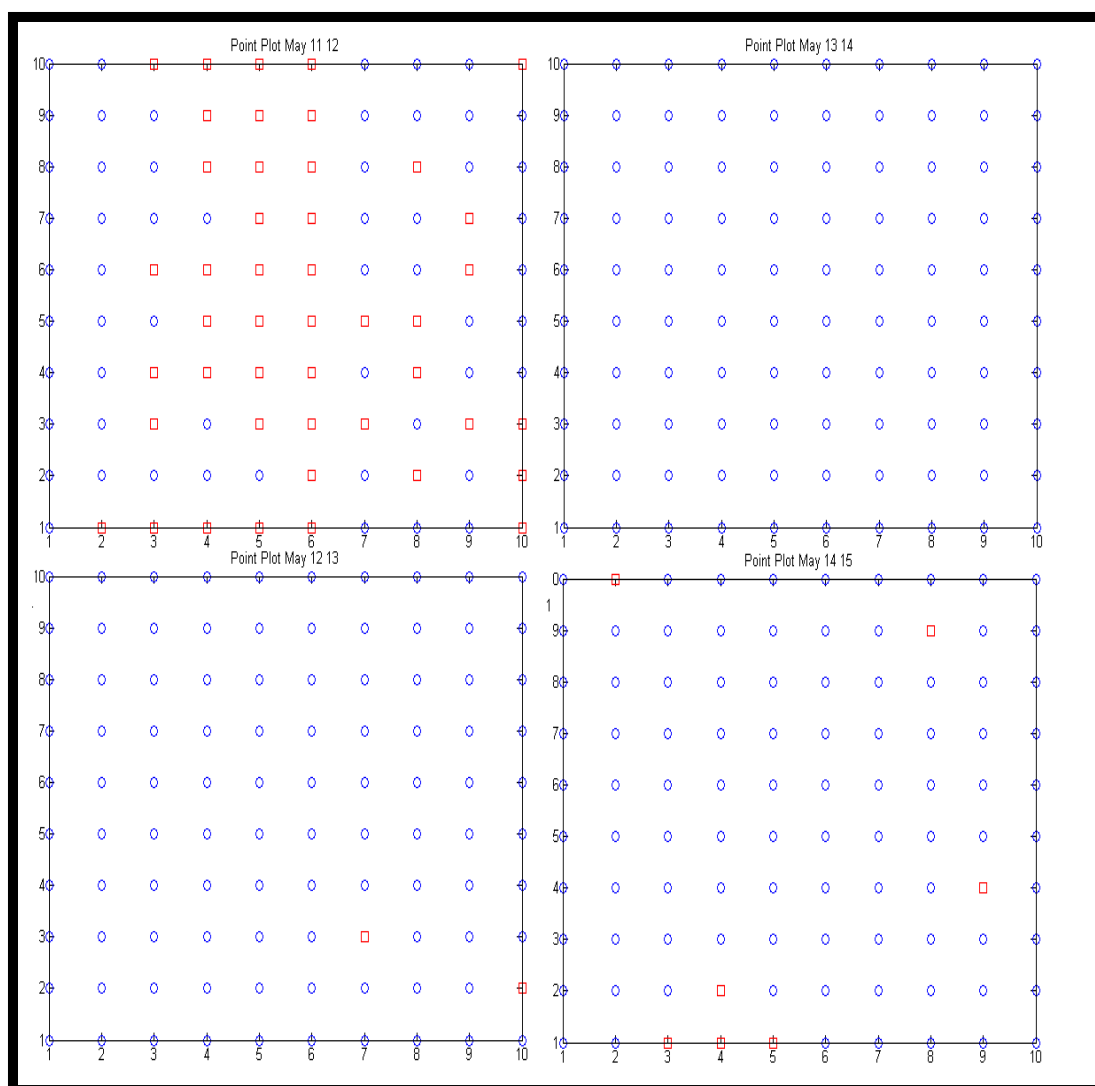


Figure 6.5c: Point plot of selected region May 11 to May 15

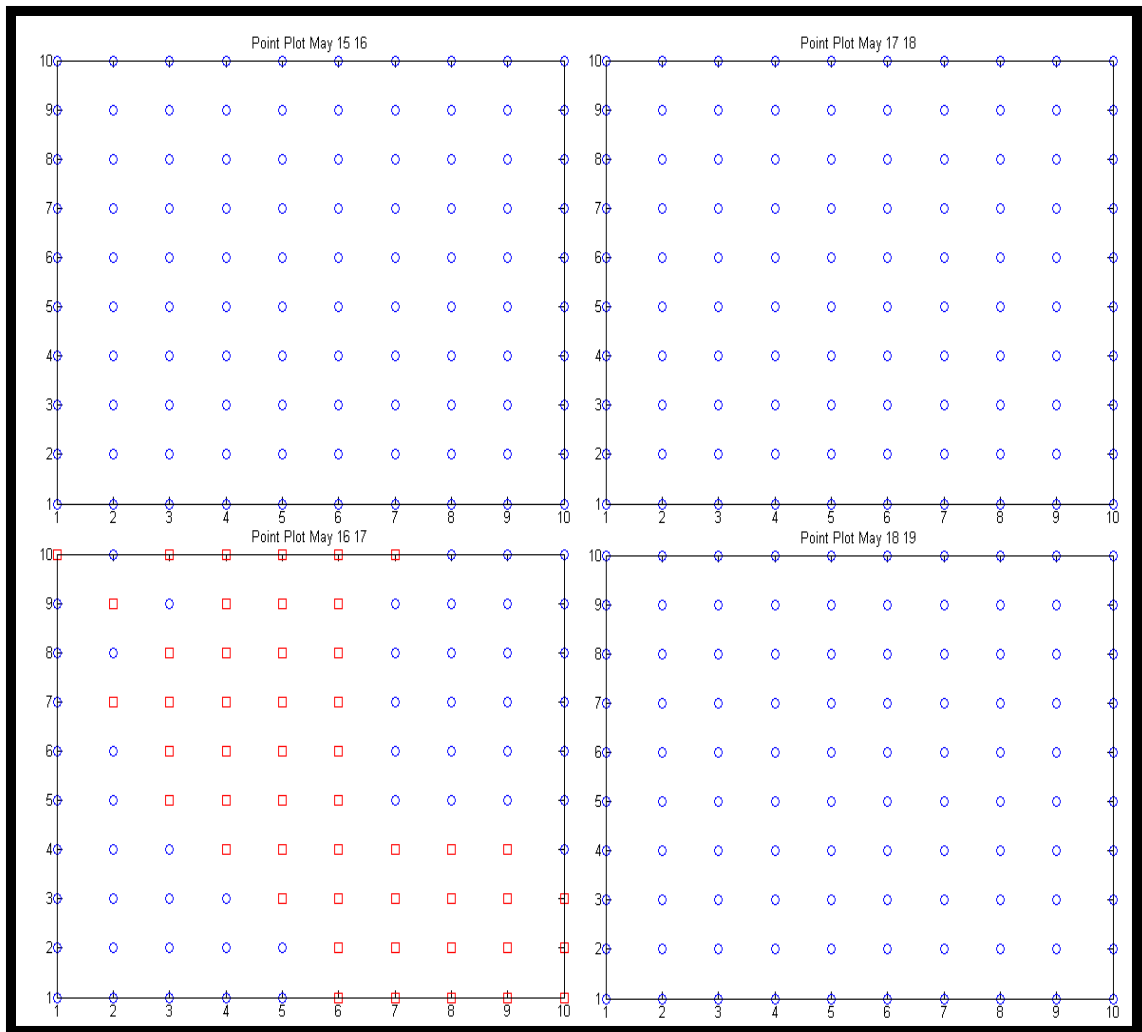


Figure 6.5d: Point plot of selected region May 15 to May 19

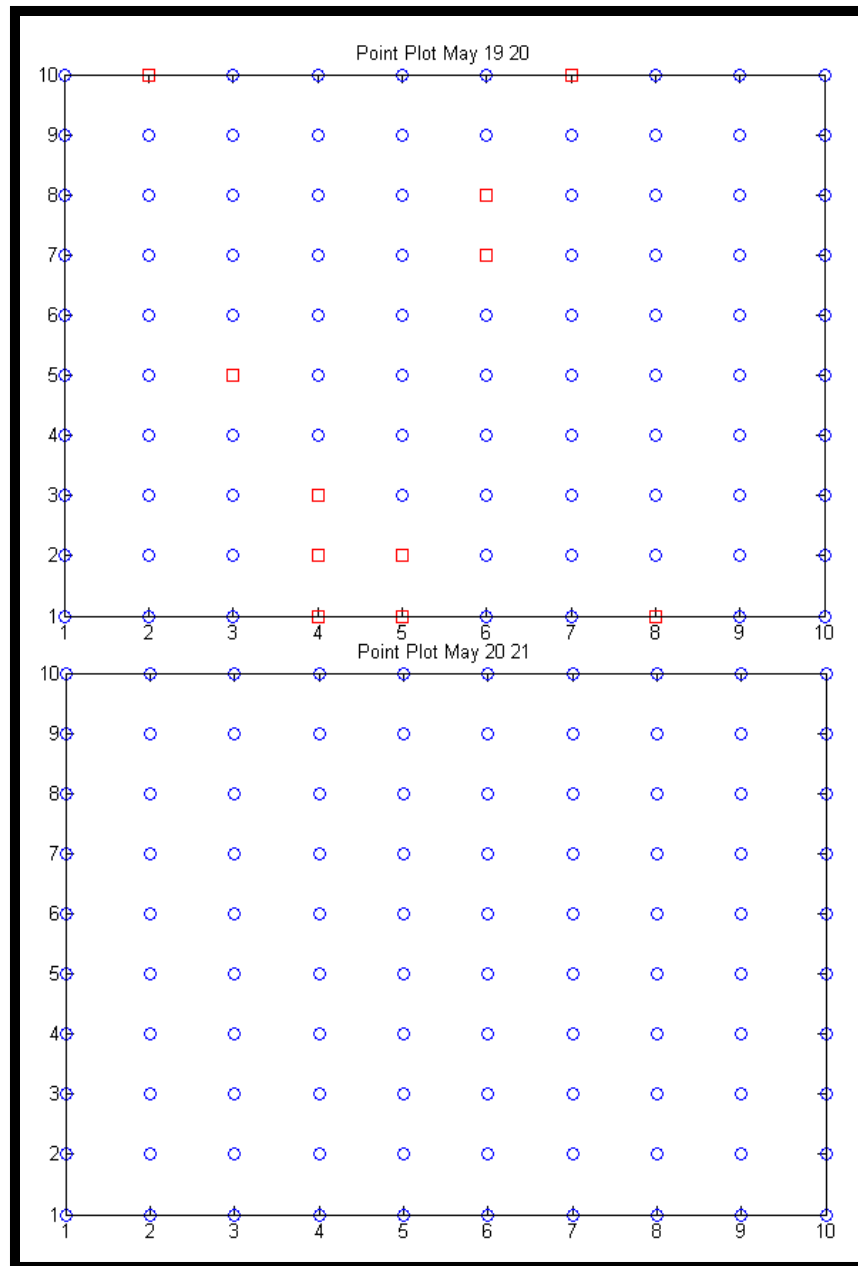


Figure 6.5e: Point plot of selected region May 19 to May 21

As observed from the grid, there is some ring formation in the central eastern region which is shown by the prediction algorithm around May 10 to May 12. The ring moves much more inward as seen from the actual map on May 28 in Figure 6.6a. It can be conjectured that the moving of the ring towards the center of the selected region can be seen in the plots of May 11 – 12 and May 16 – 17. Though the ring initially develops in the eastern region (Plot of May 10 -11) it later moves inward as shown in the plots for later days.

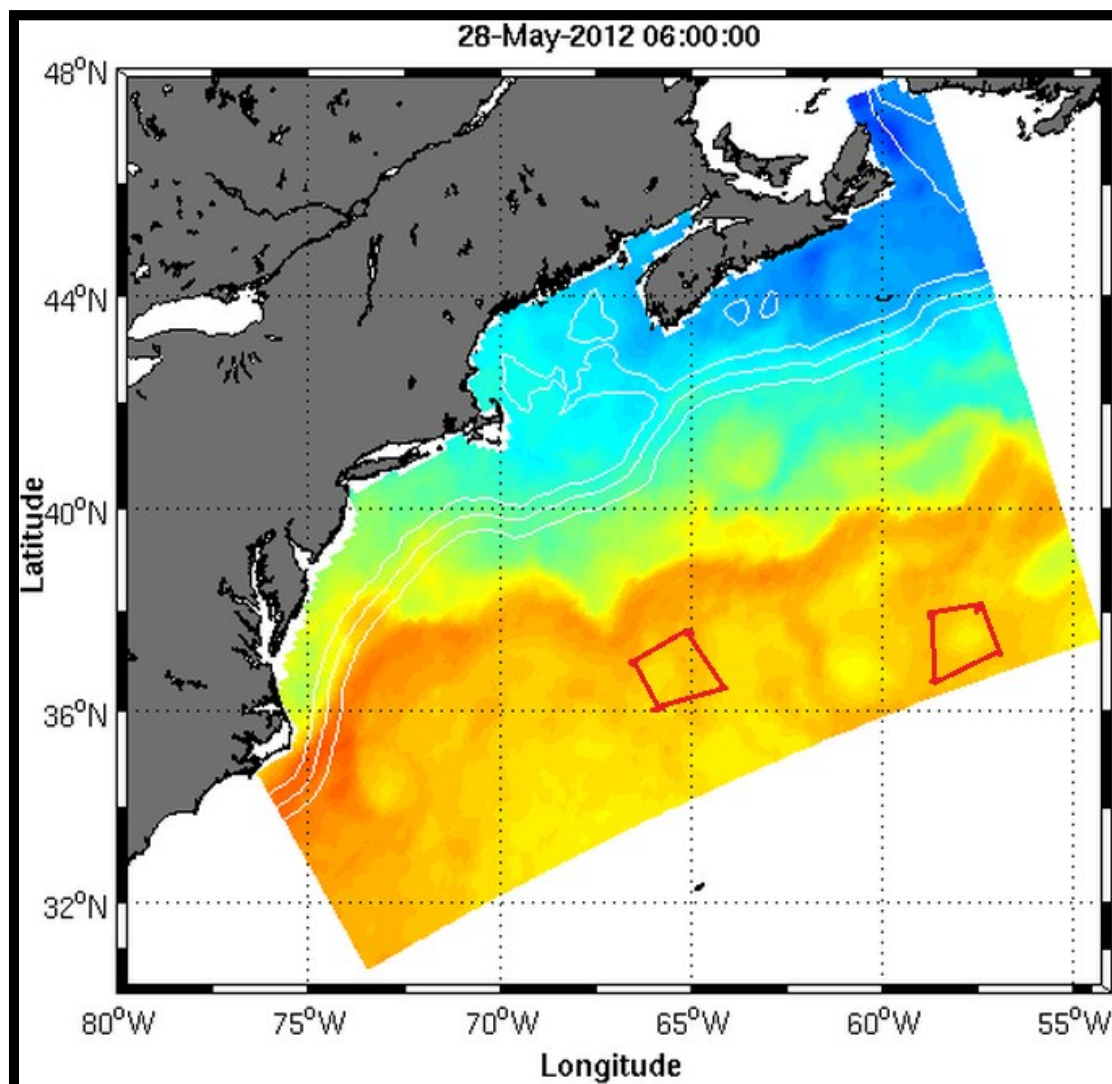
6.6b Data Set 3 - May 21

Figure 6.6a: May 28 Grid Showing the 2 Areas of May 21 Used For Analysis

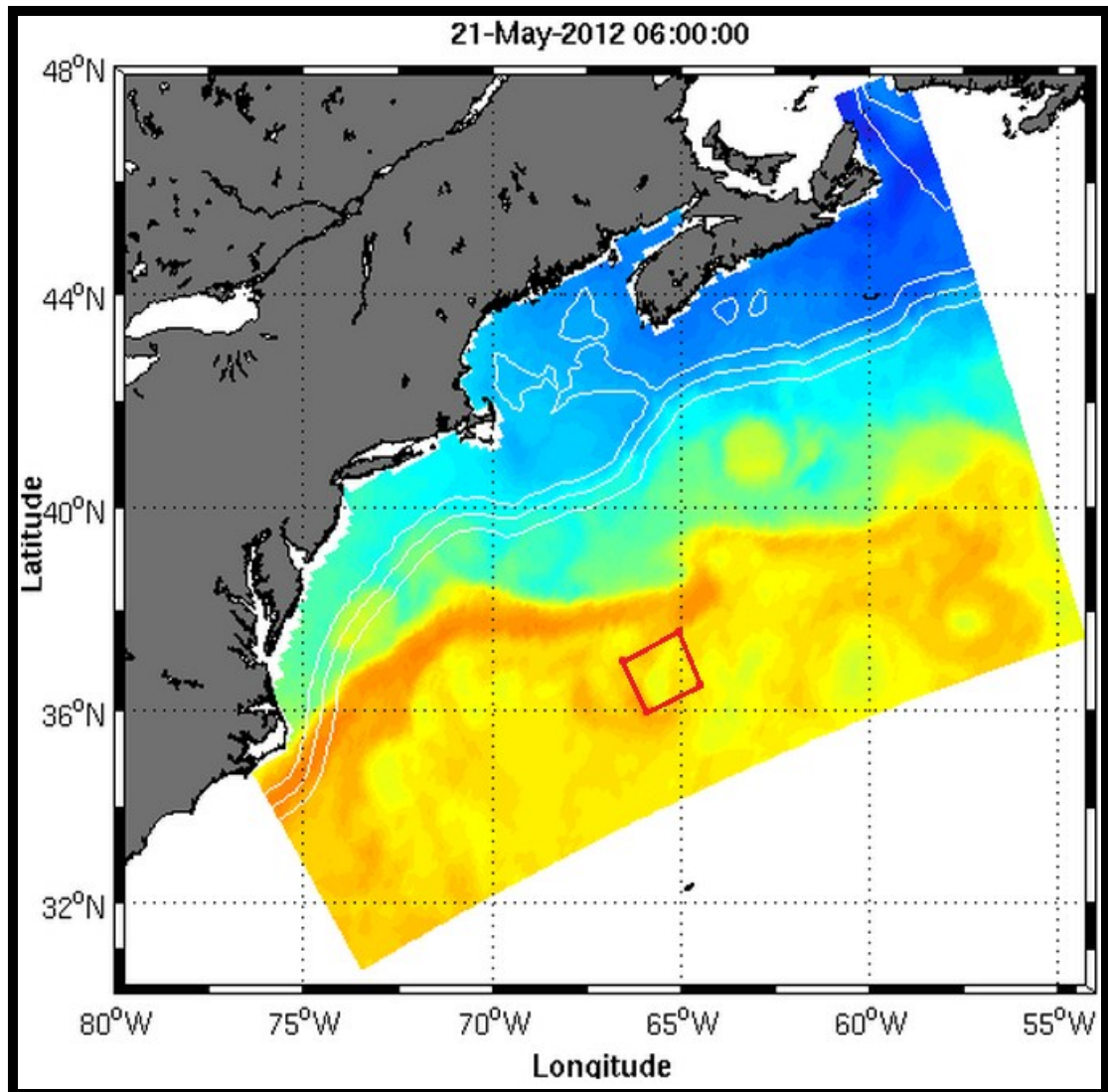


Figure 6.6b: May 21 Grid with the Selected Area for Analysis (Row 16 Col 60)

The third data set used for analysis is also selected from May 21 grids. The ring shown here has formed has a delta shaped region on May 21. The plots obtained from analysis are given below.

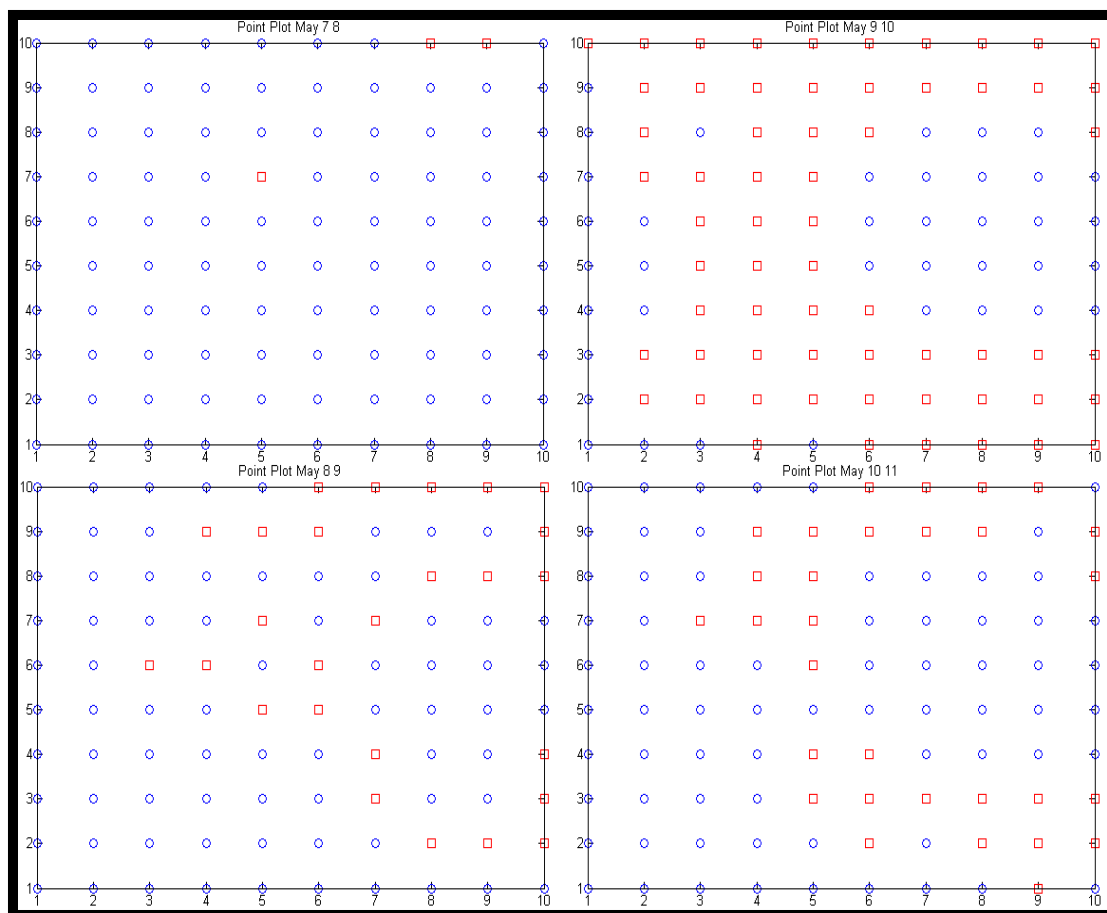


Figure 6.6c: Point plot of selected region May 7 to May 11

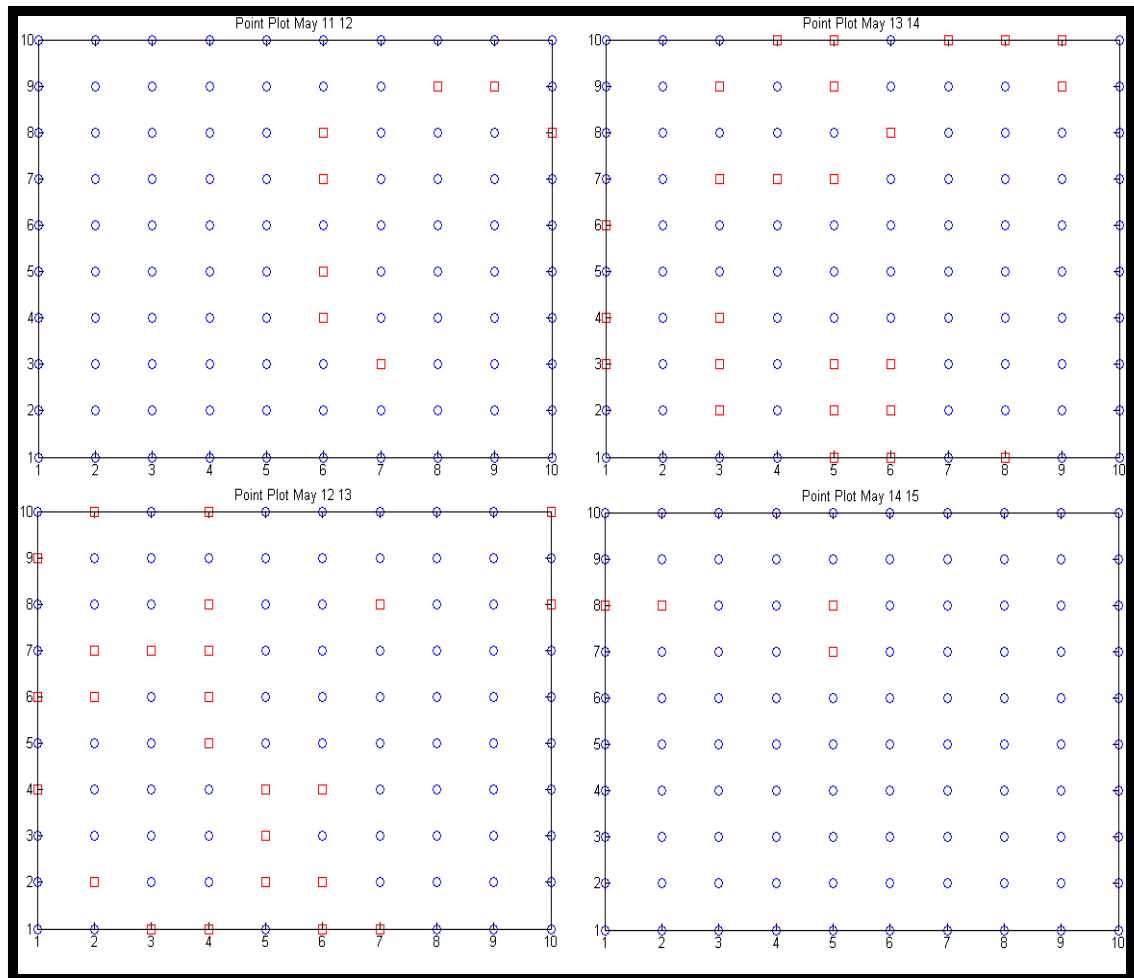


Figure 6.6d: Point plot of selected region May 11 to May 15

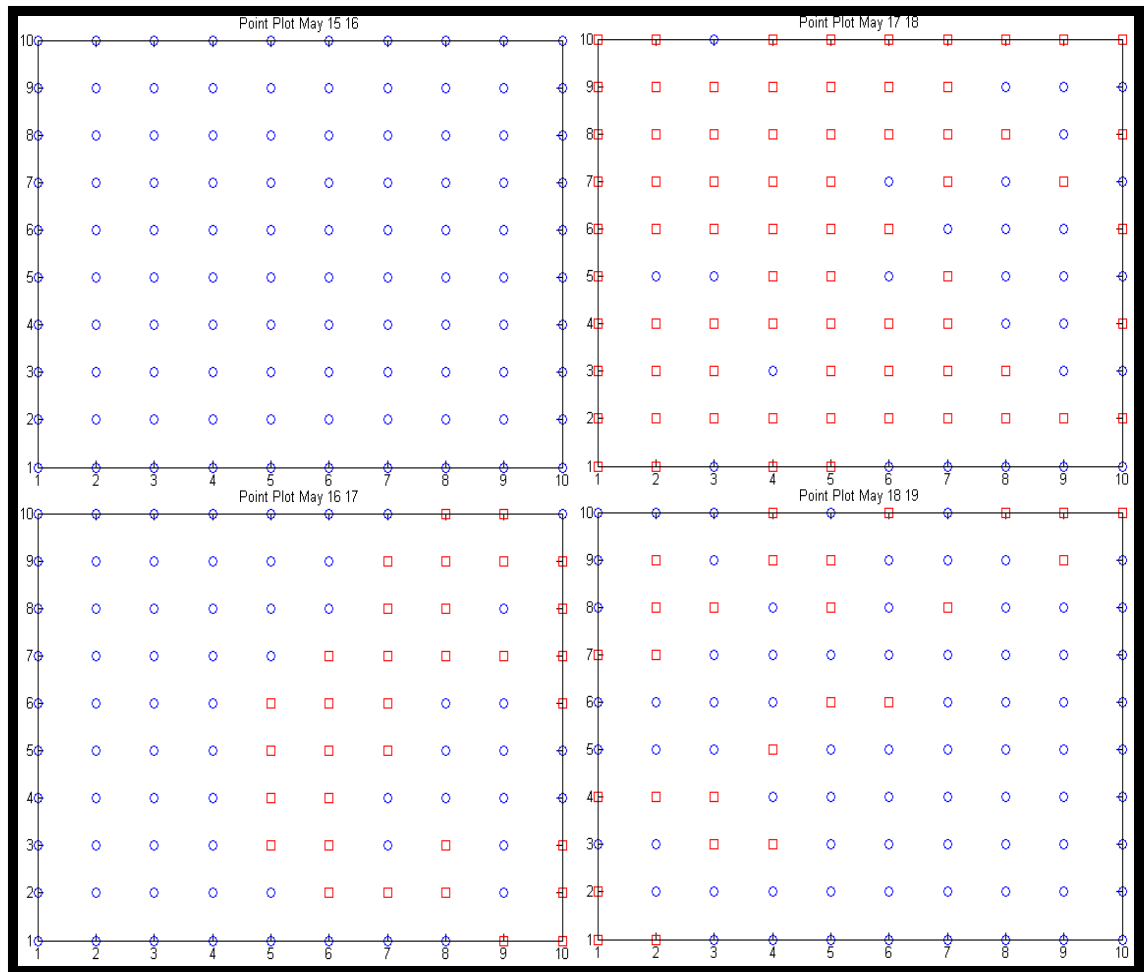


Figure 6.6e: Point plot of selected region May 15 to May 19

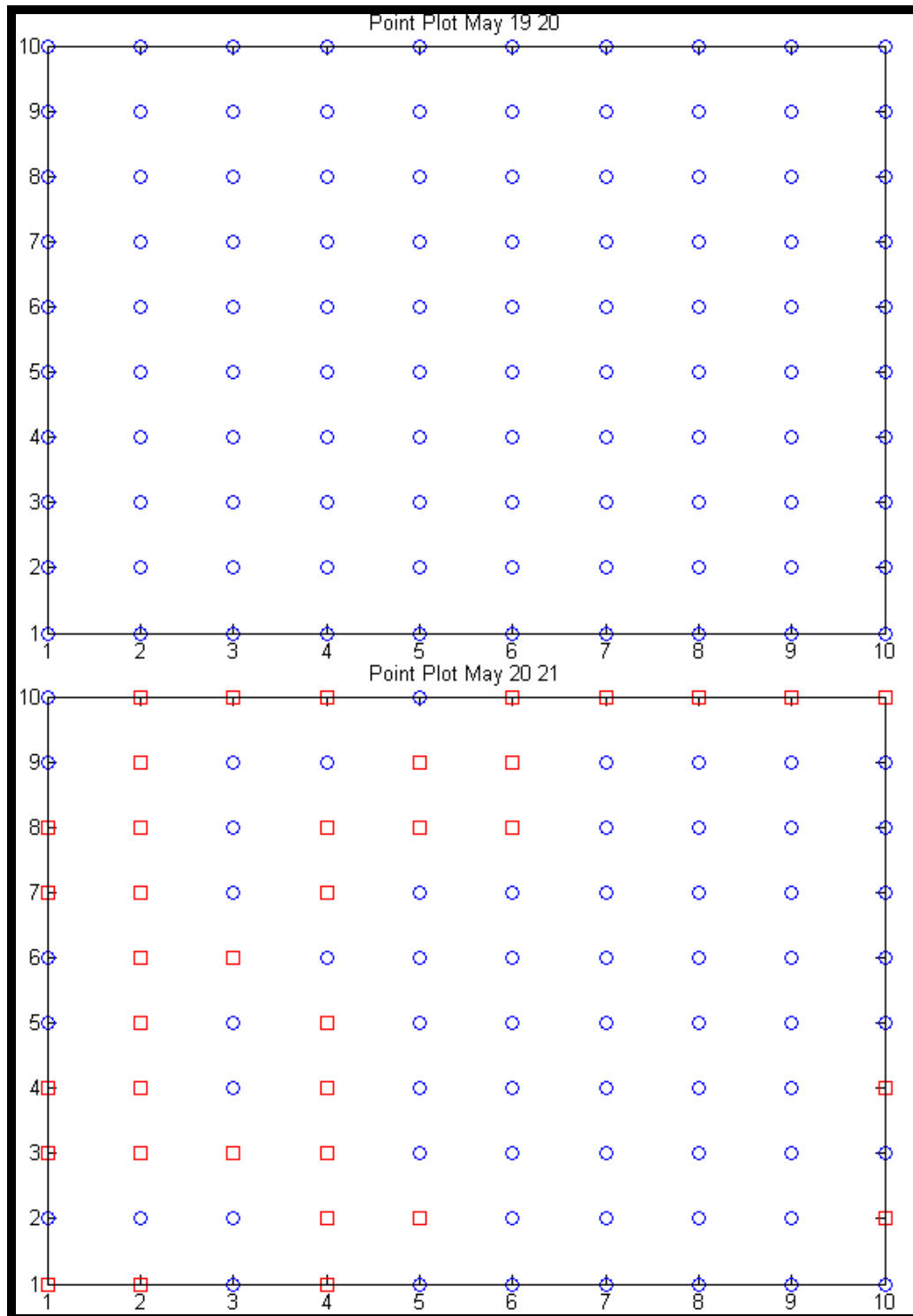


Figure 6.6f: Point plot of selected region May 19 to May 21

As it is seen from the plots predicted by the analysis, the delta shaped ring region formed by the red points can be seen in the plots of May 9 -10 and May 10 – 11 and more prominently in May 16 – 17 and May 17 - 18. However as seen from the plots, the red points seem to move to the left or west side. From the map of May 28 (Figure 6.6a) it is observed that the ring dissolves, but there is a slight trace of ring moving to the west. The same kind of trend is observed in the predicted plots of May 17 – 18. That plot shows the red points in a delta shaped ring as well as some points are present towards the left (west side) of the plot.

It can be concluded from the real maps as well as the point plots that qualitatively the results seem to match , but the prediction of the rings happen 3-4 days previous to the actual ring as seen on the real map. This could be attributed to the fact that our algorithm can only forecast based in the residual bias or predisposition that is stored in the system. Also the prediction results may have deviated from the actual results due to change in weather conditions. But overall, the results seem to depict the same trend as seen from the map.

CHAPTER 7. APPLICATION OF ALGORITHM- MACRO

ECONOMICS

7.1 Economic System Analysis

The second application of the prediction algorithm was Economic System Stability analysis. The data is obtained from the World Bank Database.

Economic indicators are traditionally analyzed with the help of time series models by observing their “trends” and “fluctuations in trend” with respect to time. However, a time series model can only treat a single uncoupled variable (a specific country in a specific dimension). The present DDP algorithm takes an alternative “systems” view of trend and stability. The prediction algorithm used here assumes that the performances of the countries in the global world are coupled. This can happen because of trade relationships – export led growth can only be as high or as low as the growth in the imports of another country. Economic performance across countries may also be coupled because of fixed amounts of specific global resources that countries have to share amongst themselves – such as funds for development from international agencies, foreign capital etc. The proposed DDP technique recognizes such competitive coupling where the countries compete for a share of the global resource “pie” that is essentially conserved.

The “systems” approach to analyze trend and stability is expected to be useful for certain purposes. For example, an international development or aid agency is deciding on the division of a fixed amount of funds and may want to identify a group of countries whose current favorable trends are expected to continue relative to each other.

In addition to this, coupling is also done between the various dimensions. The prediction algorithm that is used here couples 4 variables like GDP Per Capita at constant prices, average Lending Rate, Inflation rate as measured by the GDP Deflator and Unemployment.

The intuition behind this approach is as follows: Countries are assumed to converge to their steady states over time. At their steady states, differences in economic indicators amongst the countries are determined by differences in their fundamentals which change very slowly over time (such as natural endowments like land, mineral resources etc.; human capital; institutions; culture etc.). Homogenized differences considered in the present algorithm reflect the fundamental differences amongst countries at their steady states. The

rest of the algorithm then gives out a composite prediction that can tell whether the global system would be unstable at any point of time in the future. It also informs which dimension of the system is likely to change trend.

7.2 Choice of Variables/Dimensions

The variables of interest are GDP Per Capita at constant prices, average Lending Rate, Inflation Rate as measured by the GDP Deflator and Unemployment. These 4 variables form a conservative system. Lower lending rates imply higher GDP per capita and lower unemployment, because when banks provide loans at lower rates, costs of borrowing for businesses go down. If everything else remains equal, businesses expand; they hire more workers which result in higher GDP per capita and lesser unemployment. Lower lending rates are however usually accompanied by increase in the money supply as this the way the federal government pumps in money into an economy. A greater volume of money supply thus implies higher inflation. Thus there is an inverse relationship between inflation and unemployment.

7.3 Important Global Economic Events during 1993-2009

- The disintegration of the Union of Soviet Socialist Republics (Soviet Union) was completed in 1991. This was followed by balkanization in East Europe and Central Asia. The previously command economies (economy controlled by central government) switched to the market system (economy based on supply and demand) and went through a transition phase full of “market frictions” during the first half of the 90s.
- Major European countries began a process of forming a monetary and economic union in December 1995. This was done to replace individual national currencies by a common currency, the Euro. The European Central Bank was established in 1998 to manage the Euro.
- While in transition to a market economy, Russia went through severe economic crisis during 1997-1999 that resulted in her defaulting on its sovereign debt and a devaluation of the ruble. This crisis is known as the Ruble crisis. The crisis caused not only recessions in previously Soviet Bloc countries such as Estonia, Latvia, Lithuania, Belarus, Kazakhstan, Moldova, Ukraine and Uzbekistan but also deep financial crisis in the US and Europe where financial institutions had heavily invested in Russian sovereign bonds.

- During 1997-1999 several Asian countries such as Thailand, Indonesia, South Korea, Philippines, Malaysia and Hong Kong suffered financial and economic crises more famously known as Asian Financial Crisis that not only caused domestic recessions and their currencies to be devalued but also caused financial crisis in the US.
- In 1991, Tim Berners-Lee finally implemented the World Wide Web. This introduced a paradigm shift in communication and information technology, making information more readily available to the public. The advent of WWW also financially integrated the global economies. [Wikipedia]. Following this, the dot-com bubble ensued in the US with major global implications. Wide range speculation amid “irrational exuberance” caused NASDAQ Index to hit 5000 before collapsing starting April 2000.
- The Russian Ruble crisis and the Asian crisis of 1997-1999 were stabilized by keeping interest rates at abnormally low levels in the US till 2004. These low interest rates prompted financial institutions all over the world to heavily invest in highly risky and complicated financial assets such as mortgage backed securities and credit default swaps. The Federal Government began raising interest rates back to normal levels starting from 2004 and continued the process till 2006. This caused the housing market bubble to burst in 2006 and eventually lead to the worldwide financial meltdown of 2007-2008.
- The financial crisis of 2007-2008 was also accompanied in Europe by a series of sovereign debt crises. Several European countries either became bankrupt or came very close to it.

7.4 External factors that affect economic predictions

- In practice, economic and financial crises of every country are always stabilized by monetary and fiscal policies put in by the government so that the crisis never goes out of hand. This prevents complete and utter global economic failure. This was evident from the zoom out plots as there was no long term localization index. Thus central banks lower interest rates when there is fear of recession and unemployment or raise them when there is fear of inflation. Similarly high unemployment in the private sectors is often combated by temporary public employment programs. So in many cases when we expect that the global economic system is going towards

- failure it might be tackled immediately in by the government by putting in external policies.
- Instability predictions in the economic indicators can also be interpreted as a “predisposition” or “residual bias” built into the system because of past and present course of events. In a mechanistic sense, such residual bias or predisposition occurs in a system as its inherent structure becomes path dependent (because of accumulated excess curvature). The conservativeness of the system manages to “unload” the stress caused by stimulation, essentially by creating a dislocation. Unlike material systems, the dislocation in an economic system resides in micro-scale structural (and persistent) discrepancies, and manifests itself by introducing such predisposition or residual bias on a mathematical manifold, that mathematically embodies the underlying struggle for resources in an economic system. In other words, such dislocations pre-condition the economic system via persistent residual stress that exists with non-zero values even when equilibrium is achieved in global aggregated scales.
 - The data sets for the Lending Rate and Unemployment considered as input to this prediction algorithm had many missing data points. Interpolation methods and other (perhaps incompatible) sources had to be used to fill up the missing data points resulting in some level of “noise” in the data.

7.5 Preprocessing Data Files

The data is available from World Data Bank as a comma separated value file that lists out 81 countries and the value of the particular variable for the years 1993 to 2009. For each year there are 81 values for these 81 countries. The value for a specific year and a specific country is transformed into the same scale by dividing it by the average of all values of all countries for a particular year. These values are then arranged in a **9 x 9** matrix. This matrix serves as the sample input to the prediction algorithm.

7.6 Analysis Procedure

In the Economic Stability Prognosis primarily 2 types of analysis were done almost similar to the previous applications. The first one was Zoom Out procedure which was done to get critical localization index. The second type of analysis was done for the entire data set at every year starting from 1993 to 2009 to observe the trend for each variable (GDP Per Capita, Lending Rate, GDP Deflator and Unemployment) and predict whether the system would become unstable in the future (or reverse the trend) or not.

7.6a Critical Localization Index

The zoom out plots for the Economic System analysis are given below in Figure 7.1 which shows average of absolute values of $\kappa, \frac{1}{LTilda}, \frac{1}{L}$ against aggregation level. For the Economic system analysis only 1 type of chain length was calculated: - the short term chain length. In the case of Economic System only the extension of $\frac{1}{L}$ line meets the symmetry of the κ line.

It is so that the Economic System is kept stabilized and controlled by the Government of each and every country by monetary and fiscal policies put in by the government so that the crisis never goes out of hand. This prevents from resulting in any catastrophic results or global economic failure. That is the primary reason why there is no long term turbulence can be observed in the global economic system. If there would have been a chance of long term instability it would have shown in the zoom out plots and would have come as an intersection between the symmetry of the κ line and extension of $\frac{1}{LTilda}$ line.

The determination of critical chain length/localization index follows the same procedure as explained in section 4.5b. The intersection point of the symmetrical line of κ and $\frac{1}{L}$ line is taken to be the value of the short term localization index. The X values of these intersection points are measured. Since the zoom out plots are log scale plots, the log value of these point is converted to an actual number of points. This number of points represents the chain length that is occurring in a total of 9 points.

If the number of unstable points forms a chain greater than the short term chain length then it can be predicted the system might show instability in the future. But this instability is not long lived but rather will be a short term phenomenon.

Since this chain length is only valid for 9 points, these needs to be converted to a value that can be applicable to a set of 81 points (or the number of points being considered in the sample data set).

Short term chain length calculations for **Lending Rate** in 9 points are given as:-

$$\frac{\log_{10}^x}{\log_{10}^9} = \frac{0.836}{0.95} = 0.88$$

Keeping the ratio constant as 0.88 the chain length can be translated to a value in 81 points as given below:-

$$\frac{\log_{10}^x}{\log_{10}^{81}} = \frac{\log_{10}^x}{1.908} = 0.88 \Rightarrow x = 10^{1.908 * 0.88} = 10^{1.67904} = 47.75 \cong 48$$

So the critical short term localization index value is 48 for a set of 81 points. This is also used as the corresponding threshold value in the prediction algorithm.

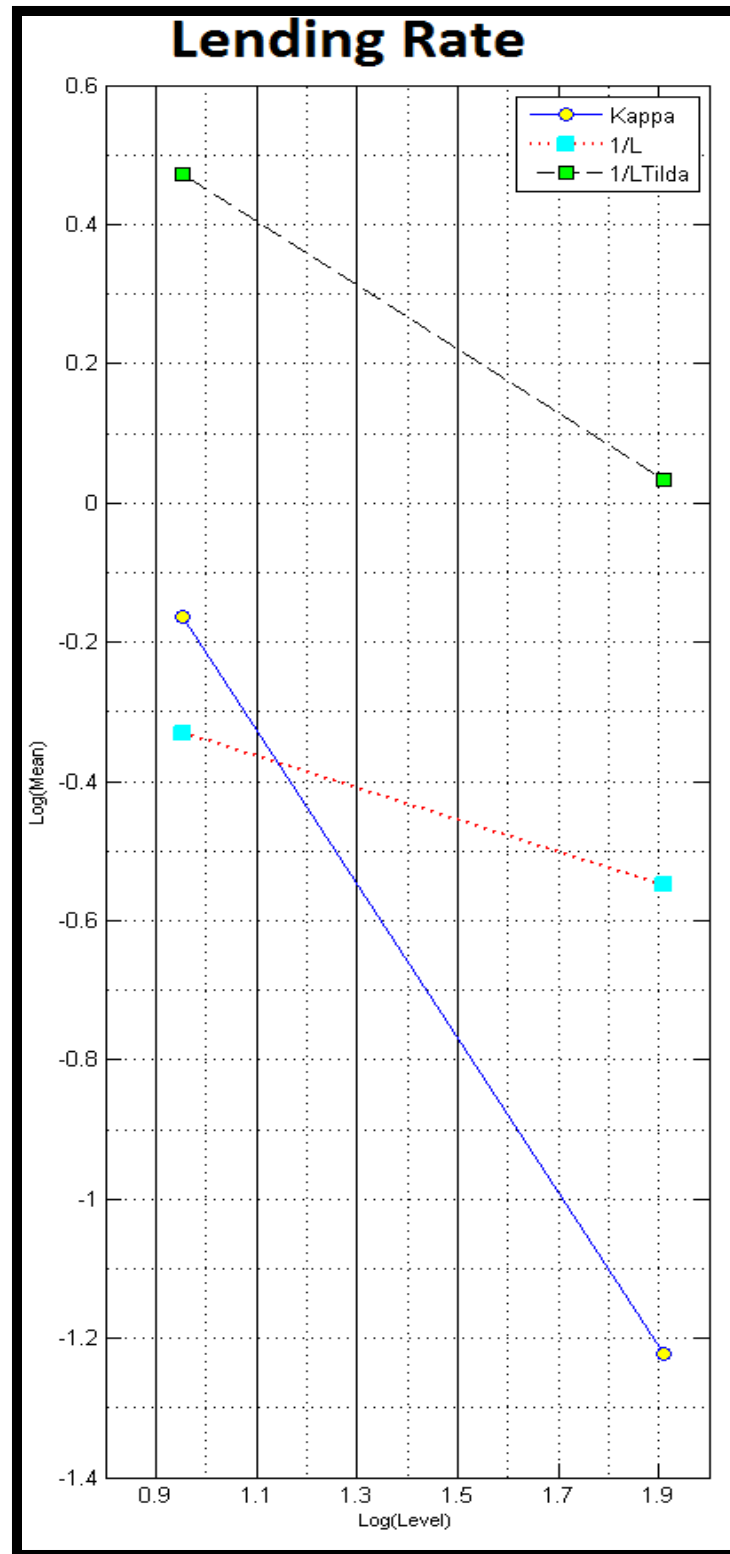


Figure 7.1: Zoom Out Plots for Macro Economic Analysis

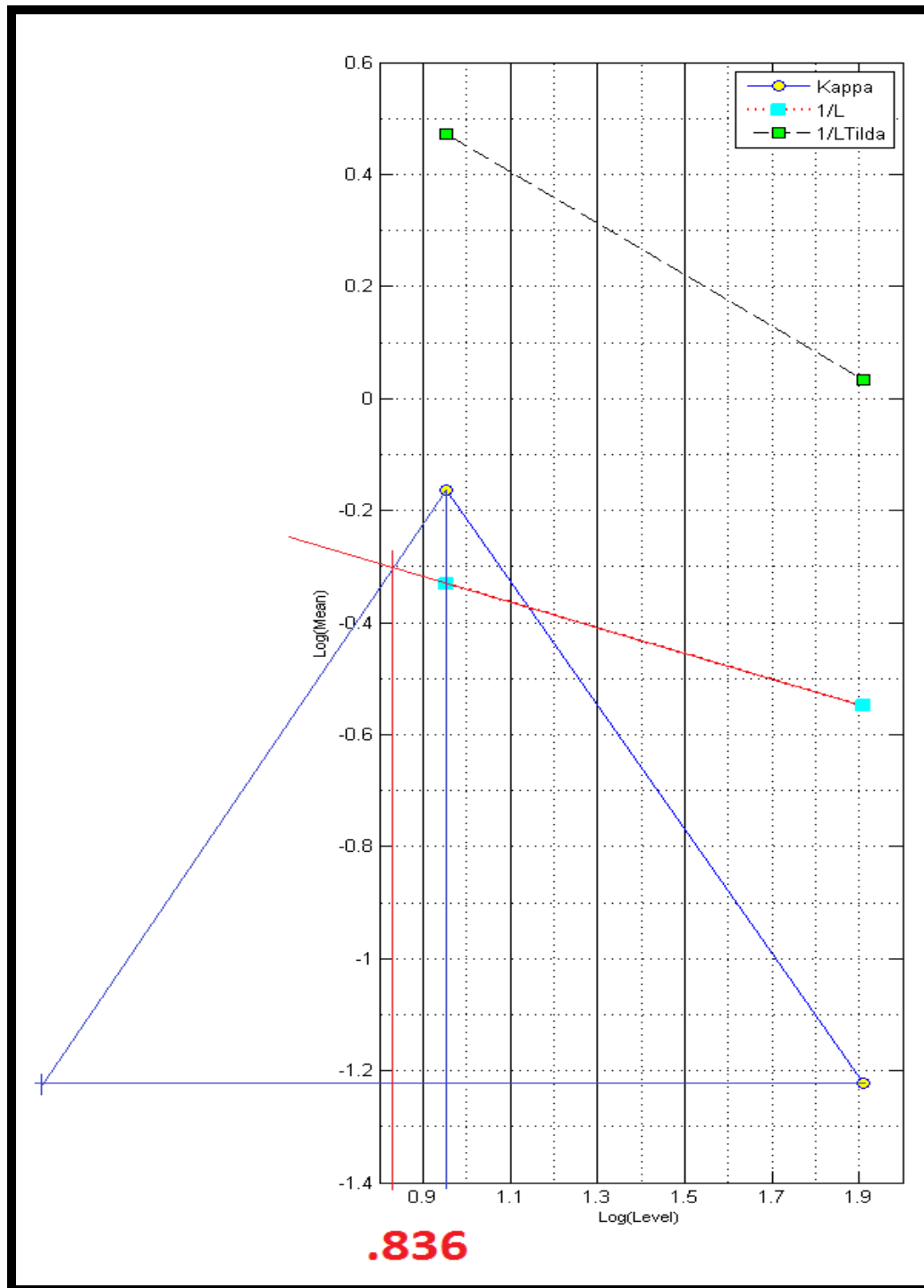


Figure 7.2: Short Term Chain Length Calculations for Economic Analysis

7.6b Path Dependency Index

The path dependency index is used individually as well as in conjunction with the above localization index to look for trend reversals in the Economic System. First the points in the sample data set are categorized according to the categories given below.

Category 1	Full Stability meaning $\frac{abs(Kappa)}{abs(KappaLong)} < 1$ and $\frac{abs(Kappa)}{abs(KappaShort)} < 1$
Category 2	Short term instability or long term stability meaning $\frac{abs(Kappa)}{abs(KappaShort)} > 1$
Category 3	Short term stability or long term instability meaning $\frac{abs(Kappa)}{abs(KappaLong)} > 1$
Category 4	Conditional Stability meaning there is scope to reduce the point's curvature to zero by making $-\frac{1}{2} < \alpha_{prime} < 1$
Category 5	Full Instability in 1 Dimension meaning Line Defect
Category 6	Full Instability in more than 1 Dimensions meaning Area Defect
Category 7 = (Original Category 7 + Category 8)	Full Instability in more than 2 Dimensions meaning Volume Defect + Chain Length Greater than Short Term Localization Index

Figure 7.3: Categorization of Points according to Path Dependency Index. (Path Independent and Path Dependent Categories)

Next the path dependency categories are used to plot the trend of all countries in all the 4 dimensions (GDP Per Capita, GDP Deflator, Lending Rate and Unemployment) for the years 1993 to 2009.

7.6c Trend Reversal Results

Following the algorithm described in section 4.7 the countries against their corresponding Path Dependency Indices are plotted for different years. These plots are done for all 4 dimensions. The plots are produced here for each dimension and there are 4 parts in each plot (relating to each dimension). To forecast economic performance, the following criteria are used:

PDI < 5: Current trend continues as extrapolated by a quadratic polynomial fit based on most recent three points.

PDI > 5: Current trend (as interpolated by most recent three points) reverses.

PDI = 5: Current trend continues as extrapolated by its tangent line at the most recent point. Thus category 5 essentially overweighs the present or most recent point in a three point extrapolation scheme.

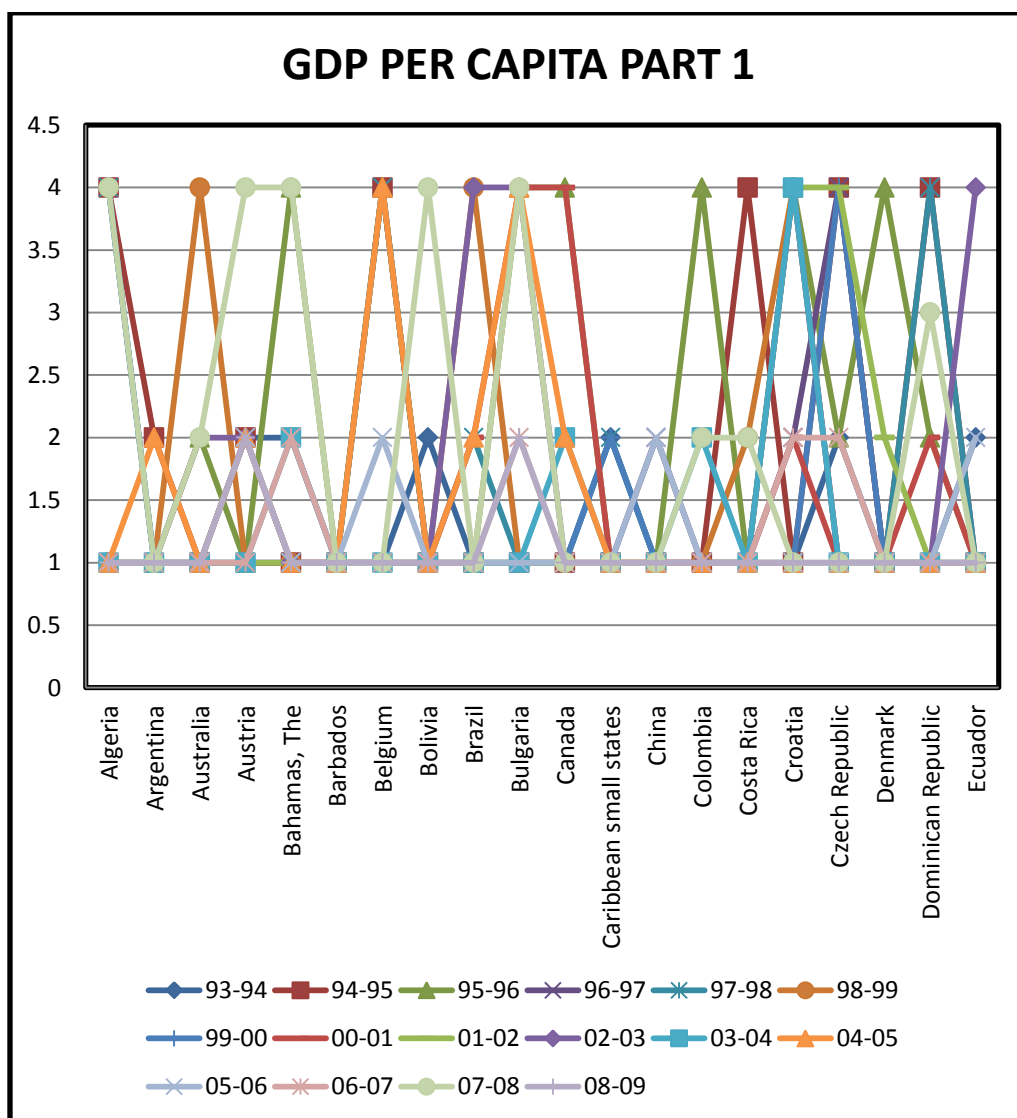


Figure 7.4a: GDP per capita of selected countries against path dependency indices part 1

The first 4 plots (Figure 7.4a, Figure 7.4b, Figure 7.4c and Figure 7.4d) shows the GDP Per Capita of the 81 countries against their path dependency indices for the years 1993 to 2009. Observing the GDP plots it is seen that the path dependency index seldom crosses 5 which is the threshold condition for declaring the system to be truly path dependent.

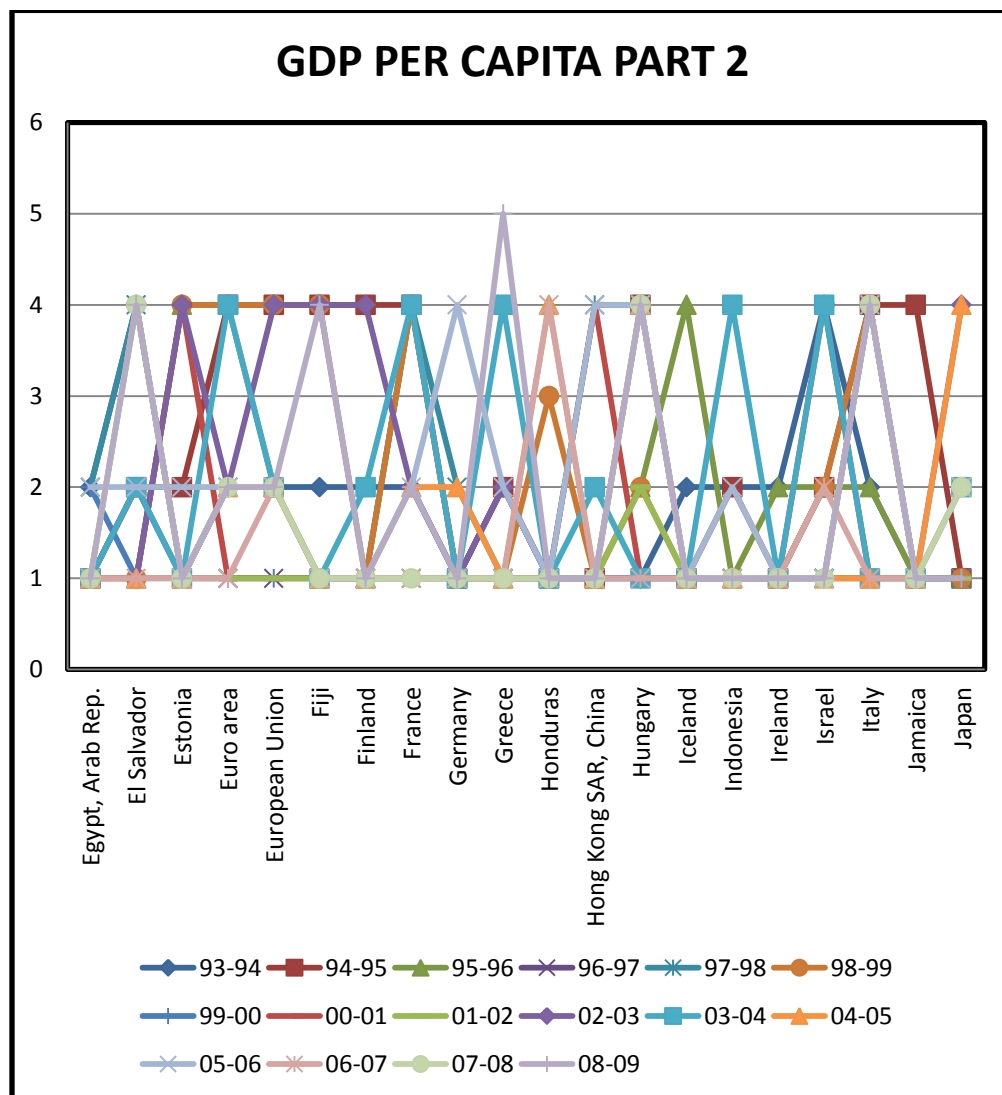


Figure 7.4b: GDP per capita of selected countries against path dependency indices part 2

The countries which show a 5 is in the year 2008 – 2009 are Greece, New Zealand, and Slovenia. This means that during those years and after that the changes in GDP Per Capita had been very smooth almost following the extrapolated tangent line drawn at the value in 2009.

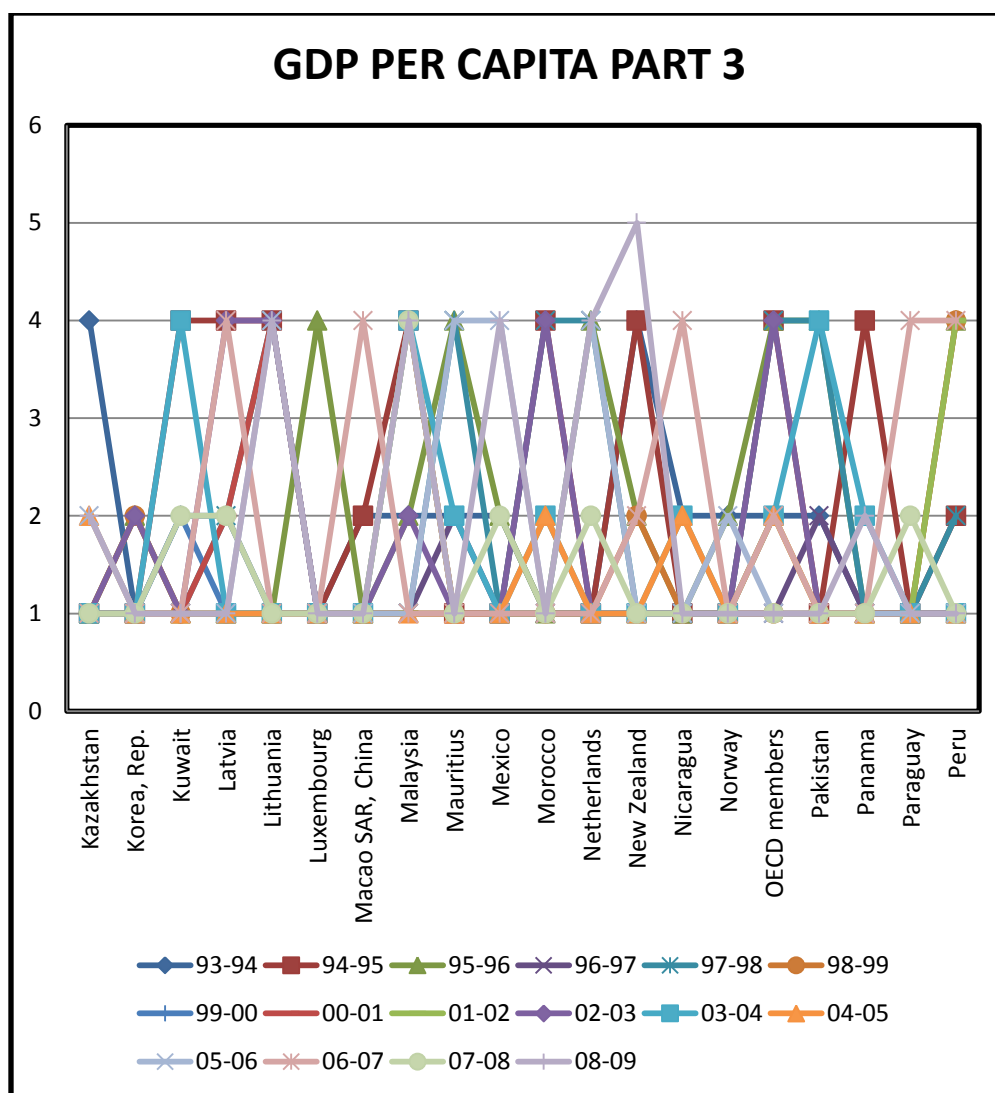


Figure 7.4c: GDP per capita of selected countries against path dependency indices part 3

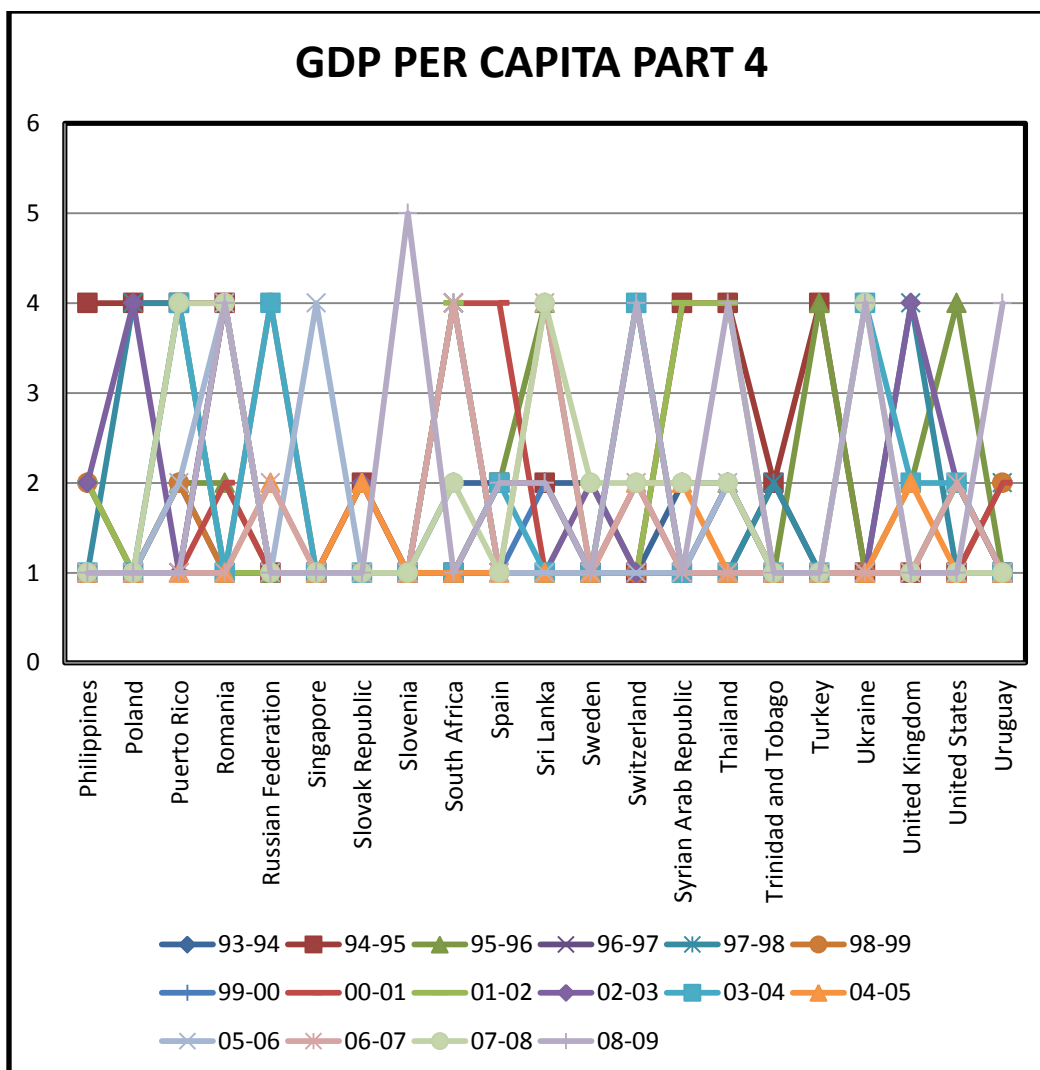


Figure 7.4d: GDP per capita of selected countries against path dependency indices part 4

The GDP per capita of Greece, New Zealand and Slovenia are shown in Figure 7.4e. From this plot it can be observed that at 2008 to 2009 there was a slight change in GDP Per Capita for these countries but after 2009 the curve for these specific countries continues with these changes very smoothly or does not change at all (it continues in a straight line with the same trend). As expected from extrapolation of present tangent line, Greece and New Zealand continues the downward trend from 2007-2008 into 2008-2009. Slovenia, however, temporarily reverses its upward trajectory till 2008 in 2008-2009, before continuing in slightly upward to flat trend.

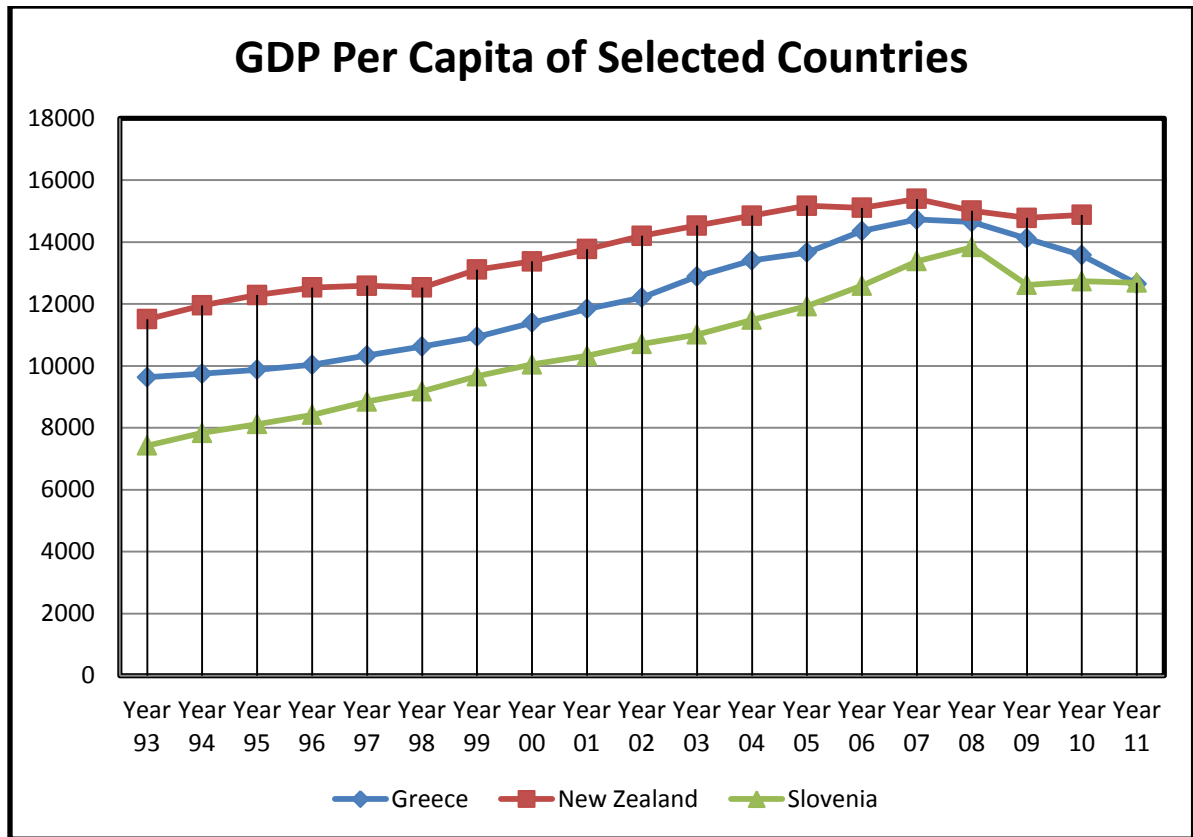


Figure 7.4e: GDP per capita of Greece, New Zealand, and Slovenia

The next 4 plots show the path dependency indices for the dimension “Lending Rate” in 4 parts. The same method as GDP Per Capita is followed in this case to interpret the results.

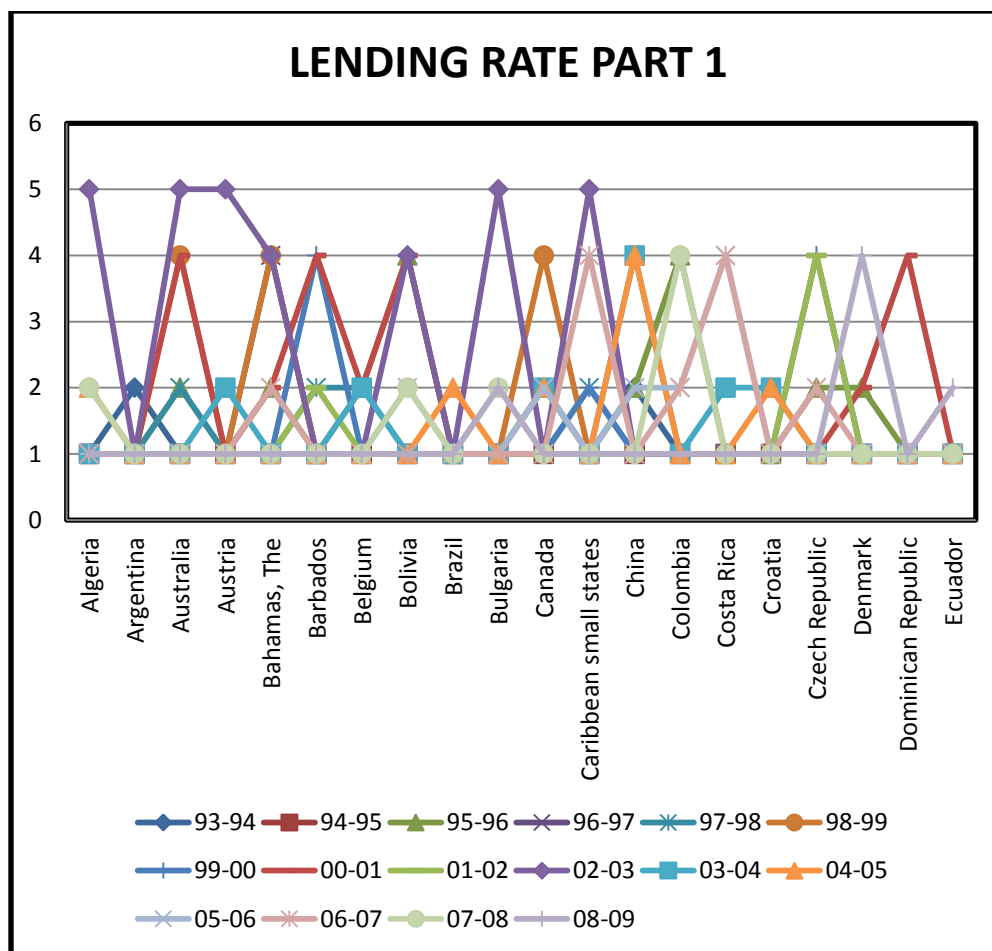


Figure 7.5a: Lending rate of selected countries against path dependency indices part

1

In lending rate also there are no countries that exceed a category of 5 in any year. The countries that have touched a category of 5 are Algeria, Austria, Australia, Bulgaria, Caribbean Small States, Hungary and Israel in the year 2002 to 2003. Some other countries like Nicaragua have reached category of 5 in the year 1995 to 1996 and Morocco, South Africa in the year 2000 to 2001. These plots of lending rate against categories are shown in Figures 7.5a, 7.5b, 7.5c and 7.5d for the years 1993 – 2009.

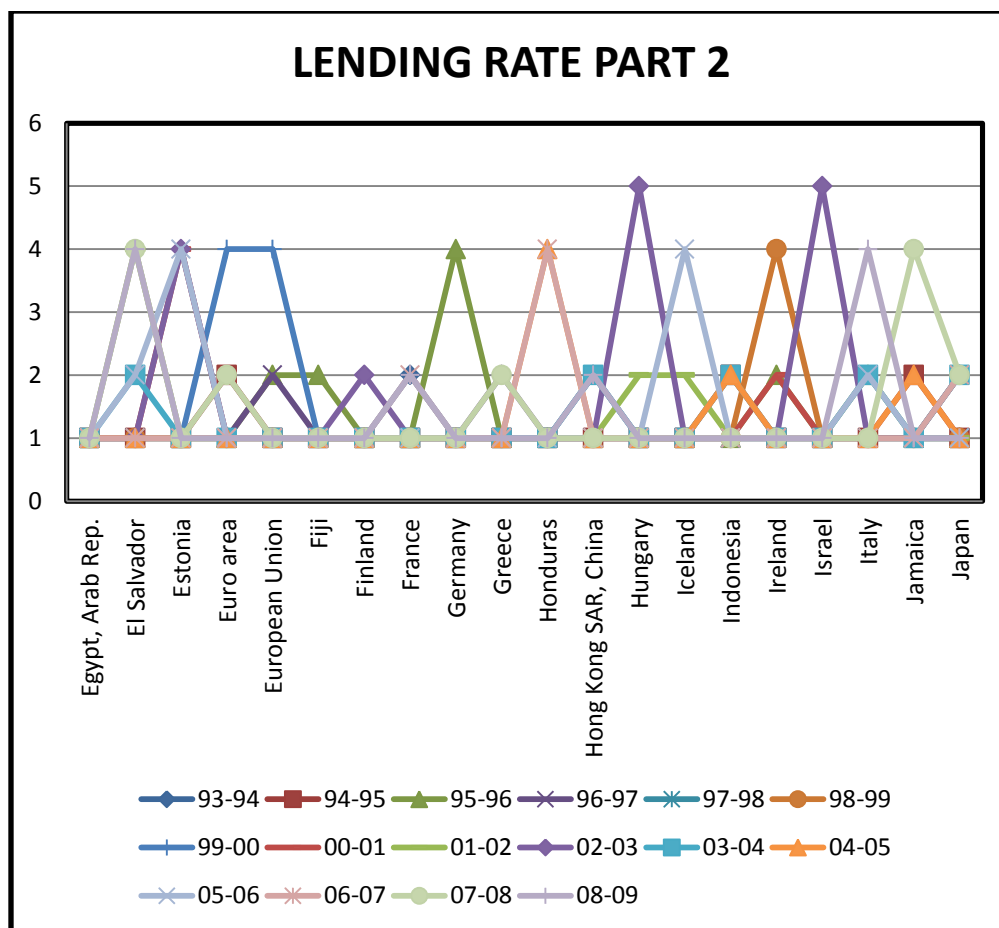


Figure 7.5b: Lending rate of selected countries against path dependency indices part 2

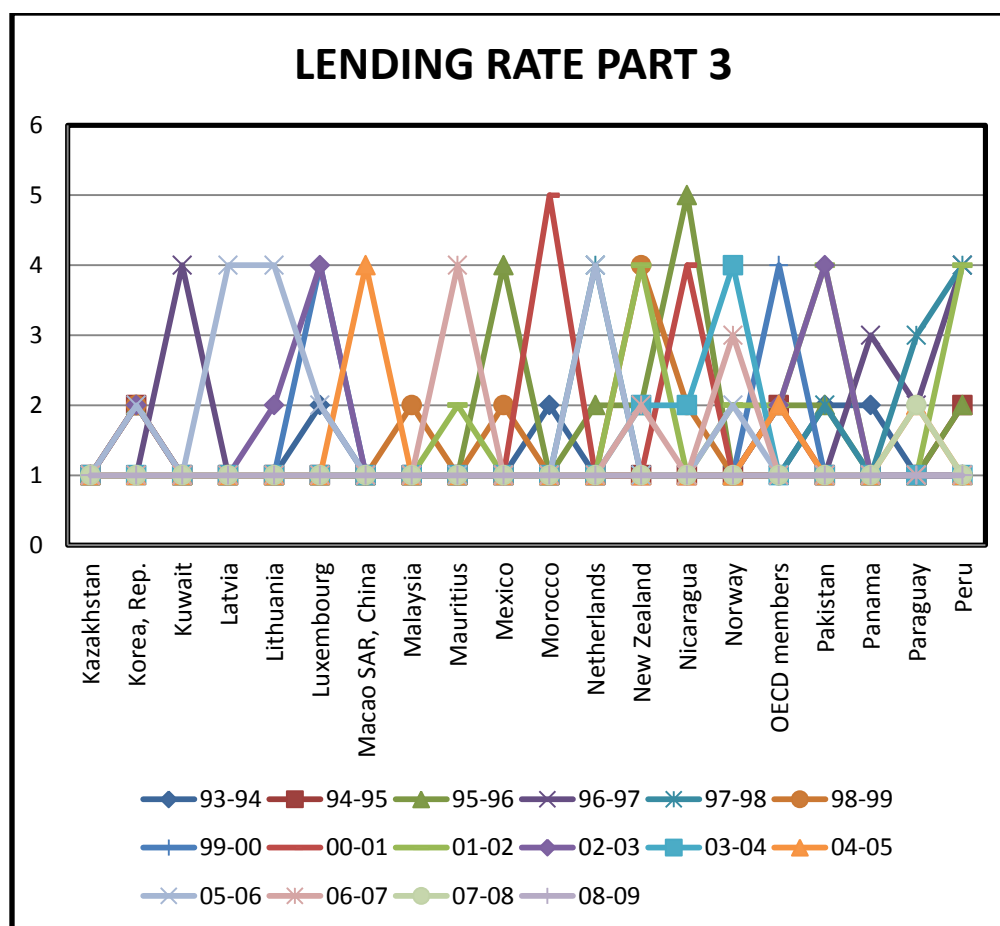


Figure 7.5c: Lending rate of selected countries against path dependency indices part 3

The “lending rate” of such countries (the ones that reached a category of 5) across time is plotted in Figure 7.5e and Figure 7.5f. As seen from the plots after 2003 the lending rate of Algeria, Australia, Hungary and Israel changed a little bit but the change was not too large and all these countries managed to remain within a band of 5% to 13% after 2003. By observing the trend of these countries over time it can be seen that other than Hungary, the countries like Algeria, Australia and Israel always remain within 5% and 20% for the time span 1993 – 2009.

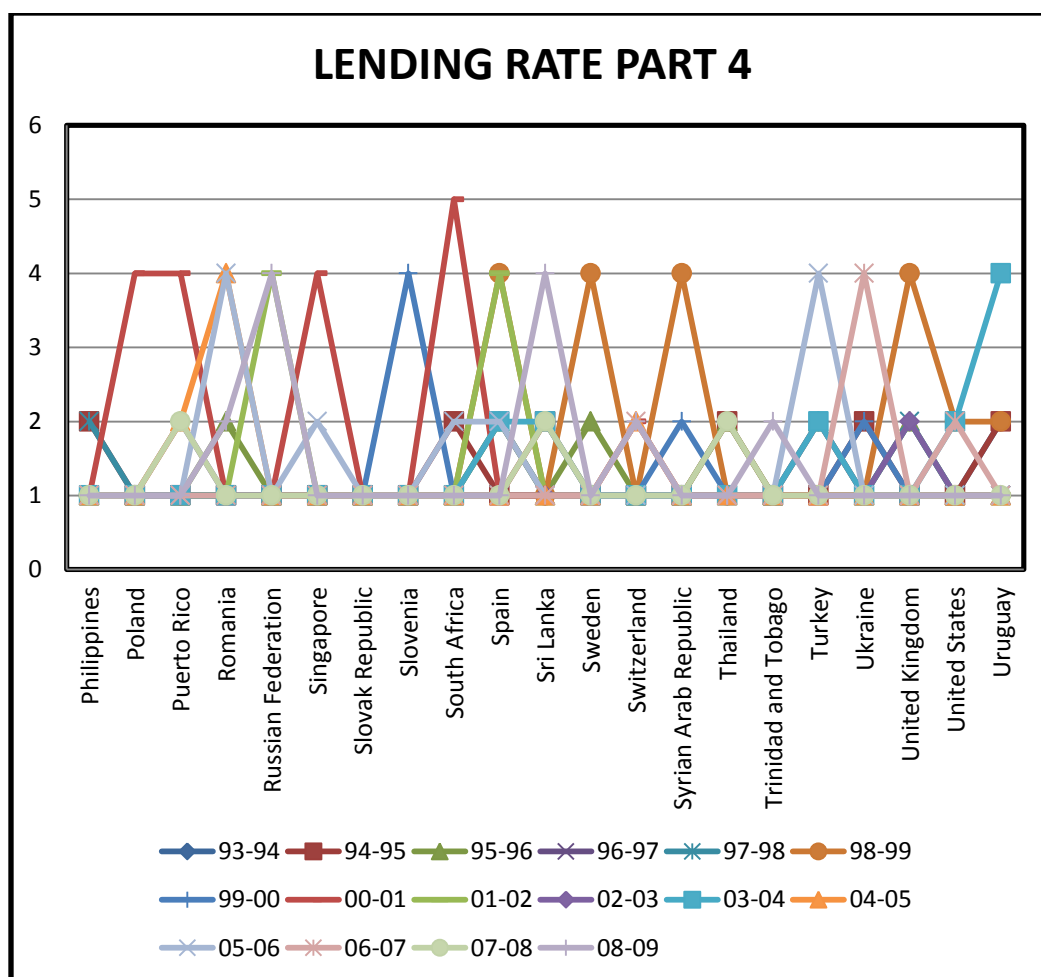


Figure 7.5d: Lending rate of selected countries against path dependency indices part 4

As expected from extrapolation of present tangent line, the curves of Algeria and Australia continues the almost flat trend from 2002-2003 into 2003-2004 seen in Figure 7.5e. The change of Lending Rate for Hungary in the year 1994 to 1995 is not captured by the algorithm probably because the change between the specific years of 1994 and 1995 was negligible but overall the change was noticeable. The curves of Hungary and Israel are slightly deviated from the extrapolation of the tangent line. Hungary shows an upward trend after 2003 which soon reverses in nature and Israel shows a downward trend which soon flattens. There was a regime change in East Europe during 1991 – 1992. So some data before and after this time period could be very noisy.

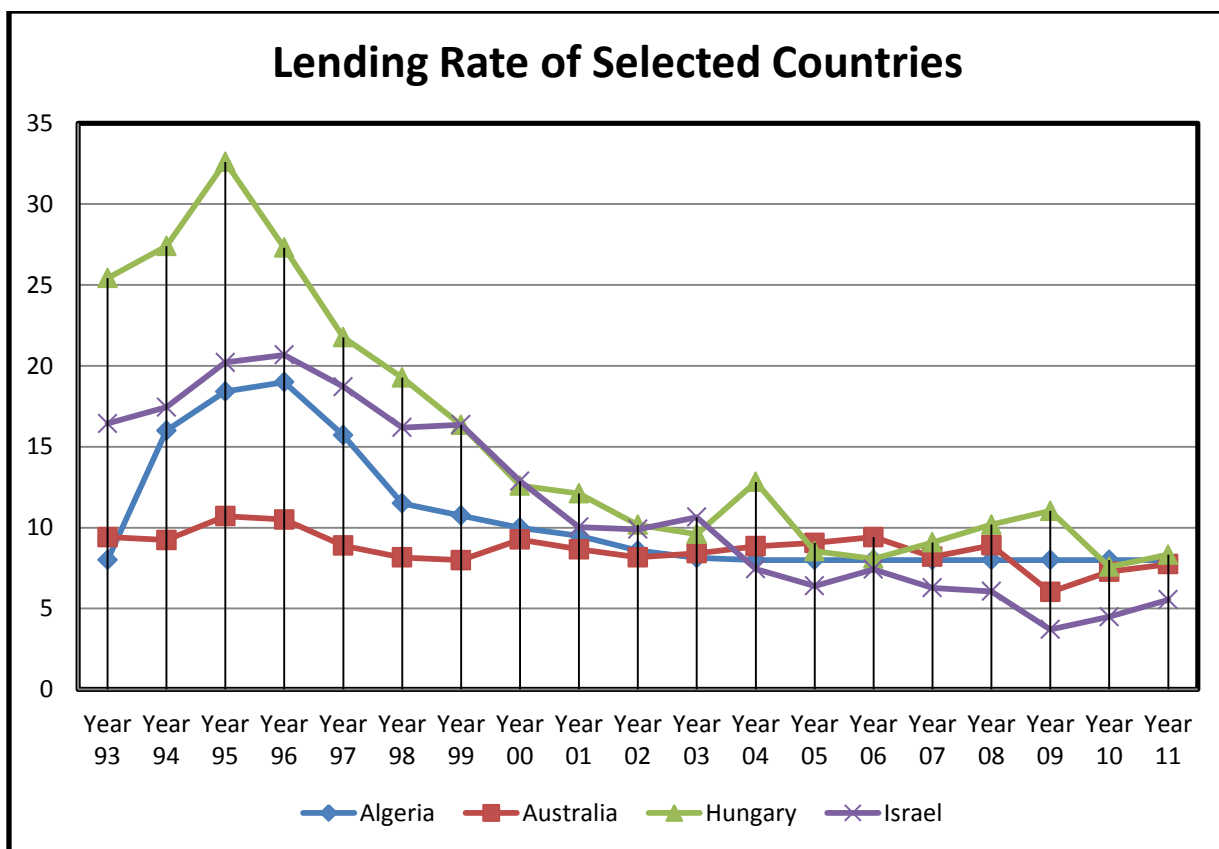


Figure 7.5e: Lending rate of Algeria, Australia, Hungary and Israel

Figure 7.5f shows the plot of Lending Rate of Nicaragua and South Africa against years 1993 to 2009. After the year 1996 Nicaragua had a slight change but mostly it continued along the tangent line. Nicaragua continues its slightly upward to flat trend from 1995-1996 into 1996-1997. Nicaragua did dip towards the downward trend in the year 1998 to 1999, which stabilized immediately continuing in a straight line from 1999. For most of the time span Nicaragua remained within 10% to 20%. As in the case of South Africa there was a slight change towards the upward trend in 2001 which is a slight deviation from the extrapolated tangent line but after this year the changes are smooth and also roughly within 10% to 20%.

In all the above cases of South Africa, Hungary and Israel can be explained to be the predisposition of the system towards the residual stress rather than the actual forecast of the events.

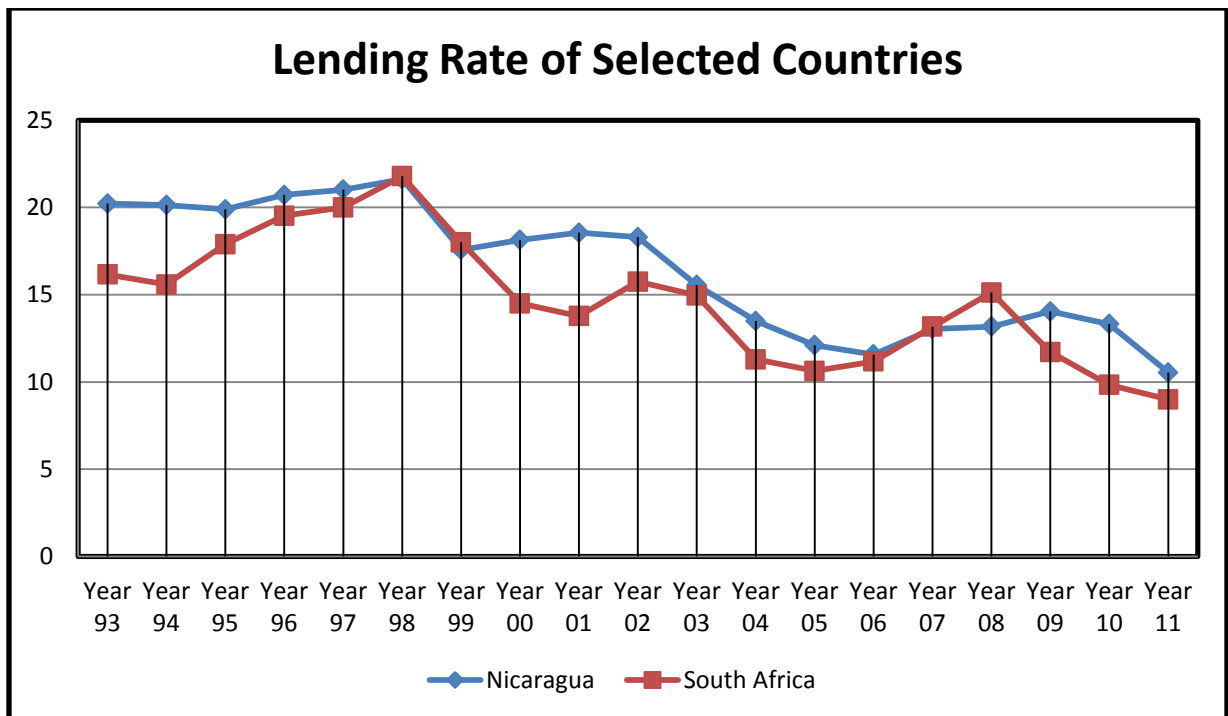


Figure 7.5f: Lending rate of Nicaragua and South Africa

The next 4 plots show the countries against their respective path dependency indices for the year 1993 to 2009 in dimension Inflation as measured by GDP Deflator.

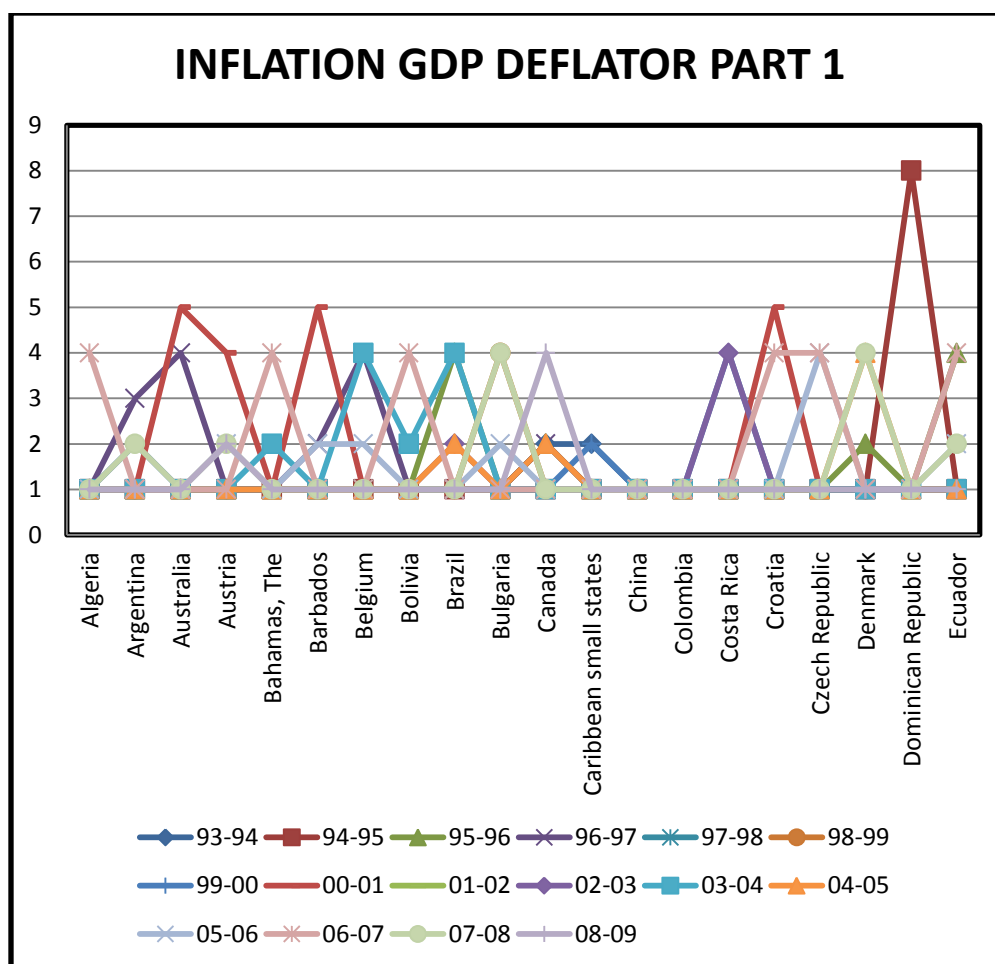


Figure 7.6a: Inflation GDP Deflator of selected countries against path dependency indices part 1

There are some countries that reach the level of 5 in the year 2000 to 2001 in GDP Deflator. These are Australia, Barbados, Croatia, Estonia, Korea Republic, Netherlands, New Zealand, Poland, Slovak Republic, Spain and Syrian Arab Republic. The only other country that shot up to a level of 8 in the year 1994 to 1995 is Dominican Republic.

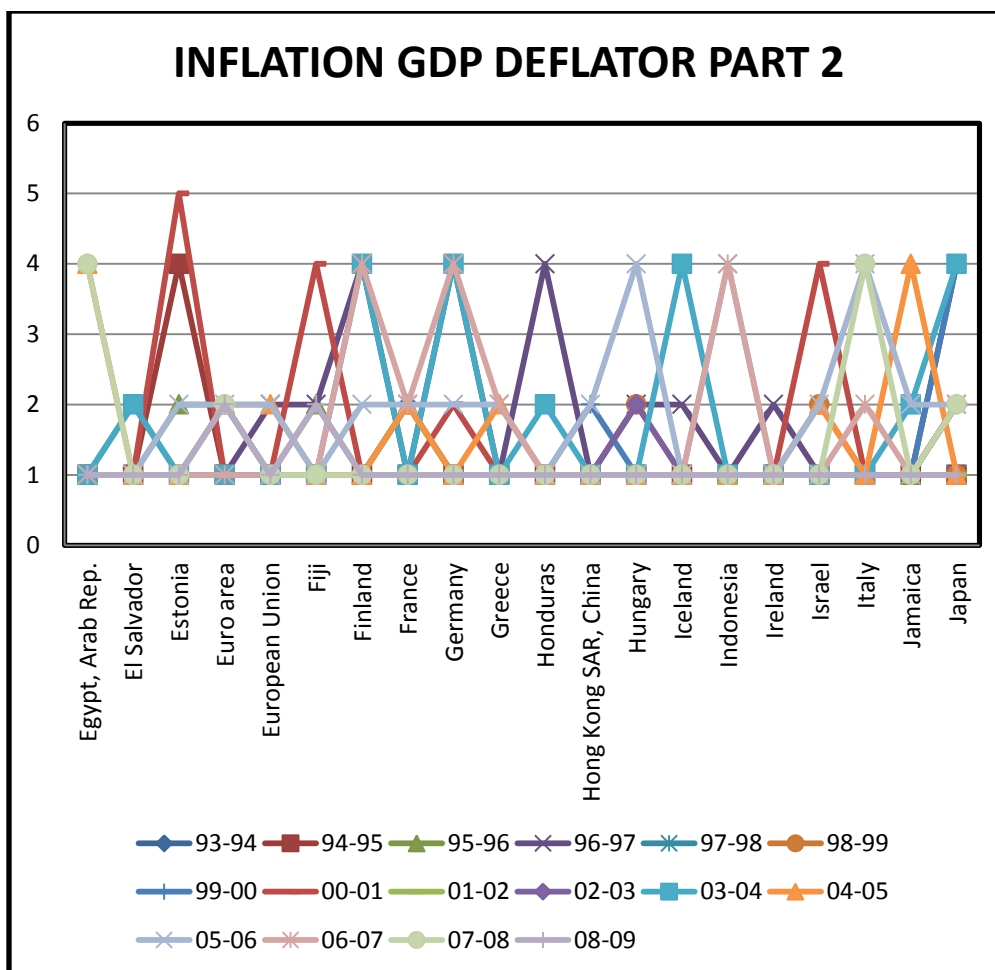


Figure 7.6b: Inflation GDP Deflator of selected countries against path dependency indices part 2

The plots of GDP deflator for some of these countries across time is given in Figure 7.6e. Other than the initial drop of Slovak Republic the plots of other countries have some oscillatory changes but all such changes remain within a band of 0% to 15%. The plot of Dominican Republic against time for GDP deflator is also shown in Figure 7.6f.

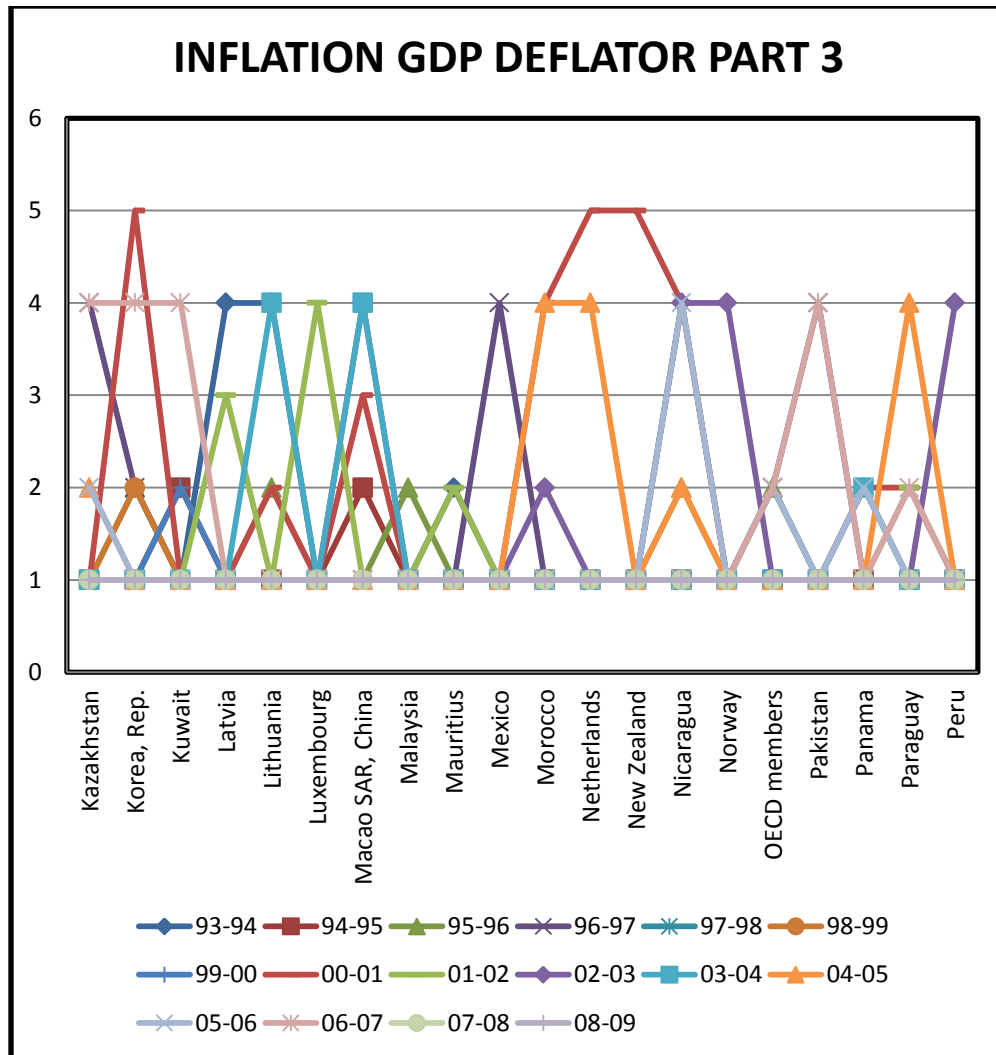


Figure 7.6c: Inflation GDP Deflator of selected countries against path dependency indices part 3

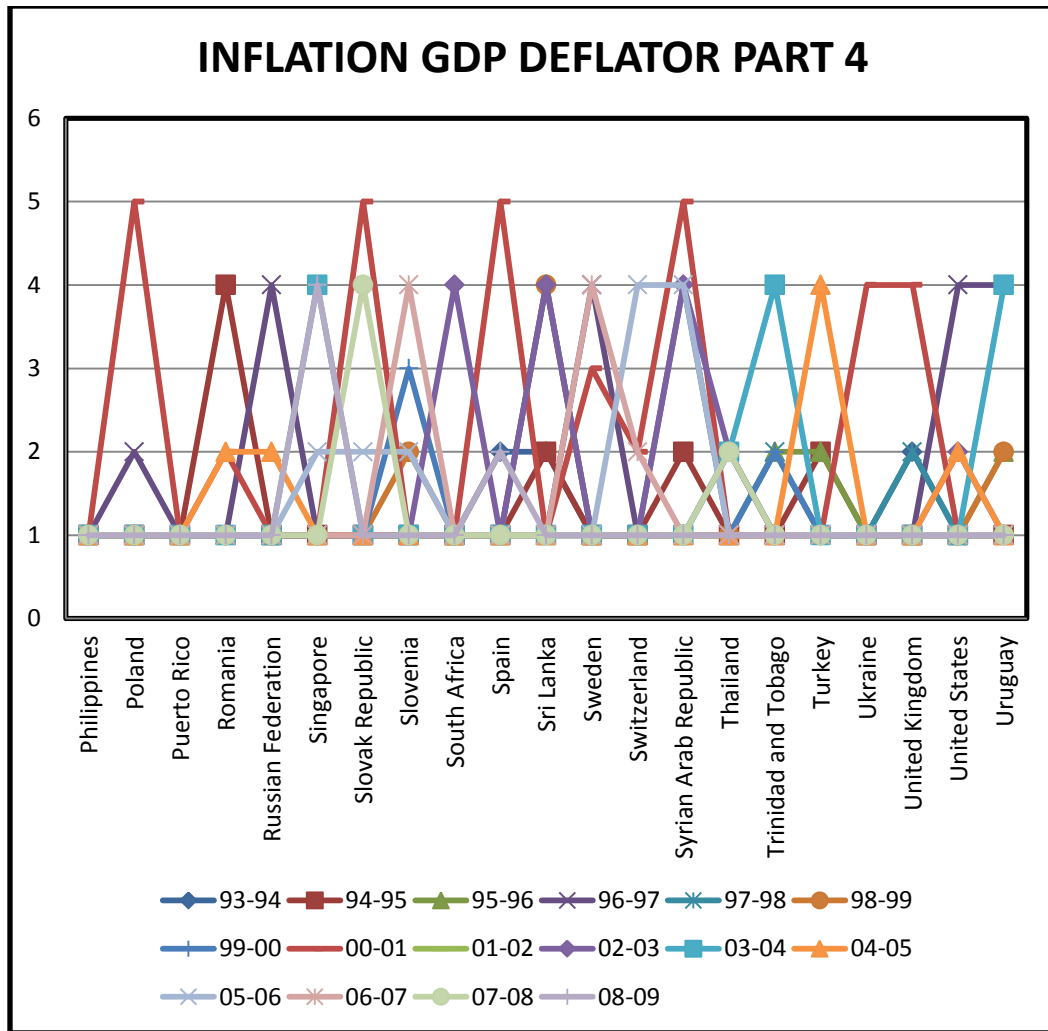


Figure 7.6d: Inflation GDP Deflator of selected countries against path dependency indices part 4

As expected from the extrapolation of the tangent line at the most recent point of 2001, the countries Korea Republic, Spain, Slovak Republic and Syrian Arab Republic continues along the tangent as expected. Korea continues with its slightly downward to flat trend, while Spain continues in the upward to flat fashion. Slovak Republic continues in its slightly downward to flat trend while Syrian Republic also continues its downward trend along the tangent line [Figure 7.6e]. The slight deviations from the extrapolated tangent line occur in the case of New Zealand and Netherlands which changes to a downward trend in 2001-2002 from the upward one in 2000-2001.

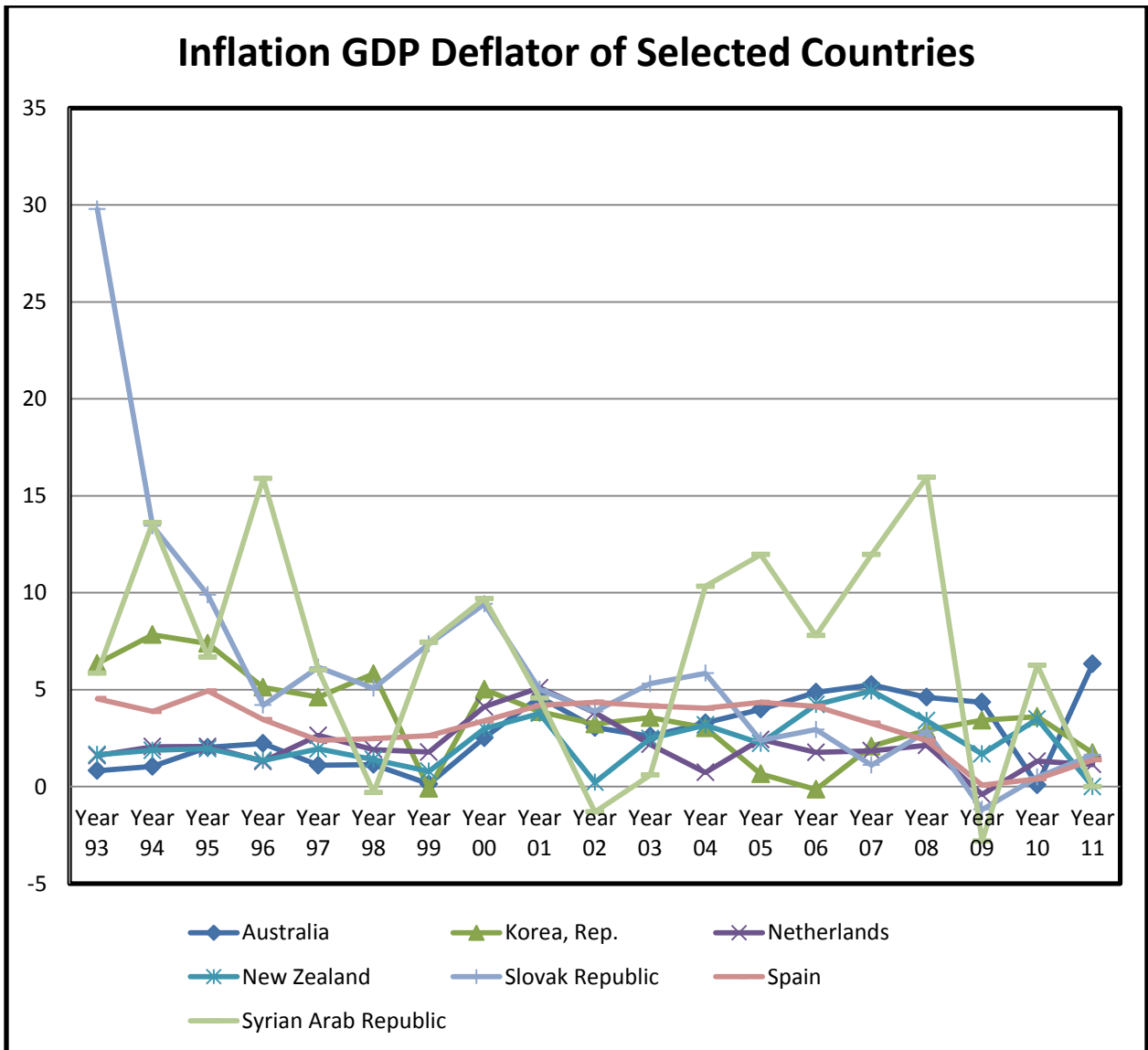


Figure 7.6e: Inflation GDP Deflator of some selected countries

From Figure 7.6f it is observed that our algorithm was not able to predict the huge inflation increase in 2002-04 for Dominican Republic, and subsequent sharp drop in 2004-05. In both of these cases, category assignment of 8 was expected. Instead a category of 8 was seen in 1994-1995, thus expecting a large change right after 1995. This did not materialize. This can be attributed to the fact that our algorithm only gives predisposition. This predisposition of the huge change happening right after 1995 may not have materialized due to extenuating circumstances such as political events or some other factors which negated the predisposition. Similar events could have taken place for the subsequent decrease in the years 2004 and 2005.

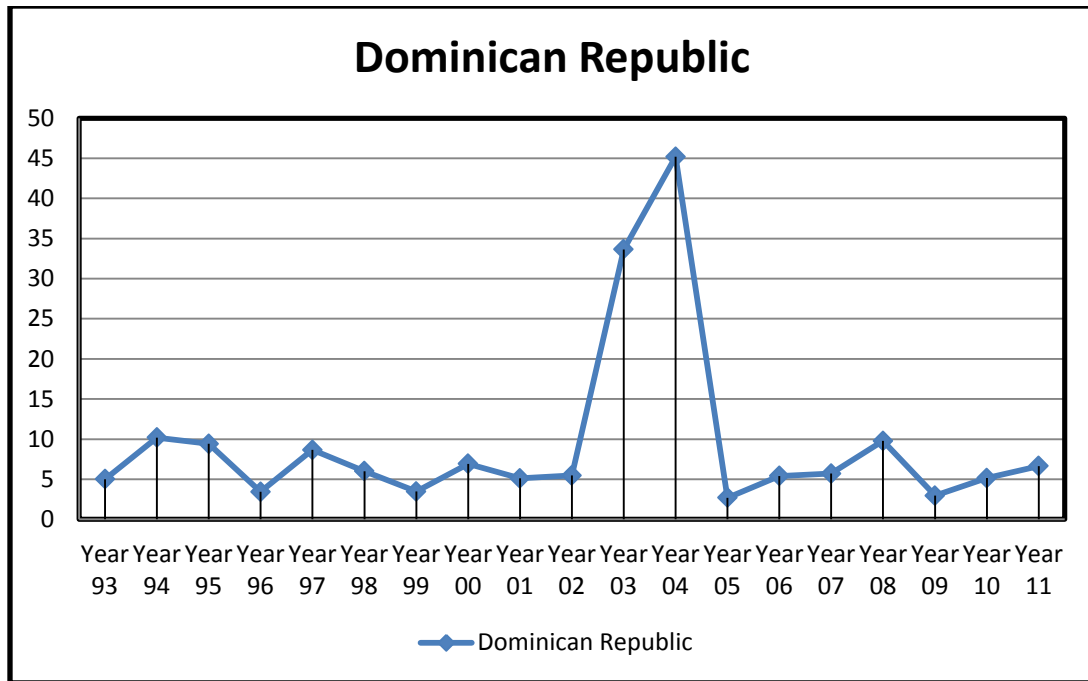


Figure 7.6f: Inflation GDP Deflator of Dominican Republic

The next 4 plots show the variation of unemployment for the 81 countries across different years against their respective path dependency indices.

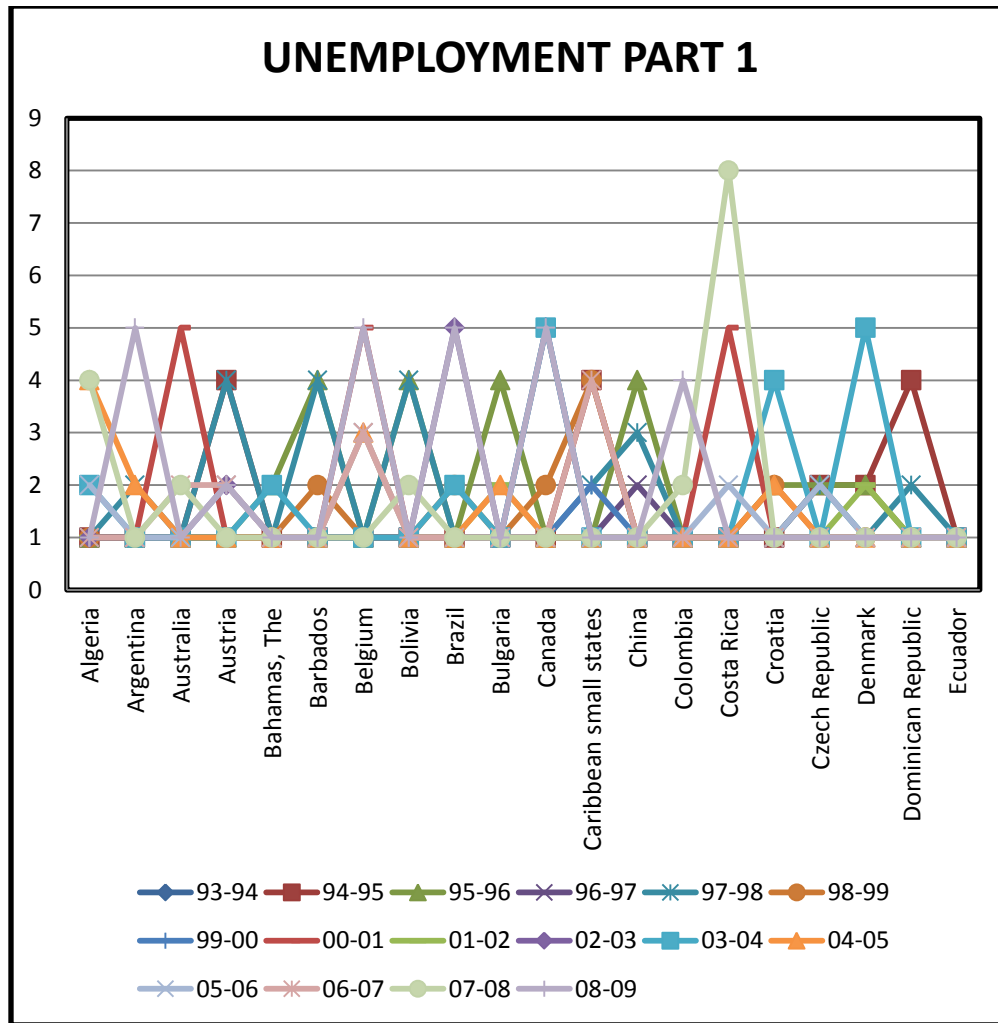


Figure 7.7a: Unemployment of selected countries against path dependency indices part 1

Here firstly the countries that have reached a path dependency index of 8 are analyzed. The countries are Costa Rica, Euro Area, France, Germany, Pakistan, Paraguay and Ukraine. All these countries reach level 8 in the year 2007 to 2008.

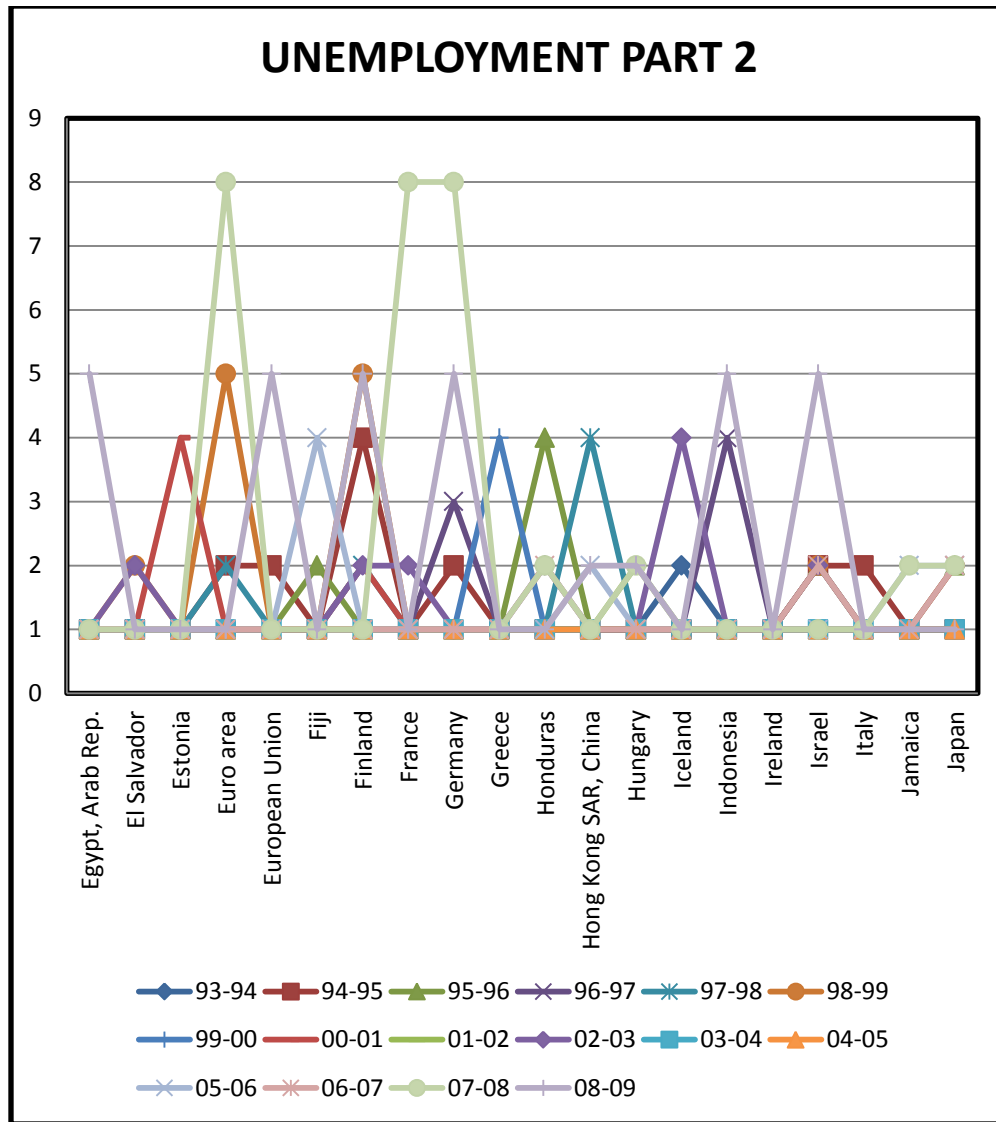


Figure 7.7b: Unemployment of selected countries against path dependency indices part 2

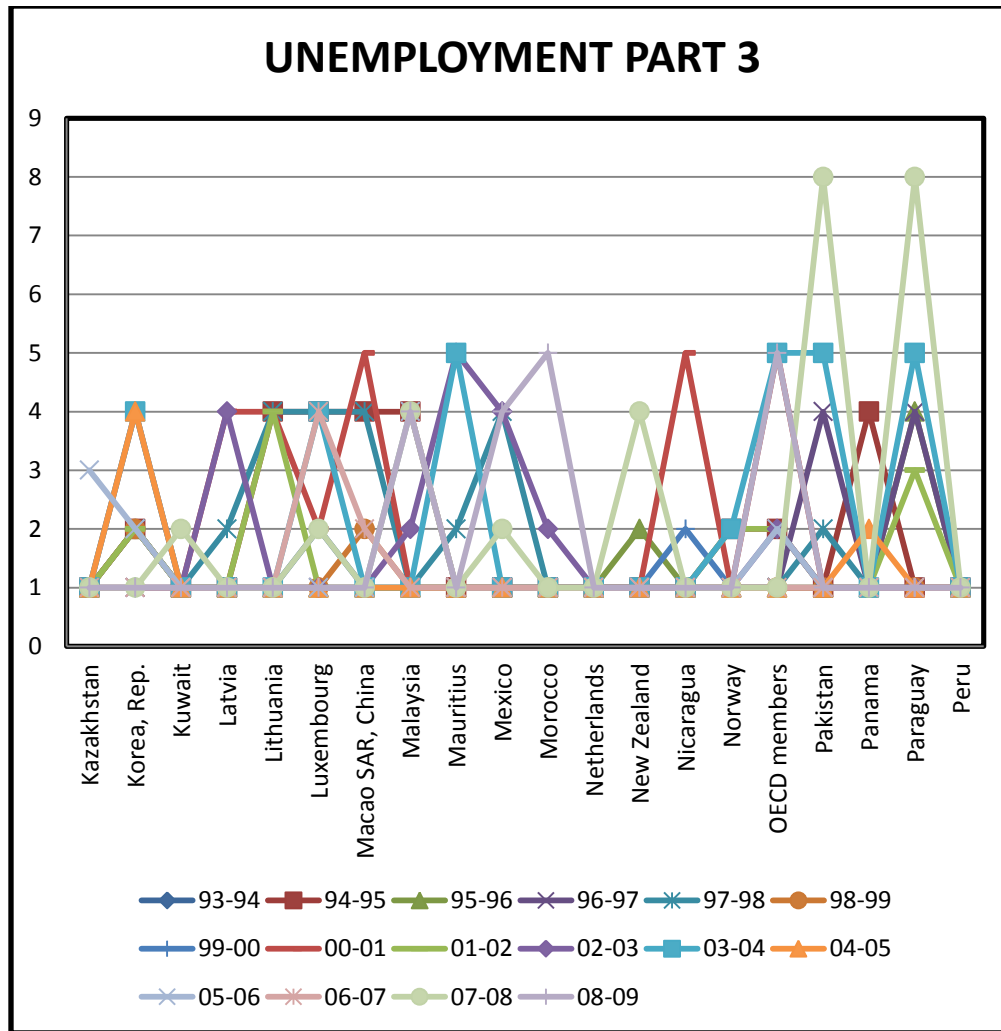


Figure 7.7c: Unemployment of selected countries against path dependency indices part 3

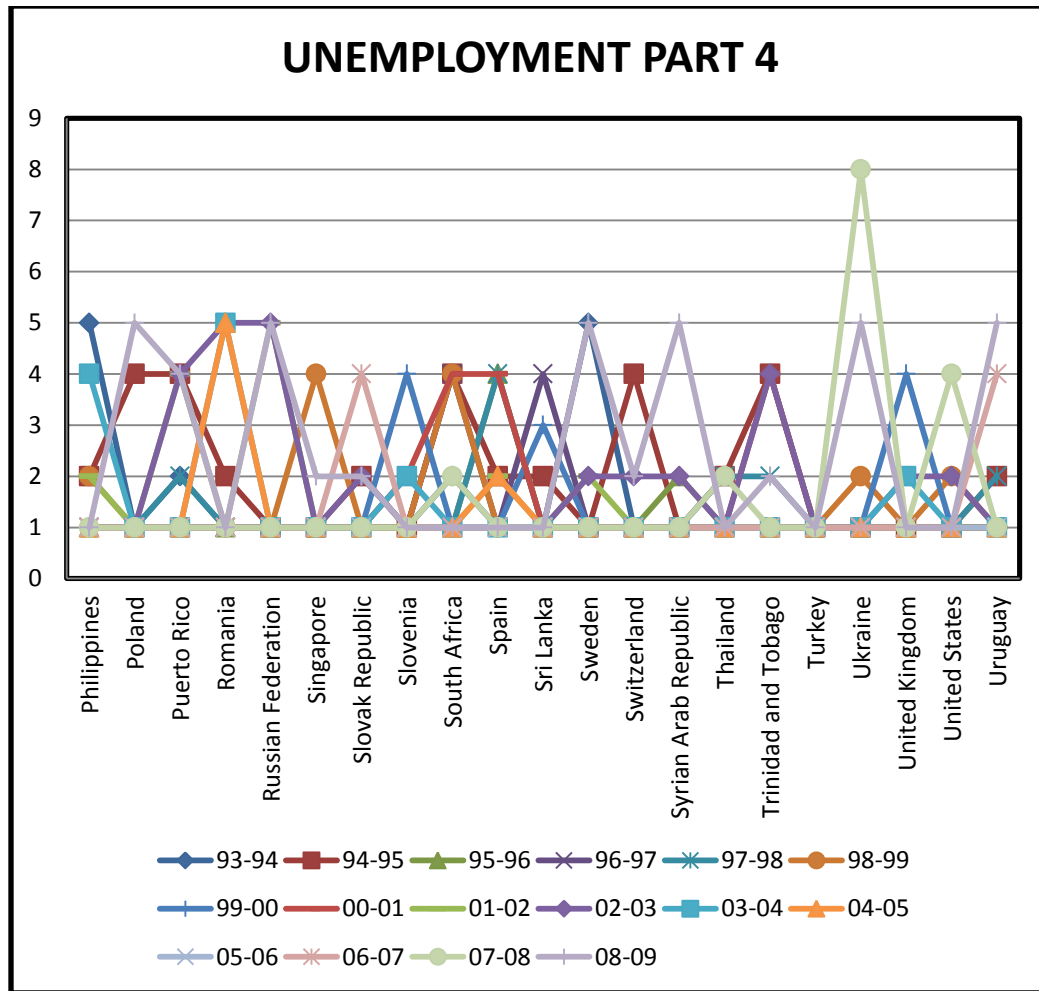


Figure 7.7d: Unemployment of selected countries against path dependency indices part 4

The plot of some of the countries which reached a level of 8 is done for unemployment in Figure 7.7e. If the plot of such countries is observed against time for unemployment rate it is seen that all the countries have a sharp increase in unemployment rate in 2008. Ukraine does have another sharp increase in the year 1997 but all other countries the changes are smoother throughout the time span. According to the plot the increase in Ukraine unemployment is a steady straight line from 1995 to 1998. According to expected results from our algorithm this should have been categorized as a 5, but such a thing did not happen. It again might be due to some external unforeseen factors that negated our prediction of an almost no to slight change curve. But other than this the graph of Ukraine had been quite smooth with only slight variations from 1998 to 2007.

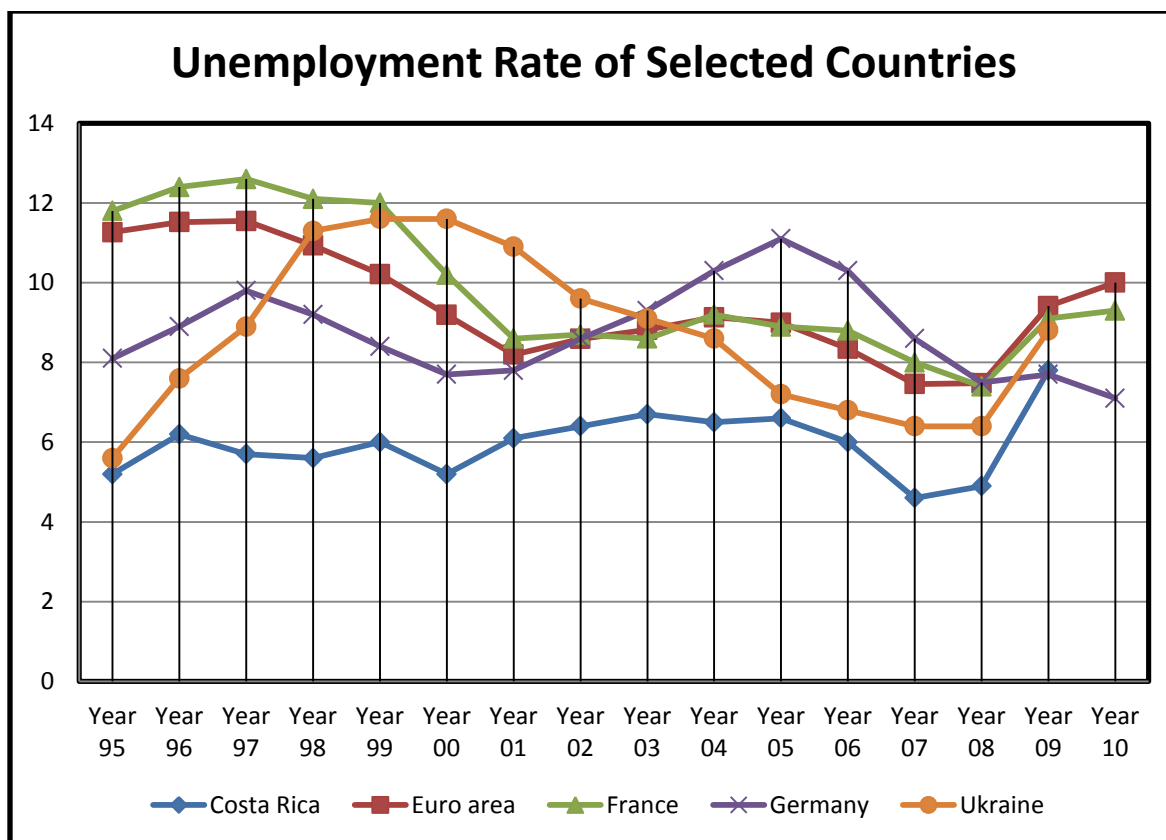


Figure 7.7e: Unemployment of selected countries against path dependency indices part 4

7.6d Residual Curvature Results

Figure 7.8 shows the percentage of roots (out of 16) which had a residual curvature drop greater than 80%. From the plot it is seen that in the year 2004 – 2005 the dimension GDP Capita had a more than 50% (more than 8) roots which had 80% or greater drop in residual curvature. This could be seen as the forecast for the financial meltdown that happened in 2007 – 2008. The US Federal Government started slashing interest rates till 2004 after which they kept increasing the rate from 2004 to 2006. This led to the burst of the housing bubble and the ultimate financial collapse in 2007 – 2008. So the instabilities in the system started cropping in the period 2004 to 2006 that is visible in this graph. Obviously the repercussions of such instabilities happened much later. The other mentionable years where the roots in specific dimensions go closer to the 50% value are 1998-1999 and 2000-2001. These can be thought of as predictions for Russian Ruble Crisis and Asian Financial Crisis that took place around that time.

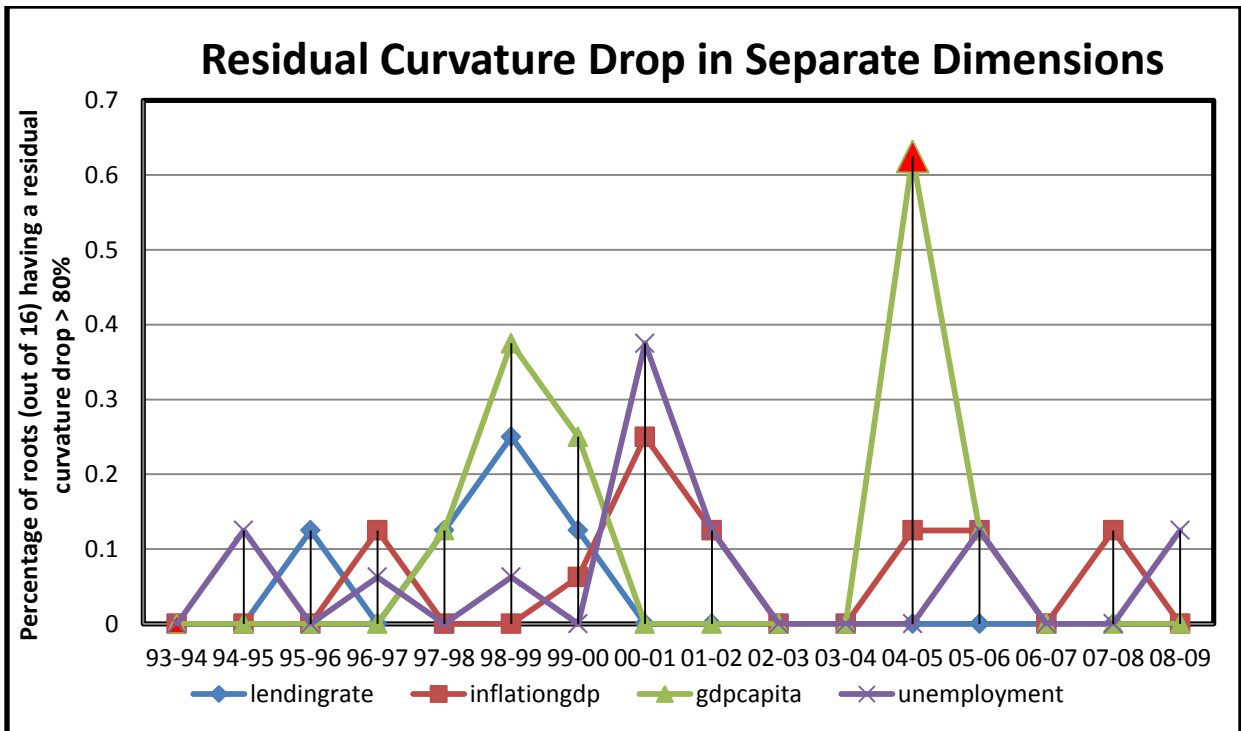


Figure 7.8: Percentage of roots (out of 16) that had a residual curvature drop greater than 80%.

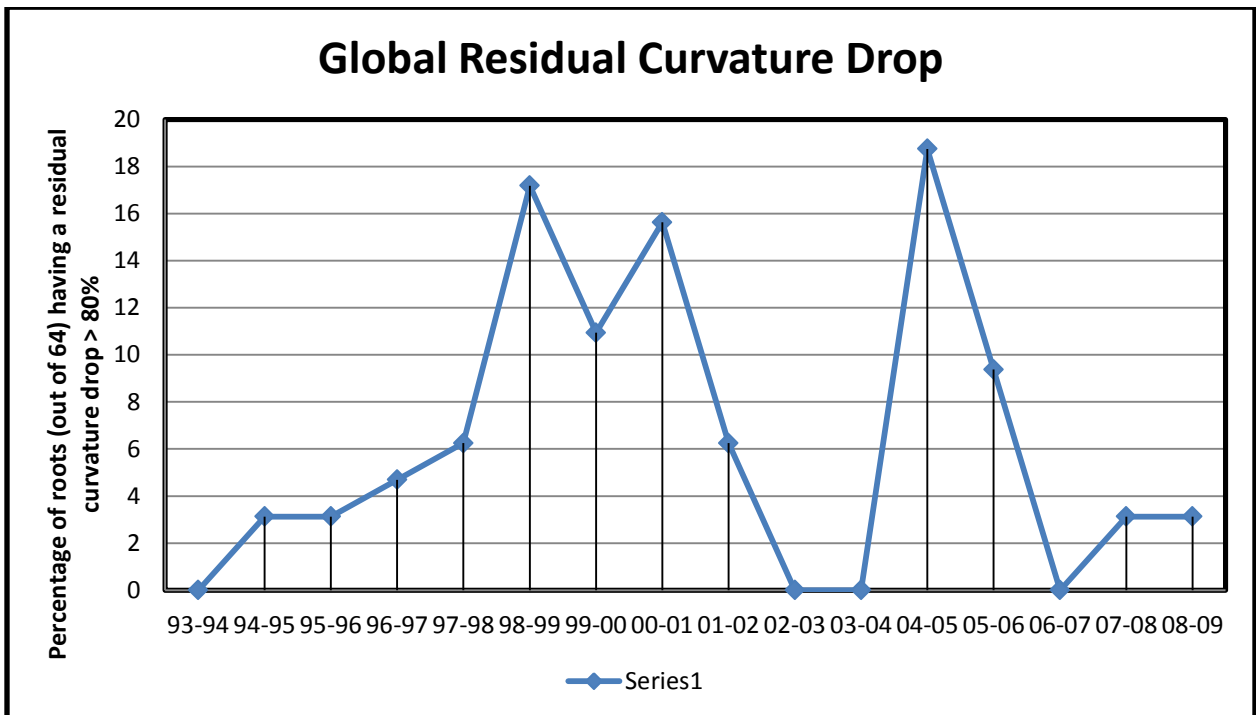


Figure 7.9: Percentage of roots (out of 64 summed across all 4 dimensions) that had a residual curvature drop greater than 80%.

Figure 7.9 shows the percentage of roots (out of 64) summed across the four dimensions that had a residual curvature drop greater than 80%. From the plot it is seen that in the year 2004 – 2005 the percentage of roots almost hit 20% (around 12 roots out of 64 in all dimensions) which had 80% or greater drop in residual curvature. This could be seen as the forecast for the financial meltdown that happened in 2007 – 2008. The US Federal Government started slashing interest rates till 2004 after which they kept increasing the rate from 2004 to 2006. This led to the burst of the housing bubble and the ultimate financial collapse in 2007 – 2008. So the instabilities in the system started cropping in the period 2004 to 2006 that is visible in this graph. Obviously the repercussions of such instabilities happened much later. The other years where the roots in specific dimensions go closer to the 20% value are 1998-1999 and 2000-2001. These can be thought of as predictions for Russian Ruble Crisis and Asian Financial Crisis that took place around that time.

CHAPTER 8. CONCLUSIONS

The results predicted from the data driven predictive (DDP) algorithm are based on data gathered in a continuous process. It takes the data, analyzes the curvature and predicts what could be happening to the system in the future based on this curvature information. But all such predictions are based on what happened to the system in the past. True predictive capability always requires determination of current state of the system. In addition, it requires knowledge of two kinds of variables: (1) predisposition of the system at present time (e.g., residual stress) and (2) the future forcing function. Out of these, the future forcing function is impossible to determine for a finite system. Hence, the present work focuses on determining the current state as well as the current predisposition of the system only. There are always external sources, other extenuating factors that may influence the system at a later time. At a specified time instant, only the past and the present can be known, but not the future. Accordingly, the model predictions obtained in this work are predictions of accumulated predisposition or “bias” at the present time. So these predictions should be looked at as predispositions at specified times rather than as forecasts of future events. These predispositions are also manifestations of induced path dependency in the system.

Although the summation of the force acting on the system across all points may be zero but the stress distribution (when stress is integrated to obtain force) at every point may not be equal to zero. This can induce a non-zero residual stress distribution in the system, even if its integral under equilibrium is zero. Such non-zero residual stress distribution may cause uneven predisposition at different locations in the system. Accordingly, in making direct comparisons (by treating these pre-dispositions as forecasts) with actual future events, it can only be hoped that the forecasts will only be stochastically valid in an ordinal sense. Certainly, detailed statistical analyses of such comparisons are needed than is made in this thesis, where only preliminary comparisons are made.

CHAPTER 9. FUTUREWORK

The algorithm that is developed here can be applied in multifaceted applications. The applications that were presented here are the 1) Balloon Burst 2) Gulf Stream Ring Formations 3) Economic Stability Analysis. Out of these applications, the balloon bursts were predicted within a maximum observed error of 12%. There were other results that were predicted only 2% or 6% before the actual failure time instant. These predictions are novel as it requires no offline testing. Considering a balloon popping experiment, the less the error the better is the result as ideally a balloon should be blown almost till the point of its bursting.

However for the Gulf Stream the cold core ring formations were predicted with a lead of 2 to 4 days before the actual ring formations took place varying between these quantities for different data sets. But the lead of 2 to 4 days is actually appreciable in the case of Gulf Stream as the fishing community needs to know in advance to travel to those specific places. Moreover we did not have the actual map pictures on every day. So it is difficult to compare the results predicted by the DDP algorithm with the actual map data. It could have happened that the ring formations were initiated much earlier as predicted by the algorithm but showed much later in the map as the map pictures were only 2 weeks or 1 week apart. Also the Gulf Stream could have been influenced by external factors like weather changes that could have made a huge difference between the predictions and the real forecast. However there were some discrepancies as some rings did appear in regions where there were no rings. This could be attributed to the fact that the model only predicts predispositions. In the future, the Gulf Stream results needs to be interpreted in a better way.

For the Economic Stability Analysis the predispositions in the system were there. But since Global Economics of the World is not a materialistic system the system had much more extenuating factors than the other two. Hence the predispositions in the system did not forecast accurately the actual events as there were much more volatile factors like government control, political influence that negated the way the system should have behaved. As a future work these external factors need to be nullified and a better prediction needs to be done. Unemployment, GDP Per Capita predictions were better than GDP Deflator and Lending rate. Most of the increases in unemployment were predicted correctly. Another reason for discrepancies that rose in the Economics predictions was the level of noise in the data that was used.

In addition to these two there are 2 other applications that are being currently considered. One such application is to study the gait analysis of functional movements including stair use and walking of individuals with anterior cruciate ligament (ACL) reconstruction. These people are at increased risk to develop knee osteoarthritis. Knee osteoarthritis is estimated to develop 5-20 years after initial ACL injury.

The second application that is being considered is that of analyzing the effect of abiotic stress (heat, cold, UVB, drought) etc. on the plant *Arabidopsis*. This would be done to understand the formation of genetic pathways, and competition of various genes within the plant for natural resources.

BIBLIOGRAPHY

- A. Chandra, A. Bastawros, K.C. Wu, O. Kar, R McCleish (2013) - Role of Velocity Control for Enhancing Planarization Rate and Stability of Chemical Mechanical Paired Grinding
- A. Chandra, S. Roy (2012) - On removing Condorcet effects from pairwise election tallies
- D. Roylance (2001) – Engineering Viscoelasticity
- D.G. Saari (1999) - Explaining all three alternative voting outcomes, Journal of Economic Theory, Vol. 87.
- D.G. Saari (2000) - Mathematical structure of voting paradoxes I and II, Economic Theory, Vol. 15
- D.G. Saari (2001a) - Chaotic Elections! A Mathematician Looks at Voting, American Mathematical Soc., Providence, RI.
- D.G. Saari (2001b) - Decisions and Elections; Expect the Unexpected, Cambridge University Press, Cambridge, UK, 2001b.
- D.G. Saari, K. Sieborg (2001) - The sum of parts can violate the whole, Amer. Pol. Science Review, Vol. 95(2).
- E. Orowan (1934) - Zur Kristallplastizität. III Über den Mechanismus des Gleitvorganges, Zeitschrift für Physik (European Physical Journal)
- G.I. Taylor (1934) - The Mechanism of Plastic Deformation of Crystals, Proceedings of the Royal Society, London
- Gulf Stream Real Time Forecasts: - <http://www.smast.umassd.edu/modeling/RTF/>
- J. Lubliner (1990) - Plasticity Theory
- J. D. Eshelby, F. C. Frank, F. R. N. Nabarro (1951) - The equilibrium of linear arrays of dislocations, Philosophical Magazine, Vol. 42.
- M. Polanyi(1934) - Über eine Art Gitterstörung, die einen Kristall plastisch machen könnte , Zeitschrift für Physik (European Physical Journal)
- Ramiro Pareja Pareja (2008) - Plastic Deformation, Dislocations and Strengthening Mechanisms
- Richard Feynman (1998) - Six Not So Easy Pieces: Einstein's Relativity, Symmetry and Space-Time
- S. Zhang, P.S. Huang (2008) -Real-Time three-dimensional shape measurement

Weisstein, Eric W. "Curvature." Math World - A Wolfram Web Resource.
<http://mathworld.wolfram.com/Curvature.html>

Wikipedia: - http://en.wikipedia.org/wiki/Osculating_circle

Wikipedia: - http://en.wikipedia.org/wiki/Gaussian_curvature

World Data Bank: - <http://databank.worldbank.org/ddp/home.do>

ACKNOWLEDGEMENTS

This material is based upon work supported by the U.S. National Science Foundation under Grant No. CMMI-1100066. The author gratefully acknowledges this support. Any opinions, conclusions or recommendations expressed are those of the authors and do not necessarily reflect views of the sponsoring agencies.

I would like to take this opportunity to express my gratitude to those who helped me at various stages of my research work and with the writing of this thesis. Firstly, I would like to thank my major professor, Dr. Abhijit Chandra, Department of Mechanical Engineering for his guidance and encouragement throughout this research and for being a wonderful mentor. I have learnt a lot from him. I am immensely grateful to him for treating me with patience and motivating me to apply this work to a variety of problems. I owe a lot to Dr. Sunanda Roy, Department of Economics, for helping me with the concepts of Stability Analysis in the Macro Economic System. I would also like to thank my committee members, Dr. Eve Wurtele (Department of Genetics, Development and Cell Biology) and Dr. David Fernández Baca (Department of Computer Science) for their support and guidance.